X-ray irradiation triggers via ROS production a canonical Ca^{2+}-dependent immune response in T-lymphocytes

Vom Fachbereich Biologie der Technischen Universität Darmstadt

zur Erlangung des akademischen Grades

Doctor rerum naturalium

Dissertation von

Dominique Tandl

1. Referent: Prof. Dr. Gerhard Thiel

2. Referent: Prof. Dr. Alexander Löwer

Tag der Einreichung: 03. Dezember.2020

Tag der mündlichen Prüfung: 22. Januar 2021

Darmstadt 2021

Dominique Tandl:
X-ray irradiation triggers via ROS production a canonical Ca^{2+}-dependent immune response in T-lymphocytes

Darmstadt, Technische Universität Darmstadt
Jahr der Veröffentlichung der Dissertation auf TUPrints: 2021
Tag der Einreichung: 03. Dezember 2020
Tag der mündlichen Prüfung: 22. Januar 2021
URN: urn:nbn:de:tuda-tuprints-154022

“If you're not failing every now and again,
it's a sign you're not doing anything very innovative.

Woody Allen

Table of contents

General Abstract

For decades X-ray irradiation has been employed in cancer therapy for eliminating malignant cells. In this treatment however not only the tumor cells but also cells in the surrounding tissue and blood are unavoidably exposed to ionizing irradiation (IR). While the cellular and molecular effects of radiation on tumor cells are well studied the impact on the immune cells, which are located coincidentally in the blood vessels and the tumor environment, remain elusive. Because of this still existing knowledge gap the present work aims to uncover the effects of X-ray as a type of IR on immune cells, especially T-lymphocytes in the blood. The primary goal is to reveal early radiation-triggered events and to elucidate their downstream effects. The work is motivated by the idea that an understanding of intracellular reaction mechanisms will help to better assess the risks of radio-therapy for tumor patients. The focus on exposed immune cells bears the possibility that X-ray may generate antagonistic or even agonistic effects in these cells, which will help to improve radiation protocols. In the case of an agonistic, hermetic effect on immune cell it even opens the potential for combining radio-immune therapy for a successful cancer treatment.

In previous studies it was shown that ionizing radiation can have beneficial effects on T-lymphocytes and stimulate an immune activation in these cells. In this scenario, redox and calcium signals serve as components in second messenger cascades where they cross react with the canonical signaling events that induce immune activation of T-cells. The latter is initiated by antigen binding to the T-cell receptor (TCR) located on the T-cell surface. This is followed by precisely regulated cytosolic calcium (Ca^{2+}_{cyt}) oscillations, which stimulate the nuclear translocation of the transcription factor nuclear factor of activated T-cells (NFAT) and therefore mediate specific immunological modulations.

The data of the current study corroborate results from previous investigations that exposing T-lymphocytes to X-ray doses between 0.1 and 5 Gy triggers an intracellular ROS/Ca^{2+}-dependent signaling cascade in Jurkat T-cells and peripheral blood mononuclear cells (PBMCs). The first resolvable events of the IR-triggered pathway are a transient increase in mitochondrial and cytosolic ROS over the first 1-20 minutes after exposure. This is followed after a lack time, within a large variation of 10-80 min after irradiation by long-lasting (>3 h) Ca^{2+} oscillations with a highly conserved frequency (~3 mHz) and a dose-dependent amplitude. The Ca^{2+} signaling cascade involves a clustering of STIM/Orai proteins forming Ca^{2+}-release activated Ca^{2+} (CRAC) channels, which in turn activates Ca^{2+}-induced Ca^{2+}-release (CICR). As a downstream consequence of the dynamic Ca^{2+} changes in the cytosol the transcription factor NFAT is translocating from the cytosol into the nucleus approximately 50 min post radiation exposure. As result of the nuclear NFAT shuffling the expression of different T-cell activation markers including the cytokines interleukin-2 and interferon-γ can be detected 24 h post irradiation with a significant expression increase compared to unirradiated controls. The X-ray triggered signaling events are similar to those observed in naïve T-lymphocytes after TCR immune stimulation. This similarity is further highlighted by the fact that not only the key molecules, which are involved in the signaling cascades are identical, but also the dynamics of the events. This includes the delay times between stimulation and onset of Ca^{2+} oscillations and NFAT translocation as well as the highly conserved frequency of calcium oscillations. In conclusion the present data underscore the assumption that X-ray exposure of T-cells to clinically relevant doses induce an immunological stimulation of these cells via an activation of the same signaling cascade that is also elicited by TCR stimulation. This agonistic effect of X-ray exposure on T-cells might in the future foster therapy approaches which combine the effects of radiation with immunotherapy.

Zusammenfassung

Seit Jahrzehnten wird die Röntgenbestrahlung in der Krebstherapie zur Eliminierung bösartiger Zellen eingesetzt. Bei dieser Behandlung werden jedoch nicht nur die Tumorzellen, sondern auch Zellen im umliegenden Gewebe und im Blut zwangsläufig einer ionisierenden Bestrahlung (IR) ausgesetzt. Während die zellulären und molekularen Auswirkungen der Bestrahlung auf die Tumorzellen gut untersucht sind, bleiben die Auswirkungen auf Immunzellen, die sich zufällig in den Blutgefäßen und der unmittelbaren Umgebung des Tumors befinden, unklar. Aufgrund dieser noch vorhandenen Wissenslücke besteht das Ziel der vorliegenden Arbeit daraus, die Auswirkungen von Röntgenstrahlung als eine Art von IR auf Immunzellen, insbesondere T-Lymphozyten, aufzudecken. Der Fokus liegt darauf, frühe durch Strahlung ausgelöste Ereignisse aufzudecken und ihre nachfolgenden intrazellulären Effekte aufzuklären. Die Arbeit motiviert durch die Annahme, dass ein Verständnis der intrazellulären Reaktionsmechanismen dazu beitragen wird, die Risiken der Strahlentherapie für Tumorpatienten besser einschätzen zu können. Die Fokussierung auf exponierte Immunzellen birgt die Möglichkeit, dass Röntgenstrahlen antagonistische oder sogar agonistische Effekte auf diese Zellen erzeugen können, was zu einem verbesserten Ansprechen der Patienten auf die Bestrahlungsprozesse führen kann. Im Falle einer agonistischen, hormetischen Wirkung auf Immunzellen eröffnet sie sogar die Möglichkeit, die Radio- und Immuntherapie für eine erfolgreiche Krebsbehandlung zu kombinieren.

In früheren Studien wurde gezeigt, dass ionisierende Strahlung vorteilhafte Wirkungen auf T-Lymphozyten haben und eine Immunaktivierung in diesen Zellen stimulieren kann. In diesem Szenario dienen Redox- und Calciumsignale als Komponenten in *second messenger*-Kaskaden, die identisch zu kanonischen Signalereignissen, die eine Immunaktivierung in den T-Zellen verlaufen. Letztere wird durch eine Antigenbindung an den T-Zell-Rezeptor (TCR), der sich auf der T-Zell-Oberfläche befindet, ausgelöst. Darauf folgen präzise regulierte cytosolische Calcium-(Ca^{2+}_{cyt}) Oszillationen, die eine nukleare Translokation des Transkriptionsfaktors *nuclear factor of activated T-cells* (NFAT) stimulieren und damit spezifische immunologische Modulationen vermitteln.

Die Daten der aktuellen Studie bestätigen Ergebnisse früherer Untersuchungen, dass die Exposition von T-Lymphozyten mit Röntgendosen zwischen 0,1 und 5 Gy eine intrazelluläre ROS/Ca^{2+}-abhängige Signalkaskade in Jurkat T-Zellen und peripheren mononukleären Blutzellen (PBMCs) auslöst. Die ersten auflösbaren Ereignisse des IR-getriggerten Signalwegs sind ein transienter Anstieg der cytosolischen und mitochondrialen ROS in den ersten Minuten nach der Exposition. Darauf folgen nach einer Latenzzeit von einigen Minuten langanhaltende (>3 h) Ca^{2+}-Oszillationen mit einer hochkonservierten Frequenz (˜3 mHz) und einer dosisabhängigen Amplitude. Die Ca^{2+}-Signalkaskade umfasst eine Anhäufung von STIM/Orai-Proteinen, die Ca^{2+}-freisetzungsaktivierte Ca2+-Kanäle (CRAC) bilden, die wiederum die Ca^{2+}-release activated Ca^{2+} (CICR) aktivieren. Als stromabwärts gerichtete Folge der dynamischen Ca^{2+}-Änderungen im Cytosol migriert der Transkriptionsfaktor NFAT etwa 50 Minuten nach der Bestrahlung vom Cytosol in den Kern. Als Ergebnis dieser Translokation kann 24 h nach der Bestrahlung die Expression verschiedener T-Zell-Aktivierungsmarker, einschließlich der Zytokine Interleukin-2 und Interferon-γ nachgewiesen werden. Die nachgewiesenen durch Röntgenstrahlen ausgelösten Signalereignisse sind nahezu identisch zu denen, die bei naiven T-Lymphozyten nach TCR-Immunstimulation beobachtet werden. Diese Ähnlichkeit wird noch dadurch unterstrichen, dass nicht nur die Schlüsselmoleküle, die an den Signalkaskaden beteiligt sind, identisch sind, sondern auch die Dynamik der Prozesse. Dazu gehören die Latenzzeiten zwischen IR-Stimulation und Beginn der Ca^{2+}-

Oszillationen und der NFAT-Translokation sowie die hochkonservierte Frequenz der Calcium-Oszillationen.

Zusammenfassend unterstreichen die vorliegenden Daten die Annahme, dass die Röntgenbestrahlung von T-Zellen mit klinisch relevanten Dosen eine immunologische Stimulation dieser Zellen über eine Aktivierung derselben Signalkaskade induziert, die auch durch TCR Bindung hervorgerufen wird. Diese agonistische Wirkung der Röntgenbestrahlung auf T-Zellen könnte in Zukunft Therapieansätze fördern, die die Effekte der Bestrahlung mit einer Immuntherapie kombinieren.

1. General Introduction

1.1 Summary for the general public

Radiotherapy is known to cure cancer patients by killing tumors. But tumors consist of more than just malignant cells; there are also normal tissue cells, blood vessels and immune cells. The actual task of immune cells is to recognize and combat malignant tumor cells, which is not always possible due to special tumor defense mechanisms. Therefore, modern tumor therapy tries to impair the defense mechanisms of tumor cells, or inversely to strengthen the activation mechanisms of immune cells. Until now, radiotherapy has almost exclusively focused on destroying the tumor cells. As a consequence, it is still unknown how and in what ways immune cells are affected. The present study shows that X-ray used in radiation therapy not only destroys the tumor cells, but also activates the immune cells that are present in the irradiated tissue. This represents a double positive effect for the patient concerned.

1.2 Social relevance for the elucidation of radiation effects on immune cells

The Robert Koch Institute reported 500,000 tumor cases in Germany in 2019, where metastatic tumors cause an estimated 180,000 deaths, representing approximately 90% of total cancer-related deaths (https://www.rki.de/DE/Content/Service/Presse/Pressemitteilungen/2019/16_2019.html;jsessionid=7FFF81339AD72C5DEC743EFADD2A4E22.internet081). That is why scientists need to investigate new therapy approaches to cure affected people. Medical experts are trying to develop more personalized therapy approaches to address the unique nature of each cancer. (McDermott and Settleman 2009; Malaney et al. 2014). In tumor patients, these therapies can consist of a combination of surgery, chemo-, immune- and radiotherapy, depending on the type of tumor. Due to immunosuppressive proteins expressed by malignant cells, the immune cells of the patient's own body are not able to recognize and destroy these degenerated cells. (McDermott and Settleman 2009; Meric-Bernstam and Mills 2012). What is actually attempted in immune therapy is the activation of the required immune cells in order to destroy the malignant cells. It is essential to understand the molecular effects of radiation on immune cells, as many studies show that these cells are not killed but rather change their immunological activation state.

1.3 Innovative aspects of the present study

Because of various genotypes and phenotypes of cancer, medical diagnostics try to develop personalized treatments to cure affected patients. For this purpose, it is necessary to determine the immune status of the patient. It is common to analyze different immune cell subtype compositions as well as expression levels of pro- and anti-inflammatory proteins in the blood of patients before and after therapy (Meric-Bernstam and Mills 2012). There is evidence that, depending on the patient condition and the tumor type, effector immune cells become active after irradiation because of an increased number of these cells as well as because of an increase of pro-inflammatory proteins. Accordingly, researchers now test for levels of inflammatory proteins, for example to see if they are up- or down-regulated in response to certain stimuli or if there are more or less cells of a certain

immune cell subtype recruited according to the stimuli. Almost nothing is known about the intracellular mechanisms of the changes in the immunological program within a cell. A new perspective of clinical application to investigate the molecular mechanisms of this phenomenon is needed. This molecular elucidation is subject of the present work. Modern molecular techniques like time-lapse life-cell imaging, FRET measurements as well as quantitative RT-PCR and FACS analyses allowed me to identify key regulators, in a before unidentified IR induced ROS/Ca^{2+}-dependent signaling. This could determine whether an organism reacts to irradiation with its immunological activation or not. This gained knowledge can be used to make tumor therapies more successful through a combination of radiation and immunotherapy.

1.4 Radiation hormesis or cell death - the influence of radiation on immune cells

The general aim of tumor therapy is to effectively kill degenerated cells, while protecting healthy tissue as far as possible. Decades of research were spent on elucidating the damaging effects of IR on living organisms, with a focus on damage to the DNA. This destructive property of radiation is used to fight tumors by exposing the tumor tissue locally, usually with fractionated, lethal doses (Castro et al. 1982; Schaue et al. 2012). Despite constant improvements in radiation technology, not only tumor tissue but also healthy surrounding tissue is exposed to a low, sub-lethal dose of radiation (Castro et al. 1982; Cuttler et al. 2017). In addition, cells that flow through the bloodstream inside the tumor tissue during the radiotherapy session are exposed compulsorily. This effect often results in metastases and secondary tumors after radiation therapy (Tucker et al. 1991). High doses of radiation are known for an immune suppression e.g. by cell cycle arrest or even death of blood cells (Manda et al. 2012; Schaue et al. 2012). However, recent studies showed that low radiation doses can also have a positive effect on the organism (Nakamura et al. 1990; Manda et al. 2012; Abuodeh et al. 2016; Cuttler et al. 2017). In this scenario, it could be determined that these low doses can lead to an activation of the immune system, for example, to faster wound healing and increased resistance to toxins and pathogens (Luckey 2006). The positive reaction to low doses of a substance, which is lethal in high doses, is described by the term hormesis. Consequently, the resulting positive phenomenon of low dose radiation is generally known as radiation hormesis (Castro et al. 1982; Luckey 2006). The awareness of the hormetic IR-triggered effect is possible, since research is no longer limited to observation on DNA, but also on extra-nuclear targets. Suzuki and colleagues (2014) were able to show that targeted irradiation of other cell organelles than the nucleus also leads to radiation sensitivity in the affected cell. This finding was possible by a specific microbeam system which can be used to target specific regions within a cell. The findings provided first insights that an onset of IR induced cell signaling events originate from cellular effects independent of DNA damage (Suzuki and Yamashita 2014; Dong et al. 2020). In this context, it has been shown consecutively that IR also has a regulating effect on kinases, phosphatases ion channels, as well as on the plasma membrane (Exton 1996; Grupe et al. 2010b; Soboloff et al. 2011; Roth et al. 2015). However, other radiation-influenced extra-nuclear targets are also conceivable.

1.5 Different cell types have diverse tasks in the humoral immune response

The humoral immune system, whose task it is to protect the organism from foreign microorganisms, viruses and other harmful substances comprises two sub-systems; the innate and the adaptive immune response (Lyte et al. 1990; Medzhitov and Janeway 1998). The first mentioned includes physical barriers like epithelial tissue but also cellular components including granulocytes and macrophages which circulate within the blood stream and eliminate unspecific foreign structures mainly by phagocytosis.

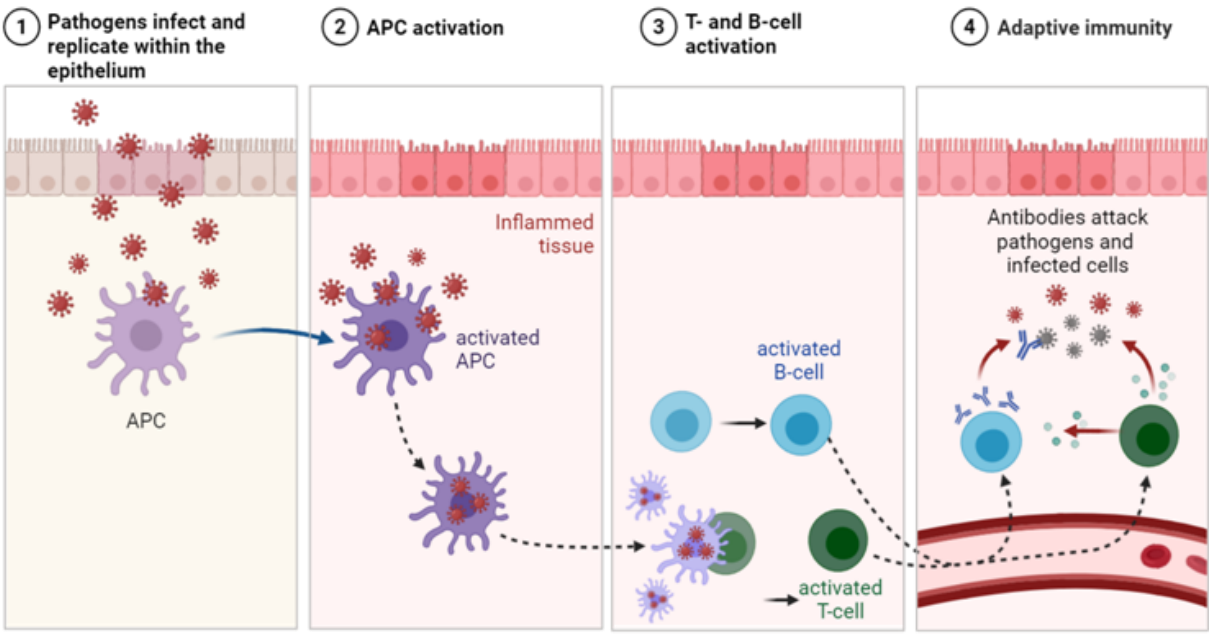

Figure 1: Schematical illustration of key players in the adaptive immune response. Pathogens that have entered the organism are recognized and phagocytized by antigen presenting cells (APC). Protein components of the phagocytized foreign bodies are then presented on their cell surface, to which T-lymphocytes can bind. Through this binding, the T-cells are activated and express messenger substances, e.g. cytokines and chemokines, to recruit further immune cells. These messenger substances can then induce the activation of B-cells, which secrete antibodies specifically against the pathogen. Created with BioRender.com.

In contrast to the innate immune response, the adaptive immune response, as illustrated in Figure 1**,** is highly specific and does not only depend on its inherited characteristics. This means, if foreign structures infiltrate an organism specific antigen presenting cells (APCs) including monocytes, macrophages and B-lymphocytes phagocyte this invader and present a part of the digested foreign structures on their surface via major histocompatibility (MHC) complex proteins (Patel et al. 1999). Together with the cells own proteins, an MHC complex is formed which is better known as antigen. Other specific immune cells are able to bind to this antigen with their cell surface receptors and therefore initiate a cell specific response signaling cascade in order to specifically attack invaders who exhibit the presented proteins. Cells who are able to generate a specific immune response are precursor immune cells, also termed lymphocytes, with an additional established expression: peripheral blood mononuclear cell (PBMCs). PBMCs are formed in the bone marpanel, but in contrast to cells of the innate immune response they have to mature to be functional. The location of their

maturation is reflected in the name of the cells. Lymphocytes are divided into two sub cell types; T-lymphocytes and B-lymphocytes. While T-precursor cells mature in the thymus, B cells mature at the site of their origin in the bone marpanel (Rolink and Melchers 1991).

Both B- and T-lymphocytes do not differentiate or proliferate before an activating stimulus (Tough and Sprent 1994). In this state, they are called naïve because they only wait for their activation. Once a cell has bound to an antigen, an intracellular signaling cascade is initiated and they begin to proliferate and differentiate into effector cells. B-cells can be activated directly by antigens that bind to the B-cell receptor (BCR) (Rolink and Melchers 1991; MacLennan and Vinuesa 2002). T-cells and dendritic cells also activate B-cells as a result of an antigen presentation to the BCR. Activated B-cells differentiate into antibody-secreting plasma cells (Rolink and Melchers 1991; van Parijs and Abbas 1998; MacLennan and Vinuesa 2002), which are specifically directed against the antigen by which the B-cell was previously activated (Lam et al. 1997).

Also, T-lymphocytes are activated by binding to antigens with their T-cell receptor, which interacts with the cluster of differentiation 3-receptor (CD3-receptor), which is also located at the T-cell surface. This entire complex is called the T-cell receptor complex and shown in **Figure 2** (Fracchia et al. 2013). If APCs and T-lymphocytes are in close proximity, the TCR complex of the T-lymphocytes can now bind to the antigen, but for a full and adequate activation, T-cells require an additional co-stimulus which is also provided by APC (**Figure 2**) (Diehn et al. 2002; Xia et al. 2018). Stimulation by the TCR alone, without any co-stimulus, causes the T-cells to a functionally inactive state where they are no longer stimulable. This state of anergy protects the organism against reactions on own tissue in case the selection in the thymus was not completely successful (Sloan-Lancaster et al. 1993; Schwartz 2003; Soto-Nieves et al. 2009). As soon as all necessary binding sites of the T-lymphocytes are occupied, a signaling cascade is initiated, which leads to the activation of the corresponding cell (**Figure 2**) (Shaw et al. 1988; Mustelin et al. 1990; Smeets et al. 2012).

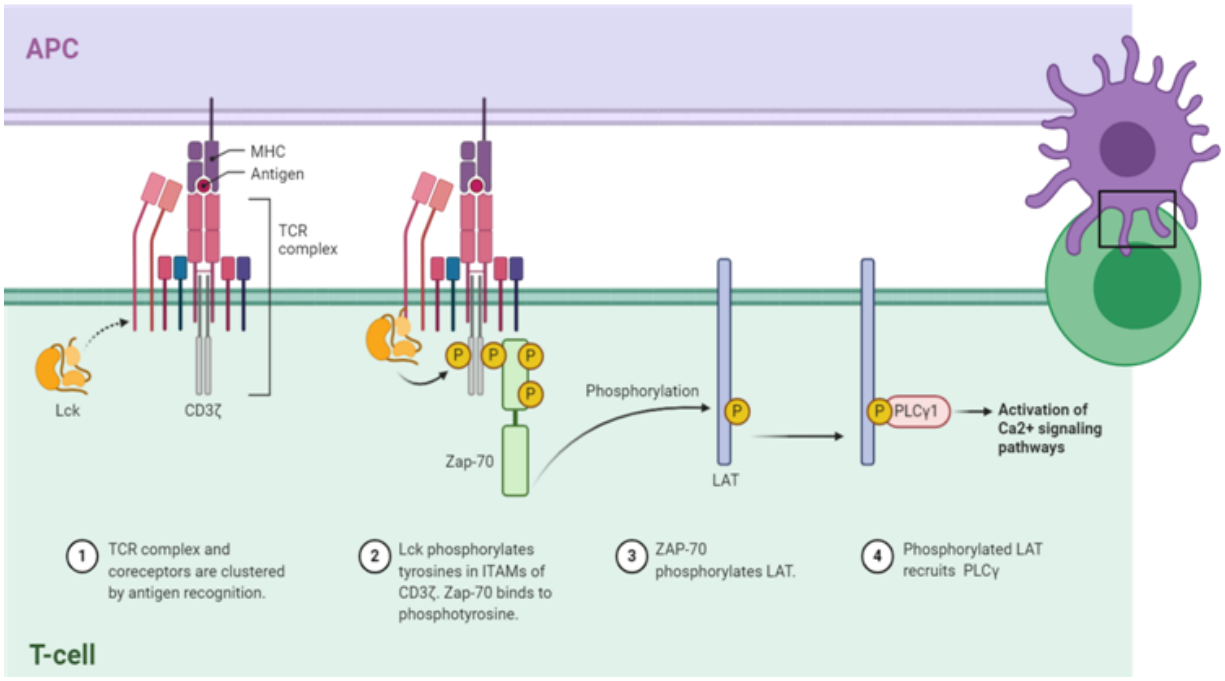

Figure 2: Schematic representation of the T-cell receptor complex. When a major histocompatibility complex (MHC) is expressed by antigen-presenting cells (APC) on their cell surface, the cluster of differentiation 4 (CD4) glycoprotein chain as well as the α and β chains of the T-cell receptor (TCR) on the T-lymphocyte surface bind to it. Via the non-covalent associated chains of CD3 and the two zeta chains, the bound signal is transmitted further into the cell. The activation motifs (ITAM) of CD3 and the zeta chains are phosphorylated after binding of the MHCII, allowing further proteins of the SRC protein kinase family to attach and foster subsequent signaling mechanisms due to PLC activation. To induce complete T-cell activation, additional stimuli are required at co-receptors on the T-cell surface. These include, for example, CD28 or CD40L, which bind to B7 or CD40 of APC. Created with BioRender.com.

However, there is not only one type of T-cells. A naive T-cell can differentiate into different T-cell subtypes through activation with in part contradictory functions. Thus, cytotoxic T-cells kill cells infected with pathogens. On the other hand, regulatory T-cells (T_{Reg}) suppress the immune response of other lymphocytes, so that only diseased tissue is attacked in order to protect healthy tissue and prevent autoimmune reactions. The post-production of lymphocytes is also regulated by T_{Reg} cells (Reinherz et al. 1980). Moreover, T-helper cells, which are also known as T-effector cells have the opposite task (Bird et al. 1998; Zhu et al. 2010). As a result of their activation, T-helper cells begin to proliferate and regulate the immune response by releasing cytokines which influence the activity of further immune cells (Diehn et al. 2002; Fracchia et al. 2013). For a long-lasting memory of the reaction to a pathogen, T-memory cells remain in the organism even after infection. In vaccination against a specific pathogen, the T-memory cells play the central role, as they can store the reaction to the pathogen and initiate it again at any time (Tough and Sprent 1994).

1.6 T-cell activation as a mediator between innate and adaptive immune response

The first step of the antigen-binding induced signaling cascade is the activation of TCR-associated tyrosine SRC kinases. Src family kinases include nine members: Src, Yes, Fyn, Fgr, Lck, Hck, Blk, Lyn, and Frk which interact with many cellular cytosolic, nuclear and membrane proteins. Src kinases modify these proteins by phosphorylation of their tyrosine residues (Giusti et al. 2000; Katz et al. 2006). In the T-cell activation process the Scr family member Lck associates with the cytoplasmic tails of the CD4 co-receptors on T-cells (Barber et al. 1989; Thome et al. 1995). As soon as the TCR is engaged by the specific antigen, Lck acts to phosphorylate the intracellular chains of the CD3 and ζ-chains of the TCR complex, allowing another cytoplasmic tyrosine kinase called ZAP-70 to bind (**Figure 2**) (Thome et al. 1995). Lck then phosphorylates and activates ZAP-70, which in turn phosphorylates another molecule in the signaling cascade called LAT (short for Linker of activated T-cells), a transmembrane protein that serves as a docking site for a number of other proteins, including the membrane-bound phospholipase C (PLC) (Thome et al. 1995). The following intracellular signaling pathway is visualized in **Figure 3.**

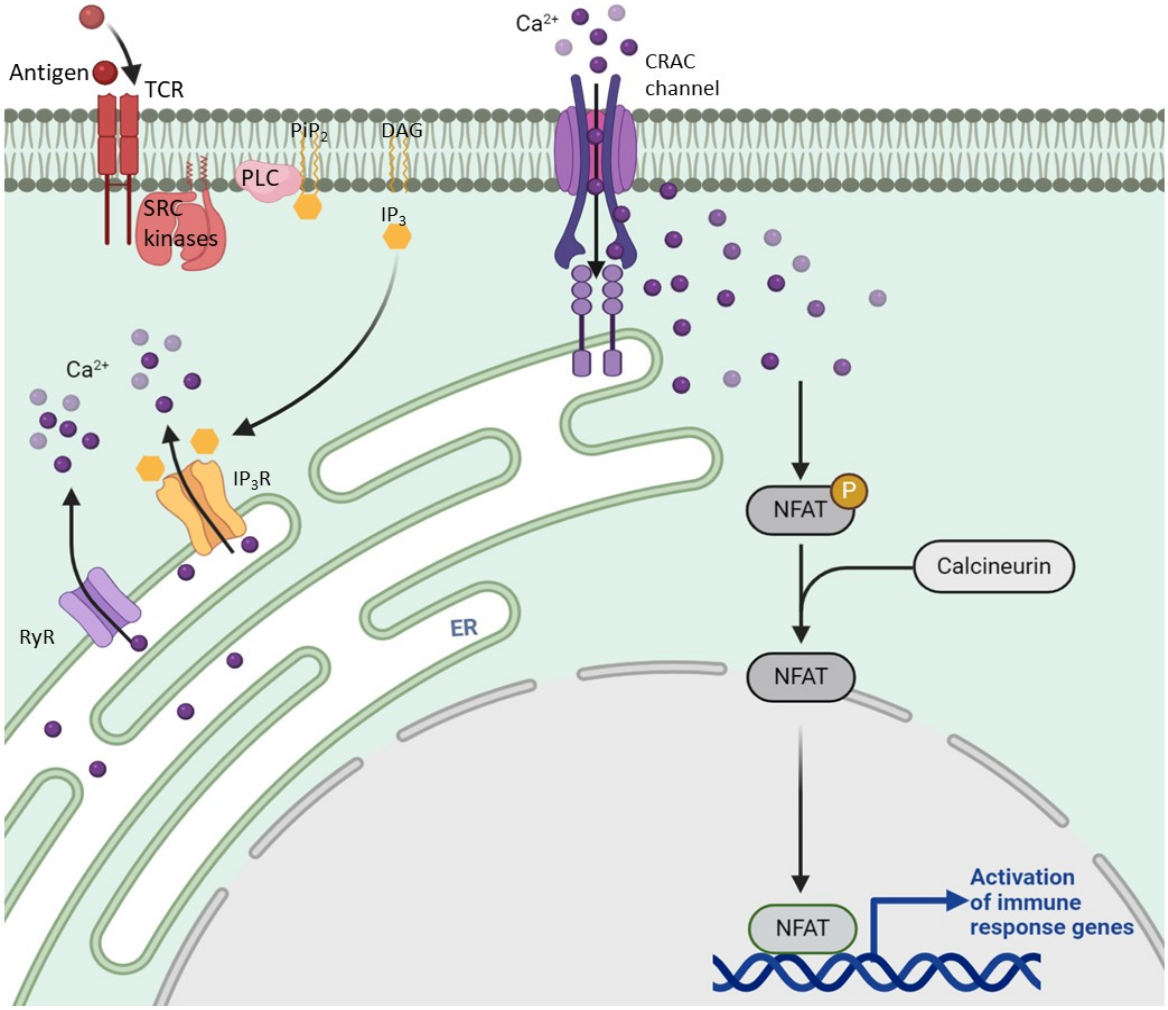

Figure 3: Schematic representation of the antigen-induced T-cell activation cascade. If a specific antigen binding to the T-cell receptor complex (TCR complex), as well as other specific stimuli at co-receptors occurs, a large number of receptor-associated protein kinases (SRC kinases) and adapter molecules are activated. Via phospholipase C (PLCγ), a calcium-dependent signal transduction cascade is initiated, which finally leads to the activation of the transcription factor nuclear factor of activated T-cells (NFAT) via calcineurin. When activated, this factor transmigrates into the nucleus, where it causes an altered transcription. Ca^{2+}_{cyt}: intracellular calcium concentration. Created with BioRender.com.

The activated PLC cleaves the phosphatidylinositol-4,5-bisphosphate (PIP_2), which is located in the plasma membrane into the two second messenger inositol-1,4,5-trisphosphate (IP_3) and diacylglycerol (DAG) (Mustelin et al. 1990; Mogami et al. 1997). As a consequence, IP_3 binds to its IP_3 receptor (IP_3R) in the membrane of the endoplasmic reticulum (ER) (Imboden and Stobo 1985; Lock et al. 2019). Since the ER acts as an intracellular calcium storage, calcium ions can now enter the cytosol along their concentration gradient via the IP_3 triggered open calcium permeant IP_3R. This increase in the cytosolic calcium concentration (Ca^{2+}_{cyt}) implies the activation of calcium- and calmodulin-dependent phosphatase calcineurin (Erondu and Kennedy 1985; Dolmetsch et al. 2001; Berchtold and Villalobo 2014). Meanwhile, the cytosol contains inactive transcription factors such as the nuclear-factor-of-activated T-cells (NFAT), which is highly phosphorylated in its inactive state (Beals et al. 1997; Cooling et al. 2009). The active calcineurin dephosphorylates NFAT, resulting in a translocation of NFAT from the cytoplasm into the nucleus, where it initiates the transcription of various target genes, which ultimately defines an immunologically active state of the T-cell (Diehn et al. 2002; Fracchia et al. 2013). The altered gene expression can now trigger a specific immune response, e.g. the activation of further immune cells mainly by secretion of pro-inflammatory proteins into the extracellular space (Amundson and Clapham 1993; Clapham 2007).

1.7 The role of the adaptive immune response in radio-immunotherapy

Recent studies suppose that immune cell activation by irradiation, which is a universal tool in medical diagnostics and therapy (Fisher et al. 1988; Armstrong and Minsky 1989; Schaue et al. 2012; Suzuki and Yamashita 2014) would provide the basis for an explanation of radiation hormesis, in which immune cells fight tumor tissue more effectively after low radiation doses (Nakamura et al. 1990; Abuodeh et al. 2016; Cuttler et al. 2017). Another well described effect playing a role in radiation therapy is the abscopal effect, which is defined as “response at a distance from the irradiated volume” by Mole in 1953. Hence, in clinical studies it could be observed that irradiation causes a reduction of tumor mass also in non-irradiated tumor parts such as metastases (R. Mole 1953; S. Demaria et al. 2005; Golden et al. 2013; Britschgi et al. 2018). However, it is supposed that radiation stimulates the immune system and this causes either tumor-specific immunity or immunogenic cell death (R. Mole 1953; S. Demaria et al. 2005; Golden et al. 2013; Britschgi et al. 2018). This could occur because radiation induced tumor cell death leads to the release of tumor antigens, which are able to stimulate APCs. Moreover, other publications showed, that IR comprises stimulatory activities on APC as their ability to capture tumor antigens is enhanced post exposure. This in turn is shown to promote APC-dependent antigen specific T-cell tumor suppression. Many studies have shown that in this scenario, dendritic cells, macrophages and eosinophils are recruited to provide T-cell activation to foster further immunological response. Despite the generally accepted paradigm that radio-treatment of cancer patients leads to consequences on immune surveillance of both; malignant and non-malignant cells (Cuttler et al. 2017), so far there exists no study that proving irradiation has no direct effect on T-lymphocytes. But if this is the case, new approaches for clinical applications for a type of "*in situ vaccination*" for radio-immunotherapy would emerge.

It is worth noting that in the present work the effect of ionizing radiation was investigated on Jurkat T-lymphocytes. This cell line belongs to the subtype of T-precursor cells with some characteristics of T-helper cells and have been used as a model cell line to characterize many signaling pathways in T-cells. In the further work, I will refer to T-cells or T-lymphocytes instead of T-helper cells for simplification.

2. Materials and Methods

2.1 Cell culture

Jurkat cells are a lymphoblastic precursor T-cell line, which were established in 1976 from the peripheral blood of a 14-year old boy with acute lymphatic leukemia. The Jurkat T-cells (ACC 282) were purchased from German Collection of Microorganisms and Cell Cultures (DSMZ, Braunschweig, Germany). They were gpaneln in RPMI 1640 medium with stable glutamine (2mM) and 2.0 g/L $NHCO_3$ (Thermo Fisher Scientifc, Waltham, MA, USA), supplemented with 10% heat inactivated fetal calf serum (FCS; PAA, Cölbe, Germany) and 50 U/ml penicillin and 5 µg/ml streptomycin (Sigma-Aldrich, Munich, Germany) at 37°C and 5% CO_2. They phenotypically gpanel in small botryoidal cluster as spherical suspension cells. Their doubling time is about 25-35 hours, with an optimal split ratio of 1:2-1:3 every two to four days with a preferable cell count of $3 \times 10^5 – 1 \times 10^6$.

Peripheral blood mononuclear cells (PBMCs) were taken from blood of healthy volunteers, and isolated from buffy coats using a biocoll-hypaque density-gradient centrifugation (Biocoll Separating Solution, Biochrom, Berlin, Germany) according to manufacturer's recommendations. Prior to assays they have been maintained in RPMI 1640 Medium with 10% FCS and 1 and 50 U/ml penicillin and 5 µg/ml streptomycin and stored at 37°C and 5% CO_2 as described previously for Jurkat cells.

2.2 X-ray irradiation

Cells were exposed to X-ray irradiation in T_{35} petri dishes using an Isovolt 160 Titan E source with a voltage of 90 kV and 33.7 mA (GE Sensing & Inspection Technologies, Alzenau, Germany), with a dose rate of 0.055 Gy/s. Doses were delivered with a source to sample distance of 30 cm with dishes placed on a 2 mm aluminum sheet.

2.3 Applied substances

Ionomycin (# ab120370, Abcam, Cambridge, UK), thapsigargin (Sigma-Aldrich, Taufkirchen, Germany) and the cell permeable Ca^{2+} sensor Fluo4 AM (Life Technologies, Carlsbad, CA, USA) were dissolved in DMSO and immediately added in external solution prior to experimental procedure in a final concentration of 5/2/1 µM respectively.

To activate human T-cells ImmunoCult™ Human CD3/CD28/CD2 T-Cell Activator (T-Act) (Stem cell Technologies, Vancouver, BC, Canada) was supplemented to the cell culture medium (25 µl/ml of cell suspension) and maintained at 37°C and 5% CO_2 for the indicated duration.

The cell permeable organelle trackers MitoTracker Red FM (#M7514), ER-Tracker Red (#E34250), CellMask Orange (#10045) and Hoechst 33342 (#H3570) were purchased from Thermo Fisher Scientifc and used according to the manufacturer's recommendations.

2.4 Confocal laser scanning microscopy

Confocal laser scanning microscopy was performed with a Leica TCS SP or SP5 II system (Leica microsystems, Mannheim, Germany) equipped with 40 × 1.30 oil UV (HCX PL APO), a 63 × 1.4 oil UV (HCX PL APO lambda blue) or 100 x 1.44 oil UV objective (HCX PL APO CS). The external buffer used for microscopy (MB) contained in mM: 140 NaCl, 4 KCl, 1 MgCl2, 5 Mannitol, 10 HEPES, 2 CaCl2, pH 7.4 with osmolarity of 310 mosmol/l.

For all microscopic recordings the custom-made setup of two metal rings and a cover slip as described in ***Figure 4*** was used. To prevent evaporation during long term recordings, this setup was sealed with laboratory grease and another coverslip.

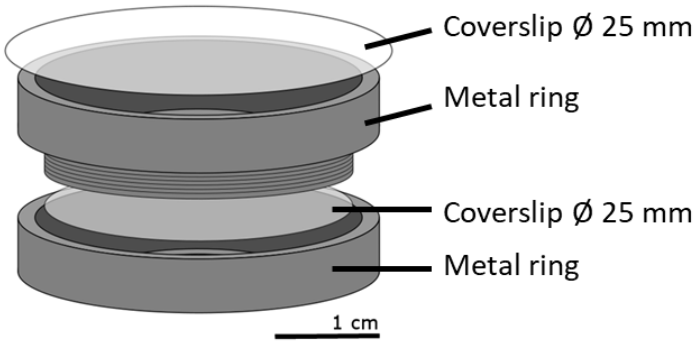

Figure 4: Schematic structure of the microscopy chamber. In order to perform long-term microscopy analyses cells are placed in this custom-made chamber. In detail, a lower metal ring, followed by a glass coverslip (Ø 25 mm) is screwed to an upper metal ring. This results in a volume capacity of about 1 ml. To avoid evaporation of the microscopy solution, the upper metal housing can be sealed with laboratory grease and a glass coverslip (Ø 45 mm).

2.5 Immunofluorescence staining

8-10 × 10^5 Jurkat cells/ml were treated with either 25 µl/ml CD3/ CD28/CD2 T-cell activator, 2 µM thapsigargin or irradiated with X-ray doses between 0.5 and 5 Gy. Afterwards, they were directly transferred to coated coverslips as described above. After 15, 30, 45, 60 or 90 min incubation at 37°C and 5% CO_2 cells were washed with PBS. Next, the cells were fixed for 30 min at room temperature (RT) in 4% paraformaldehyde (PFA) with 0.2% glutaraldehyde in PBS and permeabilized with 0.2% Triton X-100 solution. T-cells were washed in PBS and unspecific binding was blocked with 5% BSA in PBS for 30 min. Afterwards, cells were resuspended in PBS with primary antibodies for STIM1 (#PA1-46217, Thermo Fisher Scientific, Waltham, MA, USA), Orai1 (#NBP1-75523, Novus Biologicals, Waltham, MA, USA), NFATc2 (#MA1-025, Thermo Fisher Scientific) respectively. Antibodies were applied overnight at a 1:200 dilution overnight, at 4°C. Jurkat cells were subsequently washed with 0.05% Tween20 (in PBS) and incubated with anti-rabbit IgG Alexa488 secondary antibody (# A32731 anti-rabbit Alexa488 IgG, Thermo Fisher Scientific), anti-mouse IgG Alexa488 secondary antibody (# A32723 anti-mouse Alexa488 IgG, Thermo Fisher Scientific) or anti-mouse IgG Alexa647 secondary antibody (# A32728 anti-mouse Alexa647 IgG , Thermo Fisher Scientific) in a dilution of 1:2500 for 1 h at RT. Finally, stained cells were washed with 0.05% Tween20 (in PBS) and stored in PBS until microscopic analysis.

2.6 Live-cell imaging

For long-term measurements, to enable a gentle adhesion of the Jurkat cells to the glass coverslips (Ø 25 mm) the latter were prepared by cleaning in a plasma furnace (Zepto-B, Diener electronic GmbH, Ebhausen, Germany) and coated with one layer of PBS/5% BSA in a spincoater (PIN150, SPS Europe Spincoating, Putten, Netherlands) and a second layer of 0.01% poly-L-lysine (molecular weight 75–150 kDa).

2.6.1 Imaging of cytosolic calcium

The cell permeable Ca^{2+} sensor Fluo4 was loaded onto Jurkat cells by incubating cells on coated glass coverslips (Ø 25 mm) for 30 min in buffer containing 1 µM Fluo4 AM (Life technologies, Carlsbad, CA, USA). Coating was essential not only for the gentle adhesion, but also to prevent spontaneous Ca^{2+} oscillations, which usually occur when Jurkat cells are settling on glass coverslips (Fuck, 2017). The calcium dye was subsequently removed by washing cells with dye free microscopy buffer. Calcium signals were recorded in a time interval of 5 s for 60-240 min in total with an image resolution of 1024 x 1024 pixel and a scan speed of 400 Hz.

2.6.2 Transiently transfected constructs

Live cell imaging of Jurkat cells transiently transfected to express either HyPer, mitoHyper, syHyper or STIM1-eYFP/Orai1-eCFP or NFATc2-GFP using Lipofectamine 2000 (#11668027 Thermo Fisher Scientific) was performed as described previously (Kehlenbach et al. 1998) and with microscopy settings as described for Ca^{2+}-imaging.
The STIM1-eYFP/Orai1-eCFP plasmids used in this work were kindly provided by Donald Gill (Pennsylvania State University) and HyPer sensors as well as NFAT-GFP by Ralph Kehlenbach and Christine Gibhardt (University of Göttingen).

2.6.3 FRET analysis

FRET experiments with Jurkat cells, transiently coexpressing STIM1-eYFP/Orai1-eCFP, were examined with a Leica TCS SP5 II confocal microscope as described previously. Filter were set with CFP (458 Ex/460-490 Em), YFP (514 Ex/530-550 Em), and FRETraw (458 Ex/530-550 Em). Live-cell images were obtained every 30 s at room temperature with a 100 x 1.44 oil UV objective (HCX PL APO CS) for a time period of 30 min. Three-channel corrected FRET was calculated based on the following equation:

$$FRETc = Fraw - Fd/Dd \cdot FCFP - Fa/Da \cdot FYFP$$

where FRETc represents the corrected total amount of energy transfer; Fd/Dd is the measured bleed through of eCFP through YFP filter (0.473); Fa/Da represents measured bleed through of YFP through CFP filter (0.049). To reduce variations caused by differences in expression levels of CFP, the FRETc values were normalized to value of donor fluorescence (FCFP). To minimize the effect of variations of YFP expression levels on FCFP-normalized FRET signals (FRETN) and to show the relative changes as compared with resting levels, figures are shown as ΔFRETN/FRETNrest.

2.7 Determination of cell diameters

Jurkat cell diameters were measured with an EVE automatic cell counter (NanoEnTek, Seoul, South Korea). Therefore, a suitable protocol for Jurkats (cell diameter 6-18 µm) was established and all measurements were validated by visual inspection and corrected manually using the personal computer-based software EVE PC.LNK 1.0.3. Cell viability was determined by using trypan blue exclusion assay.

2.8 Taqman-Based Quantitative Real-Time PCR (qRT-PCR)

Jurkat cells and PBMCs were treated with either 25 µl/ml CD3/ CD28/CD2 T-cell activator or irradiated with X-ray doses of 1.25, 2 and 5 Gy. RNA was isolated 24 h post treatment using the NucleoSpin Kit (Macherey-Nagel, Dueren, Germany) in combination with the QiaShredder Kit (Qiagen, Hilden, Germany) according to the manufacturer's recommendations. Reverse transcription was performed with M-MLV reverse transcriptase (Promega, Mannheim, Germany) and random hexamers (Thermo Fisher Scientific). qRT-PCR was achieved with 20× Taqman Assays (Thermo Fisher Scientific) specific for IL2 (Assay ID: Hs00174114_m1) or IFNγ (Assay ID: Hs00989291_m1) with the StepOnePlus Real-Time PCR System (Thermo Fisher Scientific), ABsolute QPCR Mix, ROX (Thermo Fisher Scientific) and standard settings. Relative gene expression was calculated using the 2−ΔΔCt method relative to untreated controls with the housekeeping gene ribosomal protein L37A (RPL37A) as endogenous reference. The primer and probe sequences for RPL37A detection were as follows: RPL37A-fw 5'-TGTGGTTCCTGCATGAAGACA-3', RPL37A-rev 5'-GTGACAGCGGAAGTGGTATTGTAC-3', RPL37A probe: 5' FAM-TGGCTGGCG GTG CCT. GGA-3' TAMRA (Large et al. 2015), manufactured by Eurofins Genomics (Ebersberg, Germany).

2.9 CD25 detection by flow cytometry

Surface expression of CD3 and CD25 was analyzed either on Jurkat or PBL isolated by density gradient centrifugation as described previously. Cells were stained with fluorochrome-conjugated mAb targeting CD3 (CD3-PerCP-Cy5.5 clone SK7; Becton Dickinson, Heidelberg, Germany) and CD25 (BV510 Mouse anti human CD25 clone 2A3, Becton Dickinson) in a 1:1000 dilution for 60 min at RT. After a washing step with PBS stained cells were subjected to multicolor flow cytometry using a CytoFlexS cytometer (Beckman Coulter, Krefeld, Germany). Data acquisition and analysis were accomplished with CytExpert Version 1.2 software (Beckman Coulter).

2.10 Statistical Analysis

Data are expressed as means ± standard deviation (SD) or standard error (SE) of at least three independent experiments; number of biological replicates (n) or independent experiments (N) were denoted. Significance was estimated by using the Student's T-test in Microsoft Excel software. P values of <0.05 (*), <0.01 (**), and <0.001 (***) are indicated in the figures.

3. Results

The overall aim of the present study is to elucidate intracellular signaling mechanisms in T-lymphocytes triggered by X-ray irradiation for this investigation, five essential processes were analyzed that play a particularly important role in antigen-mediated T-cell activation. The schematic **Figure 5** illustrates the hypothesis that similar to physiological activation, irradiation can lead to 1. the increase of cytosolic ROS, 2. the generation of a CRAC channel-dependent Ca^{2+} signaling, 4. the translocation and consequently the activation of NFAT which finally leads to 5. immunological modulations and responses. The numbers shown in **Figure 5** are representative for the numbers of the chapters following in the result section.

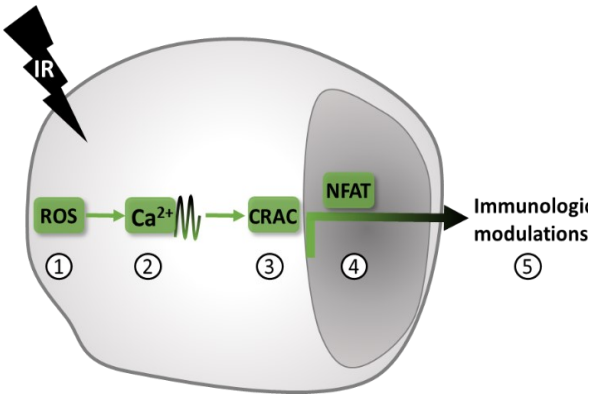

Figure 5: Graphical representation of key steps of a radiation-induced signal cascade in T-cells. X-ray triggers minutes after exposure an increase in the intracellular reactive species (ROS) concentration, which is followed by Ca^{2+}-release activated Ca^{2+} (CRAC) channels. As a consequence, the Ca^{2+}-dependent nuclear factor of activated T-cells (NFAT) becomes active and initiates immunological modulations like cell diameter increase and cytokine expression. Numbers of key steps also represent numbers of chapters in the present study.

3.1 Chapter 1 – IR induces cytosolic and mitochondrial H_2O_2

In this chapter, I designed the experiments for calibration of the H_2O_2 sensors HyPer, mitoHyPer, and syHyPer in Jurkat cells. I performed the corresponding measurements at a custom made set up for combined imaging and irradiation at the Helmholtzzentrum für Schwerionenforschung (GSI). Dr. Burkhardt Jakob provided support in the microscopical analysis and Timo Smit mainly performed experiments in the frame of a master thesis.

Abstract

It is generally accepted that ionizing radiation (IR) generates reactive oxygen species (ROS) within cells and that this is amplified by secondary effects mainly to the radiolysis of water. The key molecule in cellular ROS signaling mechanisms is hydrogen peroxide (H_2O_2). Under physiological conditions H_2O_2 is produced primarily in the mitochondria during metabolic processes. The small, diffusible molecule has a dual role in cells. At high concentrations it is toxic while it serves at low concentrations as an important second messenger within cells. As a consequence, the cell faith s depending on the intracellular H_2O_2 concentration and the redox capacity of the cells. In spite of its important function the impact of radiation on the H_2O_2 concentration in immune cells has not been sufficiently investigated. To better judge the impact of radiation therapy on this radical, the current study attempts to fil this knowledge gap.

By using high-resolution microscopy three genetically encoded, protein-based fluorescent H_2O_2 sensors HyPer, mitoHyPer, and syHyPer were used for life cell imaging in the T-lymphocyte model cell line Jurkat. After *in vivo* calibration of the sensors in cells a combined imaging/radiation setup at the GSI was employed for monitoring the intracellular or mitochondrial H_2O_2 level of living cells in real time after irradiation with a high temporal and spatial resolution. The data show that cells respond to X-ray irradiation with a fast (1-5 min) transient increase in the mitochondrial H_2O_2 concentration (in cells heterologous expressing mitoHyPer) concentration as well as a slower increase (4- 20 min) in the cytoplasmatic H_2O_2 concentration (in cells heterologous expressing HyPer). This effect is not attributed to a change of the intracellular pH, as indicated with the pH-sensitive sensor syHyPer. From the calibration of the senor it can be estimated that the H_2O_2 concentration increases in the cytosol from a low basal level of 20 nM to approximately 400 nM over, which is only slightly decreasing again within a period of 40 min in Jurkat cells exposed to 5 Gy X-ray. The fact that the lifetime of H_2O_2 is limited to only a few milliseconds but that X-ray triggered the transient increase in H_2O_2 in the cells lasts for several minutes means that the latter cannot be attributed to the direct effects of irradiation. It is much more likely that a process of ROS-induced ROS release (RIRR), which has been described in ROS signaling, is responsible for this phenomenon. From the sequence of events, in which mitochondrial H_2O_2 concentration is first increased after irradiation, it is possible that H_2O_2 spills over from the mitochondria into the cytosol where it triggers an RIRR cascade, which eventually evokes the increase of this molecule in the cytosol. Comparing the data to other recent published studies, the intracellular second messenger rise after X-ray exposure is associated with cell-activating processes such as proliferation or differentiation. Hence the data advocate a crucial role of H_2O_2 in radiation-induced T-cell activation processes.

3.1.1 Introduction

3.1.1.1 The influence of ionizing radiation on a molecular level

Ionizing radiation (IR) is a term for particles or electromagnetic energy that is able to remove electrons from atoms or molecules, resulting in a positively charged ion or molecule residue. This process is called ionization. One type of IR is X-ray, which can be described as an electromagnetic wave with quantum energies above 100 eV. This corresponds to wavelengths shorter than 10 nm, an energy range above ultraviolet light. X-rays are generated by a change in the velocity of charged particles and thus can be produced artificially in a special X-ray source. In this process, electrons are first emitted and accelerated from a cathode before hitting a metallic anode which strongly decelerates them. This energy release is called B*remsstrahlung* and is better known as X-rays. The resulting X-rays can further ionize atoms and molecules leading to secondary ionizing events. If biological material was irradiated, dose-dependent damage may occur which in response initiates a programmed cell death in the case that the damage is too high for an appropriate repair. This destructive function of X-rays is commonly used in cancer radio-therapy to eliminate malignant cells (Fisher et al. 1988; Armstrong and Minsky 1989; Hallahan et al. 1994; Trotti et al. 2000; Baskar et al. 2012).

When radiation impinges biological material the initial events of ionization are completed within fractions of a millisecond visualized in **Figure 6**. These events particularly include the production of reactive species, generally known as reactive oxygen species (ROS). ROS is a very broad term and includes different reactive species like hydroxyl radicals (OH·), ozone (O_3), singlet oxygen ($1O_2$) or superoxide anions (O^{2-}) (Lambeth 2004). They all vary in their reactivity, half-life time, site of production and detoxification reactions. Due to the high percentage of water in biological material, most of them originate from the radiolysis of water (Meesungnoen and Jay-Gerin 2009; Le Caër 2011; Roth and LaVerne 2011).Despite their common origin ROS can mainly be divided into two subgroups; either free radicals, containing an unpaired electron, or as a second subgroup non-radical oxidants, including hydrogen peroxide (H_2O_2) (Hempel and Trebak 2017). To get a detailed insight into the relation between ionizing irradiation and the resulting radicals, it is important to know that there are about 2000 ionizations per Gy of X-ray within one exposed cell (Mikkelsen and Wardman 2003). In addition, it has to be mentioned that ionization events generated by clinically relevant doses (0.1-5 Gy) are further amplified inside the cell. The primary events trigger cell responses in a so-called ROS-induced-ROS-release (RIRR) manner (Zorov et al. 2000; Zorov et al. 2006; Biary et al. 2011), which increases the ROS load of a cell and activates different downstream signaling cascades. In contrast to the short-lived ROS production from a direct irradiation, this RIRR processes could last for long-term periods up to minutes and in some cases even up to hours (Zorov et al. 2000; Gouspillou et al. 2015).

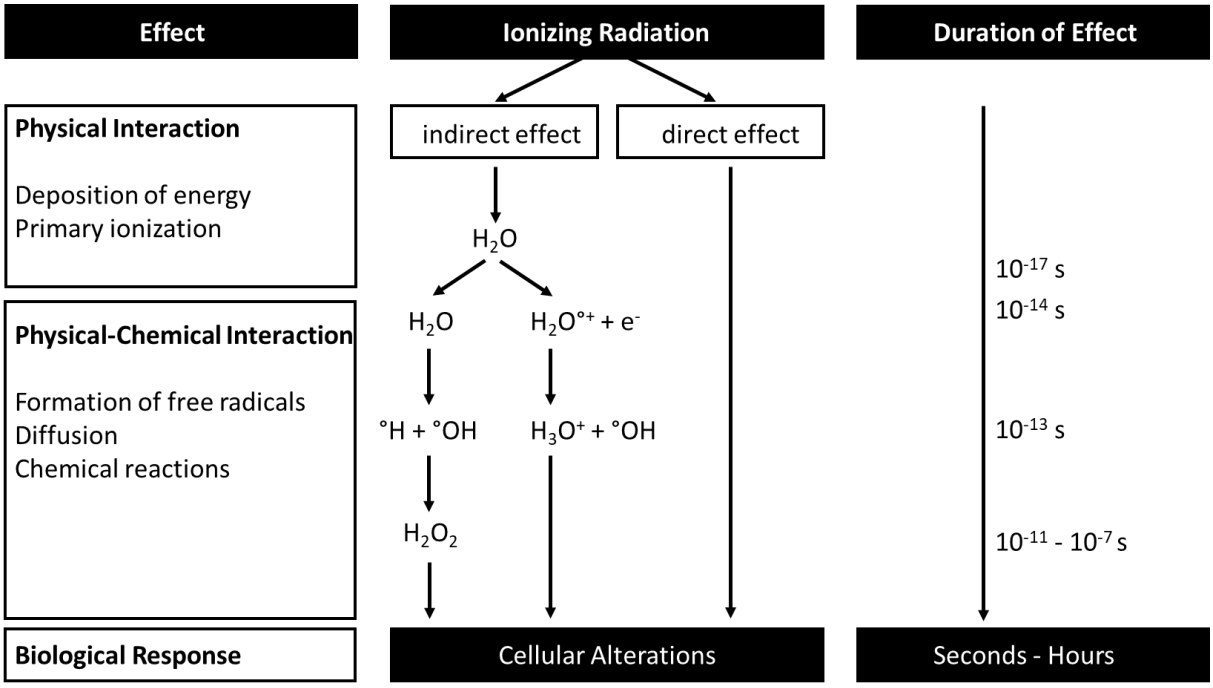

Figure 6: Timeline of early effects of ionizing radiation. First physical interactions of ionizing radiation (IR) within biological material occur within the first femtoseconds. This is followed by the physical-chemical stage, where the generated reactive oxygen species (ROS) further react and diffuse in an exposed cell. The generated ROS can cause cellular responses, which can last up to hours.

3.1.1.2 **Effectiveness of reactive oxygen species (ROS) on a cellular level**

In addition to the artificially generated ROS, they also occur naturally within all cells. Large ROS surges are also known as “oxidative stress”. They are primarily associated with widespread oxidation of macromolecules and irreversible cellular damage. Sublethal concentrations of ROS in contrast contribute to cellular redox signaling (Hempel and Trebak 2017). Externally applied ROS, e.g. as a result of radiation exposure as well as their intracellular generation in metabolic processes, are well known for their role in mediating both physiological and pathophysiological signal transduction (Saito et al. 2006; Driessens et al. 2009; Roth et al. 2015). In this context the process of inflammation is again an interesting mechanism. It is a protective response of multicellular organisms to recognize and localize, as well as to eliminate or remove harmful stimuli and to recover damaged tissues (Dantzer and Kelley 1989; Wilder 1995; Ozinsky et al. 2000). In this scenario ROS are crucial for the initiation and progression of the inflammatory response because of its action as a second messenger in numerous intracellular signaling cascades (Apostol et al. 1989; Schreck and Baeuerle 1991; Hallahan et al. 1994; Neuenschwander et al. 1995). The function of ROS can mainly be attributed to its influence on the posttranslational modification of proteins, where redox-sensitive cysteine residues are oxidized to form disulfide bonds (Chan et al. 1997; Buhrman et al. 2005; Yang et al. 2014). At the same time, there is clear evidence that overproduction of ROS may result in cell and tissue injury and contribute to chronic inflammation. This can be the reason for neurodegenerative, cardiovascular, and metabolic diseases, which are associated with an altered redox balance (Finkel 2003; Sies et al. 2017; Sies 2017). In addition, it was demonstrated that also cancer cells show an increase in cellular ROS because of an elevated metabolism (Szatrowski and Nathan 1991).

Understanding the role of ROS signaling in the regulation of metabolic activity, inflammatory activation, and diseases associated with metabolic dysfunction like Alzheimer (La Monte and Tong 2014) or Huntington's disease (Bpanelne et al. 1997) is important in our pursuit of novel therapies to treat these diseases.

3.1.1.3 **Sources of ROS generation within distinct cellular organelles**

Endogenous ROS are primarily generated as by-products of numerous enzymatic reactions or, as part of basal metabolic functions, in various cell compartments including the cytoplasm, cell membrane, endoplasmic reticulum (ER), mitochondria (Feinendegen 2002; Murphy 2009), and peroxisomes (Bedard and Krause 2007). In this whole orchestra, one enzyme retains a special role in immune cells: the nicotinamide adenine dinucleotide phosphate (NADPH) oxidase (short: NOX). The plasma membrane bound NOX catalyzes the production of superoxide free radicals by transferring one electron from NADPH to an oxygen (Lambeth 2004; Bedard and Krause 2007; Lee and Yang 2012; Cortés-Ríos et al. 2017; Daiber et al. 2017). This process is known to be relevant during infections in order to kill pathogens. It is suspected that superoxides have a direct damaging influence on pathogens by lipid peroxidation (Krishnamoorthy et al. 2012), although its underlying mechanism is not yet fully understood. Additionally, cytokines and gpanelth factors, which are secreted by activated immune cells, are able to induce NOX phosphorylation and consequently its activation. The fact that NOX are either modulated by intracellular metabolic processes or external stimuli turns it into an interesting target for immune therapy.

However, originally described as the "powerhouse of the cell", mitochondria have been long appreciated for their bioenergetic and biosynthetic properties within the cell. Since, it is becoming increasingly evident that mitochondria also play an essential role in other signaling pathways. Through their production of mitochondrial ROS (mROS), mitochondria are the major source of ROS within a cell (Murphy 2009). It is well known that mitochondria generate oxygen radicals (O_2·) from the reduction of oxygen as a byproduct of oxidative phosphorylation during the respiratory chain for ATP synthesis (Murphy 2009; Dröse and Brandt 2012). In context of the latter, the O_2· generated by the electron transport chain complexes I and II located in the mitochondrial matrix is rapidly converted into H_2O_2 by the mitochondrial superoxide dismutase 2 (SOD2) (Fridovich 1997). In opposite to that O_2· produced by complex III in the intermembrane space is able to travel through voltage-dependent anion channels (VDACs) through the outer mitochondrial membrane and subsequently into the cytosol, where it can be converted into H_2O_2 by cytosolic SOD1 (Kim et al. 2005a; Kil et al. 2012). Once H_2O_2 has arrived in the cytoplasm, it can cause the oxidation of various targets and contribute to the generation of secondary ROS within the cell interior, causing RIRR.

3.1.1.4 **H_2O_2 – a second messenger with contradictory cellular functionality**

The key molecule in cellular ROS signaling mechanisms is H_2O_2 (Burdon and Rice-Evans 1989; Hallahan et al. 1994; Neuenschwander et al. 1995; Kim et al. 2005b; Saito et al. 2006; Jiang et al. 2011; Enyedi and Niethammer 2013; Zorov et al. 2014). Since H_2O_2 is not a radical, it is more stable and able to persist for up to 1 millisecond in a cell (Reth 2002). In addition, it can diffuse to some extend until reacting with other molecules (Mishina et al. 2013). The nonpolar second messenger H_2O_2 is not only

able to diffuse within the cell but also across biological membranes. Bienert and colleagues (2007) were able to show that H_2O_2 can enter cells from the extracellular medium via aquaporins (Bienert et al. 2007; Bienert and Chaumont 2014). In spite of its membrane permeability there is a H_2O_2 concentration gradient across the membrane which is as high as 1:200- 1:500 (Ermakova et al. 2014b).

In the last decades it was recognized that H_2O_2 has not only damaging effects but acts at low concentration as a second messenger. The cellular signaling pathways on which H_2O_2 has an impact are illustrated in **Figure 7**. They vary significantly, from initiation of proliferation at low 1- ~100 nM (Burdon and Rice-Evans 1989; Sies 2017; Sies et al. 2017) to apoptosis at high >1 µM intracellular H_2O_2 concentrations (Szatrowski and Nathan 1991; Dumont et al. 1999; Hiniker et al. 2012). It must be mentioned that information and concentration may vary depending on the cell type and their different redox sensitivities. Hence, depending on the cell function, different cell types have specific levels of basal ROS and specific thresholds for certain cell processes. In addition, the occurrence and the amount of antioxidants play a major role in the redox sensitivity of a certain cell type (Iñarrea et al. 2007; Rodemann and Blaese 2007; Kil et al. 2012).

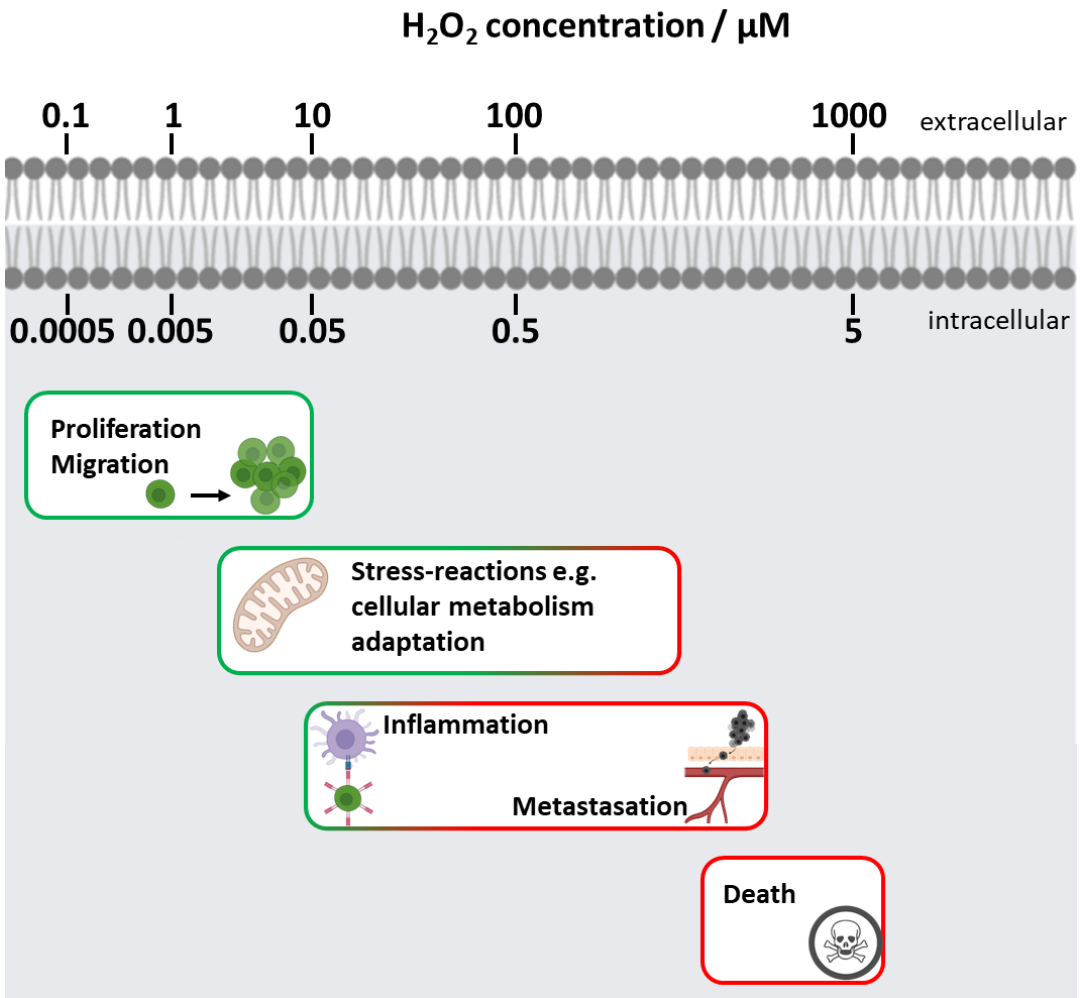

Figure 7: The functional role of H_2O_2 in cells varies depending on its concentration. External addition of H_2O_2 is able to diffuse into the cell with a concentration drop by a factor of approximately 200 across the plasma membrane. Positive H_2O_2 triggered effects on the cellular/ organismic survival are marked in green, negative effects in red. Taken from Sies, 2017, modified according to Gibhardt *et al.*, 2015, created with BioRender.com..

3.1.1.5 **The role of mitochondrial ROS in T-cell activation**

Notably, mitochondria are dynamic and motile organelles that move within a cell depending where they are needed the most for cellular signaling mechanisms (Frederick and Shaw 2007; Al-Mehdi et al. 2012). The property of cellular mobilization has also been observed within T-cell activation. Before any activation processes, naïve T-cells exist in a quiescent, catabolic state and after TCR stimulation they have to switch into an anabolic state to support synthesis of macromolecules. These macromolecules are needed for the cell's proliferation and cytokine expression in order to fulfill their assignments in the adaptive immune response (Weinberg et al. 2015). This switch to anabolism requires an increase in glycolysis, as well as in mitochondrial metabolism, which are both in the need for an appropriate adenosintriphosphate (ATP) and reduced Nicotinamide adenine dinucleotide phosphate ($NADPH/H^+$) production (Carr et al. 2010; Gomes et al. 2013). Besides the fact that mitochondria are essential for biosynthetic properties, they also contribute to T-cell activation through their production of mROS (Brand et al. 1984; Zorov et al. 2006; Gomes et al. 2013; Zorov et al. 2014). Additionally, in the Jurkat T-cell line, mitochondria were found to translocate to the immunological synapse. At the synaptical side their production of H_2O_2 is required for an appropriate TCR signal transduction and following T-cell activation and proliferation (Mustelin et al. 1990; Smith-Garvin et al. 2009; Smeets et al. 2012; Fracchia et al. 2013). Here, the initial phase of activation-triggered proliferation of naïve T-cells is intimately associated with an increase in mitochondrial mass, mitochondrial DNA (mtDNA) content, and oxidative phosphorylation (Darzynkiewicz et al. 1981; Ogura et al. 2009; Carr et al. 2010). Although mtDNA encodes proteins that are components of the mitochondrial electron transport chain (Ogura et al. 2009), damage to mtDNA results in increased production of ROS, conversely causing neurodegenerative diseases and various types of cancer (Browne et al. 1997; La Monte and Tong 2014; Tomita et al. 2019).

3.1.1.6 **Buffering of the cellular ROS concentration by ROS scavenger and antioxidants**

Because of the multiple functions of ROS in general and H_2O_2 in particular, it is important for cellular survival and signaling to precisely regulate their intracellular concentrations. For this reason, cells have developed several mechanisms to counteract oxidative stress. The most important mechanisms for redox regulation are ROS scavengers and antioxidants, which play a major role in the homeostasis of the oxidative molecules. In this scenario it is important that the reaction of these scavengers and buffers with ROS molecules is reversible, which is a necessary feature of sustainable cellular signaling. Enzymes such as superoxide dismutase (SOD) (Halliwell 1974), catalase or glutathione peroxidase (Foyer and Halliwell 1976) actively reduce ROS, while antioxidant proteins such as glutathione buffer ROS (Chaudière and Ferrari-Iliou 1999; Trachootham et al. 2008). There are also natural and synthetic chemical molecules that prevent oxidative stress, such as vitamin C, N-acetylcysteine (NAC), and Dithiothreitol (DTT). A healthy cell attempts to balance ROS production and its degradation leading to a chemical equilibrium (Trachootham et al. 2008) to either quickly initiate signal cascades or reduce harmful ROS concentrations.

3.1.1.7 **The early beginnings of ROS detection within immune cells**

In the mid-1980s initial observations of antioxidants which were added to T-lymphocytes inhibited both; TCR-induced transcription of cytokines and the proliferation of the cells, suggesting a regulatory role of ROS in T-cell (Passwell et al. 1982). Later, TCR-triggered ROS production was demonstrated activation (Mori et al. 2004a; Mori et al. 2005; Nambiar et al. 2011; Li et al. 2015; Patwardhan et al. 2015; Tavassolifar et al. 2020). Many studies have shown that a transient generation of low physiologically relevant levels of ROS, i.e., a hydrogen peroxide-mediated oxidative signal, facilitates the activation of oxidation-dependent transcription factors like NFAT, NFKB and AP-1 in immune cells (Nakamura et al. 1990; Jackson et al. 2004; Feinendegen 2005; Dagoglu et al. 2019). But, from an experimental point of view, it was difficult to measure ROS immediately after a stimulus, e.g. exposition of cells to X-rays. Because of its very short life-time, ROS production was mostly indirectly measured in the time frame of minutes to hours after oxidative stress (Narayanan et al. 1997; Shaposhnikova et al. 2007; Hafer et al. 2008; Gouspillou et al. 2015). Due to its ability to diffuse within the cell, traverse biological membranes, and a comparably long half-life it has been suggested that H_2O_2 may be a suitable second messenger and major contributor to redox signaling within cells.

3.1.1.8 **New perspectives with the genetically encoded, fluorescence-based H_2O_2 sensor: HyPer**

To enable a time resolved high-resolution microscopic analysis of the intracellular concentration of the relatively long-persisting ROS, H_2O_2 was thought to be a suitable target. In 2006 Belousov et al. constructed for the first time a genetically encoded, fluorescence-based H_2O_2 sensor: HyPer (Belousov et al. 2006). This sensor enables a precise ratiometric, reversible and highly sensitive analysis of generated H_2O_2 already during irradiation exposure (Belousov et al. 2006; Bilan et al. 2013; Mishina et al. 2013; Ermakova et al. 2014a). Furthermore, in contrast to previous methods, the dynamical switch of the sensor is no longer the limiting factor, which allows measurements with a high temporal and special resolution. The ROS sensor incorporates a permutated YFP and the well characterized regulatory domain of OxyR, a transcription factor of E. coli (Choi et al. 2001). Binding of H_2O_2 to OxyR within the HyPer protein leads to the formation of a disulfide bridge between Cys199 and Cys208. This results in an increased fluorescence intensity for the oxidized state at an excitation wavelength of 488 nm and a decreased fluorescence intensity for its reduced state upon an excitation wavelength of 405 nm. Because of this antagonistic change in fluorescence intensities for the two different excitation wavelengths the corresponding ratio of the fluorescence 488 nm/405 nm can be used as a measure of the H_2O_2 concentration. The ratio increases upon oxidation of HyPer with bound H_2O_2 and decreases as a result of reduction. In the present study I used this genetically encoded sensor to detect H_2O_2 immediately before, during and after exposing Jurkat T-cells to X-ray. One additional advantage of this reporter protein is that it can be selectively sorted into cellular subcompartments via specific targeting sequences. One shortcoming of the HyPer sensor is that it reacts also to changes in pH (Belousov et al. 2006; Bilan et al. 2013; Roth et al. 2015). To discriminate between changes in H_2O_2 and pH the scientists also created a pH sensitive, but H_2O_2 insensitive variant of HyPer (syHyPer). A third variant of the sensor which is sorted into the mitochondria in order to investigate the possible generation of H_2O_2 in these ROS generating organelles was developed, designated mitoHyPer. Thus, it is possible to obtain a better understanding not only of the ROS kinetics, but also of their origin within the cells. In addition, the

sensors can be transiently expressed in different cell types, allowing comparisons to be made for different cell and tissue types which is important due to the discriminative redox capacity in different cells.

3.1.1.9 **Important connections to previous studies with HyPer based experiments**

In previous studies data from the above-mentioned sensors indicated that IR induced biological reactions are not only dependent on the primary ROS which are generated as a direct result of X-ray exposure (Roth et al. 2015; Huang et al. 2017). Moreover, an RIRR mechanism lasting several hours post irradiation in A549 cells was observed (Ogura et al. 2009). Hence, it is thought that the most probable source of these secondary produced ROS are mitochondria where ROS are amplified (Gill and Levine 2013; Kamiński et al. 2013; Diebold and Chandel 2016). Moreover, Gibhardt (2014) demonstrated that the ratiometric HyPer signal remained stable over 120 min in resting A549 lung cells. External addition of 30 µM H_2O_2 elicited a dramatic increase in the 488 nm/405 nm ratio indicating a rise in cytosolic H_2O_2 concentration. This experiment confirms that the HyPer sensor is functional and that it is possible for the externally applied H_2O_2 to enter the cell. In addition, Gibhardt performed an *in vivo* calibration of HyPer using external H_2O_2 concentrations from 10 to 500 µM. This resulted in a K_{ox} value of 31.3 µM. In the same experiments it was also reported that irradiation of A549 and HEK293 cells with either 1, 5 or 10 Gy X-rays elicited rapid, transient burst of H_2O_2 concentration immediately after exposure to X-ray irradiation.

To examine if the same cellular reaction occurs in Jurkat cells, Fuck (2017) used this experimental setup for the just named T-lymphocytes. In these experiments he found that Jurkat cells reacted unlike the aforementioned cells in a variable manner to X-ray irradiation with 1 or 10 Gy. In some cells the HyPer signal remained unaffected by irradiation while others exhibited a small increase in the 488 nm/405 nm ratio. The results of these experiments suggest that Jurkat cells react with respect to a H_2O_2 production differently to X-ray irradiation than other cells. However, since the HyPer signal was not specifically calibrated for Jurkat cells, Fuck could not exclude that the fluorescent sensor has a different sensitivity to H_2O_2 in the T-lymphocytes.

3.1.2 Results

The aim of the present chapter is to elucidate potential Jurkat cell-specific H_2O_2 signaling events as a cellular response to ionizing radiation and to compare these reactions to those observed in other cell lines used by Gibhardt (2014) and Fuck (2017). Therefore, I performed live-cell measurements with a high temporal and spatial resolution using the H_2O_2 sensor HyPer. Because of its ratiometric properties it is possible to monitor exact changes of the intracellular H_2O_2 concentration. In order to quantify the concentration of this second messenger, it is crucial to calibrate the HyPer sensor in the cell line in which the experiment is performed. This is relevant since different cell lines may have different redox buffer capacities with the effect that a rise in H_2O_2 concentration could be high (low buffer capacity) or low (high buffer capacity) in response to the same stimulus.

3.1.2.1 *In vivo* calibration of the HyPer sensor

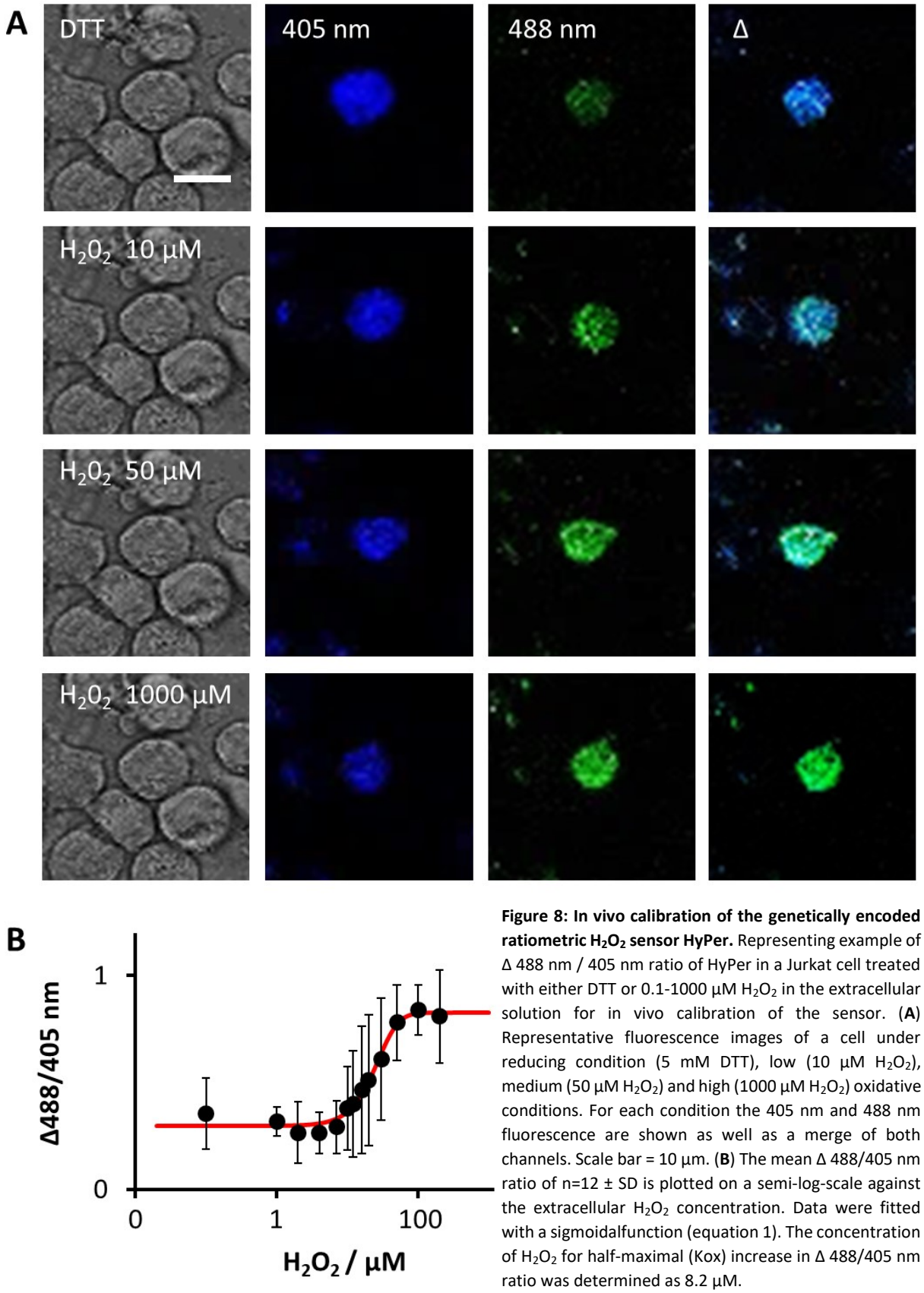

Figure 8: In vivo calibration of the genetically encoded ratiometric H_2O_2 sensor HyPer. Representing example of Δ 488 nm / 405 nm ratio of HyPer in a Jurkat cell treated with either DTT or 0.1-1000 µM H_2O_2 in the extracellular solution for in vivo calibration of the sensor. (**A**) Representative fluorescence images of a cell under reducing condition (5 mM DTT), low (10 µM H_2O_2), medium (50 µM H_2O_2) and high (1000 µM H_2O_2) oxidative conditions. For each condition the 405 nm and 488 nm fluorescence are shown as well as a merge of both channels. Scale bar = 10 µm. (**B**) The mean Δ 488/405 nm ratio of n=12 ± SD is plotted on a semi-log-scale against the extracellular H_2O_2 concentration. Data were fitted with a sigmoidalfunction (equation 1). The concentration of H_2O_2 for half-maximal (Kox) increase in Δ 488/405 nm ratio was determined as 8.2 µM.

Jurkat cells were transfected with the HyPer plasmid to identify the properties of the genetically encoded, fluorescence-based H_2O_2 sensor in these T-lymphocytes. **Figure 8A** shows that HyPer is homogeneously distributed within the cell; the basal 488 nm/405 nm ratio is low with 0.25 ± 0.07. In a next step the Jurkat cells were challenged with different concentrations of H_2O_2 in the extracellular buffer over a range from 0.1 to 1000 µM for calibration. Representative images of a single cell under reducing conditions (5 mM DTT), slight oxidative (1 µM H_2O_2), medium oxidative (50 µM H_2O_2) and high oxidative conditions (1000 µM H_2O_2) are illustrated in **Figure 8A**. The data show that a rise in extracellular H_2O_2 causes a concomitant increase in the 488 nm/405 nm ratio. The resulting mean ratio from 12 independent experiments is plotted as calibration curve on a logarithmic scale in **Figure 8B**. The curve indicates that the fluorescent ratio 488 nm/405 nm of the HyPer sensor changes with a saturating kinetic as a function of the extracellular H_2O_2 concentration. The curve can be fitted with a sigmoidal function (**Equation 1**).

$$f(x) = \Delta r_{min} + [\frac{(\Delta r_{max} - \Delta r_{min})}{(1 + \left(\frac{x}{K_{Ox}}\right)^{n})}$$

Equation 1

Here Δr_{min} and Δr_{max} represent the minimal and maximal change in 488 nm/405 nm ratio of HyPer fluorescence respectively. Fitting of the data yields a value of 8.2 µM for the half-maximal (K_{ox}) increase in 488 nm/405 nm ratio as a function of H_2O_2 concentration.

Gibhardt (2015) performed the same kind of experiments in A549 cells and reported a K_{ox} value of 31.3 µM. This value is also in the range of micromolar concentrations but higher than the estimated K_{ox} value of 8.2 µM for Jurkat cells. From these experiments we can conclude that the HyPer sensor behaves in Jurkat cells not fundamentally different than in other cells. However, the affinity of the sensor seems to be about 4 times higher in Jurkat cells compared to A549 cells. The finding that the affinity of the sensor varies in different types of cells is possible since *in vitro* calibrations of HyPer by Belousov *et al.* (2006) demonstrate a dynamic range of between a K_{ox} value ranging from 25 nM up to 250 nM. This deviation between *in vitro* and *in vivo* calibrations implies that the cellular environment can have an impact on the sensor performance.

One additional factor which influences sensor calibration in cells is related to the membrane permeability of H_2O_2. Several studies have shown a 200-500-time difference in the internal to external H_2O_2 concentration (Bilan et al. 2013). The discrepancy between the *in vivo* and *in vitro* calibration is explained by the fact that the plasma membrane acts as a diffusion barrier for H_2O_2. If this is taken into account in the calculation of the intracellular H_2O_2 concentration, it is in the range of approximately 20-400 nM before the HyPer sensor saturates, which in turn fits well with *in vitro* measurements.

3.1.2.2 **IR induces a long-lasting increase in cellular H_2O_2**

After the calibration of the H_2O_2 sensor I measured the immediate generation of H_2O_2 in Jurkat cells expressing the HyPer sensor after exposing the cells to 5 Gy X-ray. The dynamics of intracellular H_2O_2 changes were measured in Jurkat cells with a high temporal and spatial resolution over a period of 30 min. These experiments were possible thanks to a special experimental setup at the Helmholtzzentrum für Schwerionenforschung (GSI) which allows fluorescence imaging of living cells simultaneously to X-ray irradiation. For this purpose, an X-ray chamber is directly coupled to a fluorescence microscope. With this setup I measured the fluorescence emission intensity of both, excitation wavelength 405 and 488 nm. The 488 nm/405 nm fluorescence ratio was calculated and further normalized to its highest value. These values were then plotted as a function of time, where the time point of irradiation with 5 Gy X-ray is indicated by a black arpanel. It occurred that Jurkat cells responded in a variable manner to IR as an external stimulus. Based on this variability, the cellular responses can be divided into three different categories. Cells responding with a: i. low basal H_2O_2 level and a slow H_2O_2 increase (**Figure 9A**) ii. low basal H_2O_2 level and a fast H_2O_2 increase (**Figure 9B**) and iii. marginal to no change in the cellular H_2O_2 concentration (**Figure 9C**) after irradiation. The majority of monitored cell reactions could be assigned to category i. (5 out of 11) with a rather slow rise in H_2O_2. The remaining second half of the examined cells behaved as described in category ii. with fast kinetics (3 out of 11), or did not react at all (category iii., 3 out of 11). The results of these experiments underscore that the absence of a HyPer signal in Jurkat cells following X-ray irradiation is unlikely related to an altered sensitivity of the H_2O_2 sensor in the T-Lymphocytes. The data suggest different populations of Jurkat cells, which exhibit different responses to the radiation stress. The reason for the variability of individual cells in the radiation triggered H_2O_2 production remains unknown.

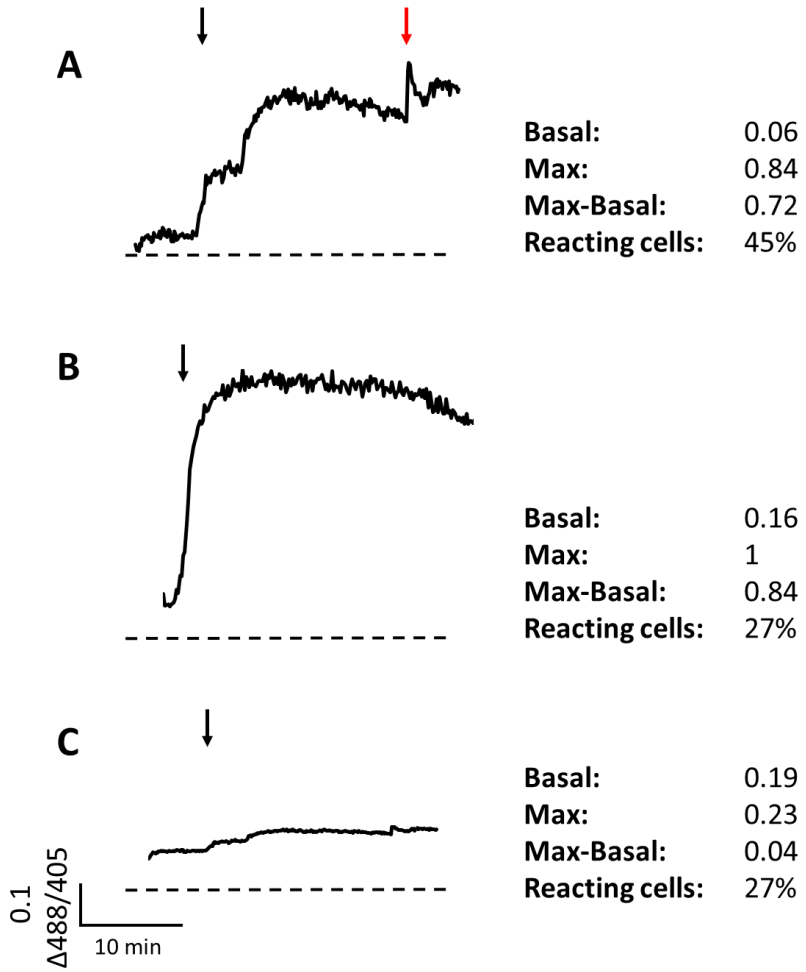

Figure 9: X-ray irradiation elicits various phonotypes with respect to H_2O_2 generation in Jurkat T-cells. Three exemplary Jurkat cells transiently expressing the H_2O_2 sensor HyPer were irradiated with 5 Gy X-ray and the fluorescence intensity was monitored with a confocal microscope. The Δ 488/405 nm ratio is shown as a black line. The basal value (Δ0) is shown as a dotted line. The exposure of the cells to X-ray irradiation is indicated by a black arrow and the time point of addition of 1 mM H_2O_2 for a maximal increase in the cytosolic H_2O_2 with a red arrow. The variable phenotypes of reactions could be divided in three categories: (**A**) low basal H_2O_2 level and a slow H_2O_2 increase (phenotype i), (**B**) low basal H_2O_2 level and rapid H_2O_2 increase (phenotype ii) and (**C**) no significant H_2O_2 elevation post irradiation (phenotype iii). For each measurement the value for the basal and the maximal Δ 488/405 nm ratio as well as the increase from basal to peak value (Max-Basal) is indicated.

In the following experiments I focused on cells, which exhibited a category i. type response (**Figure 9A**). In the example shown in **Figure 9A** the H_2O_2 signal reached a maximum at approximately 9 min post X-ray exposure before it slightly started to decrease. But, even 20 minutes after irradiation the H_2O_2 level remained at a very high value. Further addition of externally applied 1 mM H_2O_2 (red arpanel) again evoked an increase in the HyPer signal to a new maximum confirming that the sensor was still reactive and was not in saturation before.

The result of this experiment shows that 5 Gy X-ray elicits a long-lasting rise in the cytosolic H_2O_2 concentration. In 9 out of 17 cells the 488 nm/405 nm ratio exhibits an excursion over a range of 0.43 ± 0.21. Based on the HyPer calibration curve this mean rise of the sensor signal is comparable to that obtained by adding 50-200 µM H_2O_2 to the external solution. If we consider that the real cytosolic concentration is 200 times lower than the external concentration (Gibhardt 2015) the real peak value of cytosolic H_2O_2 after irradiation with 5 Gy X-ray translates into a concentration of 400 nM. This further indicates that IR is able to trigger a slow progressing, medium high and long-lasting H_2O_2 response in a population of Jurkat cells. With this general message the results of the present study are in agreement with the measurements reported by Fuck (2017). Important to note is that the generated H_2O_2 signal remains elevated over a period of several minutes bevor it decreases. This finding is surprising since

H_2O_2 has only a short half-life of less than one millisecond. Hence, it must be assumed that IR does not directly induce all of the monitored ROS. It seems more likely that an initial rise in ROS elicits a cellular reaction in which ROS is gradually evolving via a RIRR or even a calcium-induced-calcium-release (CIRR) mechanism; these secondary effects could be the main source for the prolonged H_2O_2 signals.

3.1.2.3 **IR induced H_2O_2 elevation is pH independent**

It has been mentioned that HyPer is also pH dependent (Markvicheva et al. 2011; Mishina et al. 2013). Hence, the X-ray induced excursions of the HyPer signal are not necessarily caused exclusively by H_2O_2. To test whether the IR induced effect on HyPer is the result of a change in H_2O_2 concentration and not the pH, the pH sensitive but H_2O_2 insensitive syHyPer was implemented in the present set-up. It was calibrated in the same way as the HyPer sensor (**Figure 8**). In **Figure 10A** the syHyPer calibration curve is shown, where syHyPer expressing cells were treated with extracellular H_2O_2 concentrations ranging from 0.1 to 1000 µM. Again, the monitored 488 nm/405 nm fluorescence ratio is plotted as a function of the H_2O_2 concentrations. As in the experiments reported in **Figure 10**, syHyPer expressing cells were irradiated and analyzed at the special setup at the GSI. In contrast to the measurements with HyPer, the fluorescence signal reacts very homogeneous within the tested Jurkat cells. Unlike the HyPer calibration curve, there is no concentration-dependent change in the 488 nm/405 nm ratio. Seven out of eight cells show no appreciable change in the 488 nm/405 nm ratio. The ratio remains constant around a value of 0.54 over the measured period. A representative measurement in **Figure 10B** illustrates the response of a single cell to X-ray exposure. One out of the eight measured cells showed random fluctuations in the syHyPer fluorescence intensity and was therefore neglected. Two conclusions can be drawn from these results: The HyPer measurements visualize the redox status of H_2O_2 within the cells. Additionally, no change in the intracellular pH value occurs upon irradiation.

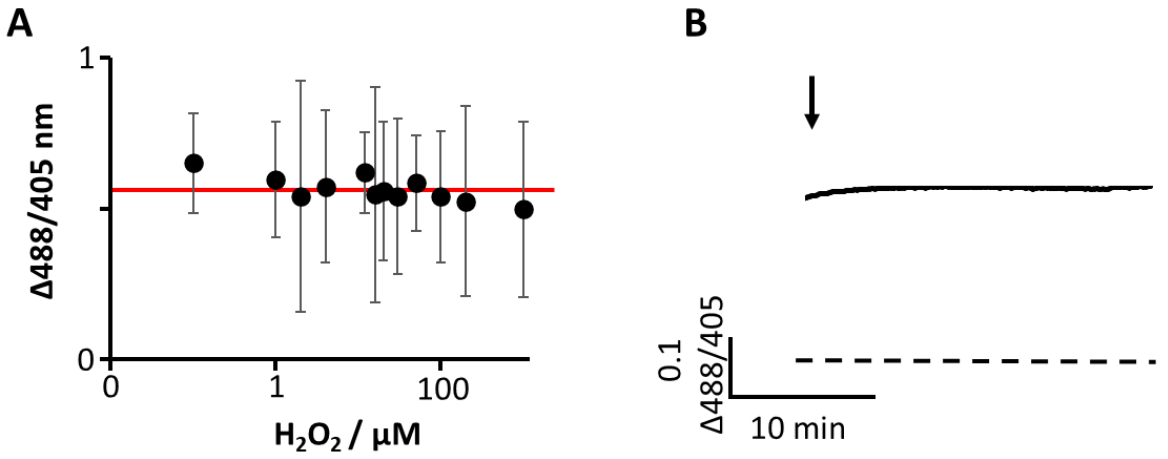

Figure 10: *In vivo* calibration of the genetically encoded ratiometric H_2O_2 insensitive, but pH sensitive sensor syHyPer. syHyPer expressing Jurkat cells were challenged with 0.1-1000 µM H_2O_2 in the extracellular solution for *in vivo* calibration of the sensor and analyzed by confocal microscopy. (**A**) The mean Δ 488 nm/405 nm ratio of n=8 ± SD is plotted on a semi-log-scale as a function of extracellular H_2O_2 concentrations. The data were fitted with a linear function. The Δ 488 nm/405 nm ratio of the calibration curve of syHyPer *in vivo* shows no H_2O_2 concentration dependency. (**B**) A representative recording of a single syHyPer expressing cell irradiated with 5 Gy X-ray (time of X-ray irradiation is indicated by a black arpanel). The Δ 488 nm/405 nm ratio of the syHyPer protein remained stable over 30 min of recording, indicating that no pH changes occur after irradiation

One question remains unsolved: Which process causes a long-lasting H_2O_2 signal within the irradiated cells? To tackle this question, I want to examine the possibility of RIRR mechanisms as a source of the long lasting H_2O_2 signal. It is reasonable to assume that such a mechanism is caused by the largest H_2O_2 producer of a cell: the mitochondria. To answer the question whether these organelles are involved in the sustained generation of H_2O_2 post irradiation, I monitored the effects of X-ray irradiation on H_2O_2 production in mitochondria (**Figure 12**).

3.1.2.4 *In vivo* calibration of mitoHyPer with externally applied H_2O_2

To examine whether the mitochondria are initiators of cellular H_2O_2 production after irradiation, I repeated the same experiments as in **Figure 8** for calibration of the mitoHyPer signal in the mitochondria of Jurkat cells. To my knowledge this sensor has previously not been tested in the lymphocytic cell lines. In a first assay the cellular localization of the genetically encoded, fluorescence-based H_2O_2 sensor mitoHyPer was examined in Jurkat cells. Cells transiently expressing mitoHyPer were therefore additionally stained with the established fluorescence mitochondrial marker mitoTracker red (Minamikawa et al. 1999). With this combination it was possible to monitor potential fluorescence colocalization.

Figure 11A shows representative images of Jurkat cells, which expressed mitoHyPer and were stained with the fluorescent mitoTracker dye. The distinct colocalization of both fluorescence signals confirm that the H_2O_2 sensor is indeed targeted into the mitochondria.

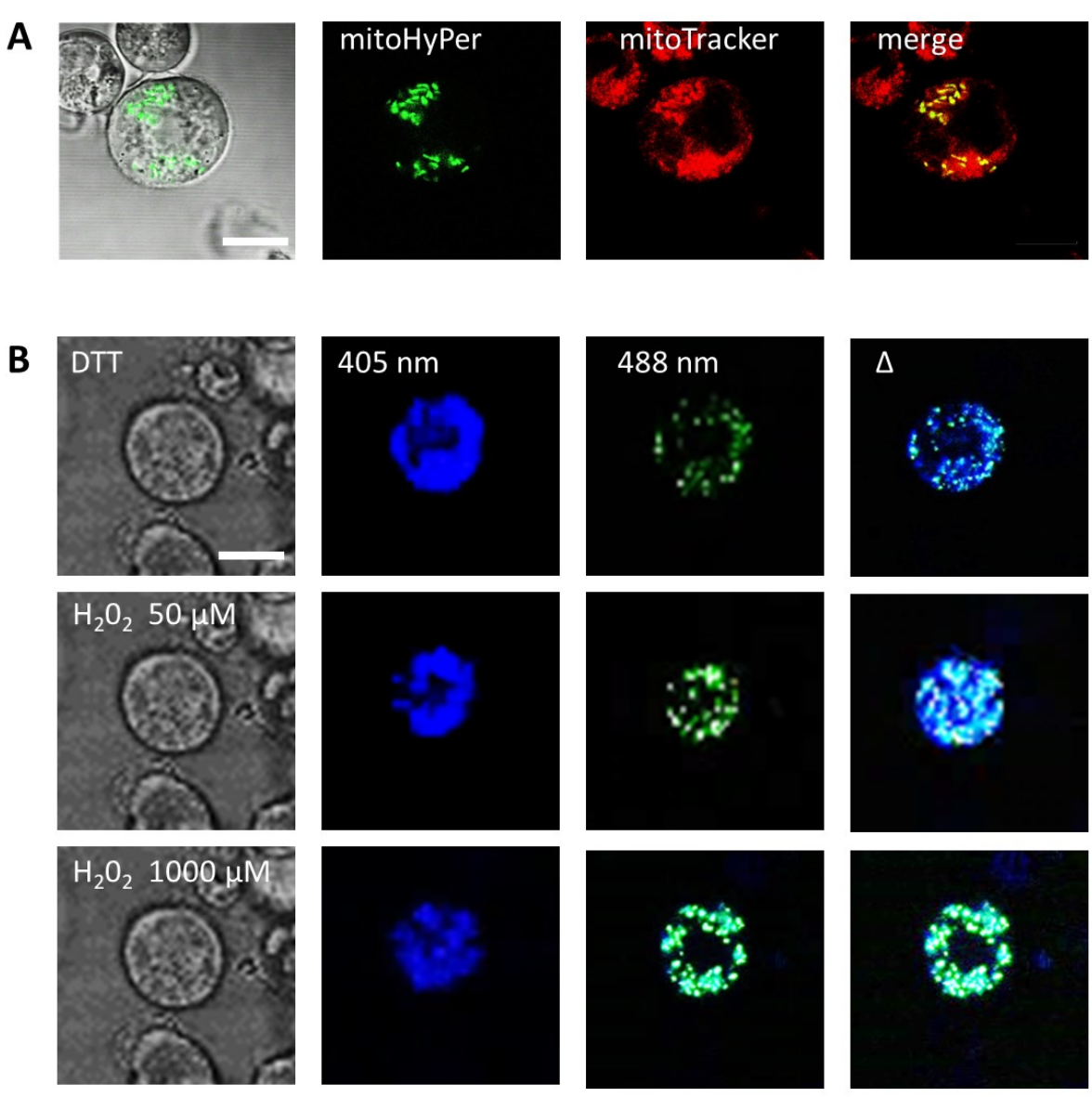
A
mitoHyPer
mitoTracker
merge
B
DTT
405 nm
488 nm
Δ
H2O2 50 µM
H2O2 1000 µM
C
Δ488/405 nm
1
0
0
1
100
H2O2 / µM

Figure 11: *In vivo* calibration of the genetically encoded mitochondrial and ratiometric H_2O_2 sensor mitoHyPer. Represantative example of Δ 488 nm/405 nm ratios of mitoHyPer in Jurkat cell treated with either DTT or 0.1-1000 µM H_2O_2 in the extracellular solution for *in vivo* calibration of the sensor. (**A**) Representative confocal images show live cell images of mitoHyPer (green) and mitoTracker red (red) as well as their merged images. The images confirm mitochondrial localization of the mitoHyPer sensor (scale bar = 10 µm). (**B**) Representative fluorescence images of a cell under reducing conditions (5 mM DTT), medium (50 µM H_2O_2) and high (1000 µM H_2O_2) oxidative conditions. For each condition the 405 nm and 488 nm fluorescence is shown as well as a merge of both. Scale bar = 10 µm. (**C**) The mean Δ 488/405 nm ratio of n=12 ± SD is plotted on a semi-log-scale versus the extracellular H_2O_2 concentration. The data were fitted with a sigmoidal function (equation 1). The concentration of H_2O_2 for half-maximal (K_{ox}) increase of the Δ 488 nm/405 nm ratio was determined as 24 µM. The Δ 488 nm/405 nm ratio of the calibration curve of mitoHyPer *in vivo* shows a H_2O_2 concentration dependency.

In the following step, mitoHyPer was calibrated in the same manner as the cytoplasmic HyPer variant. Therefore, H_2O_2 was externally applied in a concentration range of 0.1-1000 µM, assuming that the membrane permeant H_2O_2 reaches also the mitochondria.

Figure 11B again shows representative microscopic images of a single cell under reduced conditions (DTT), medium oxidative (50 µM H_2O_2) and high oxidative conditions (1000 µM H_2O_2). A comparison between measurements with the cytosolic HyPer and mitoHyPer show that both sensors exhibit a similar sensitivity to the external H_2O_2. In the latter, the calibration curve is slightly flatter. The large SD values obtained with mitoHyPer indicate that the measurements of mitochondrial H_2O_2 are more variable than that within the cytosol. Since both calibration curves exhibit the same shape, the mitoHyPer data can also be fitted with a sigmoidal function (**Equation 1**). This yields a K_{ox} value of 24 µM, which is in the same range of the K_{ox} determined for the cellular HyPer. In summary, this value also fits to the published data of Gibhardt and *the in vitro* measurements of Bilan *et al*. For this reason, I concluded that mitoHyPer is also functional in Jurkat cells.

3.1.2.5 **IR induces a rapid, transient increase in mitochondrial H_2O_2**

After successful *in vivo* calibration of the mitoHyPer H_2O_2 sensor I measured the generated H_2O_2 concentration in the Jurkats mitochondria after 30 min of 5 Gy X-ray exposure. In this experimental setting I observed again different cell populations, which can be distinguished by their H_2O_2 kinetics after irradiation. In this sense the response of the mitochondria is similar to that of the cytosol. There are three different categories of cellular response: i. cells with a high basal mitochondrial H_2O_2 level a small, but rapid increase (**Figure 12A**), ii. cells with a low basal H_2O_2 level in the mitochondria and a rapid increase that was quickly buffered to the pre-irradiation level (**Figure 12B**) and iii. cells with a marginal to no change in mitochondrial H_2O_2 concentration upon irradiation (**Figure 12C**). From a total of 25 cells analyzed, twelve, six, and seven cells can be classified into the categories i., ii. and iii., respectively.

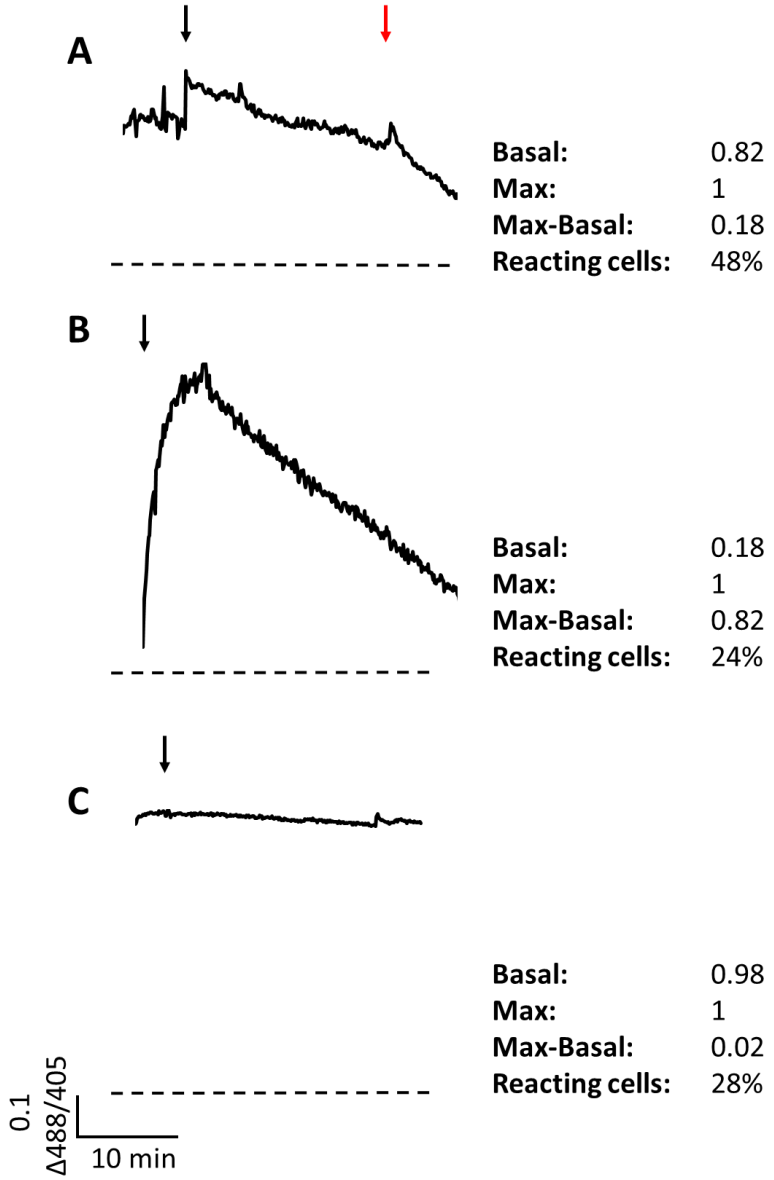

Figure 12: X-ray irradiation elicits variable phenotypes of changes in the mitochondrial H_2O_2 concentration of Jurkat T-cells. Three exemplary Jurkat cells transiently expressing the H_2O_2 sensor mitoHyPer were irradiated with 5 Gy X-ray and the fluorescence intensity was monitored with a confocal microscope. The Δ 488 nm/405 nm ratio is shown in black and the baseline level (Δ0) is indicated by a dotted line. The time of X-ray exposure is indicated by a black arrow and the time of addition of 1 mM H_2O_2 for a maximal increase in the cytosolic H_2O_2 with a red arrow. The variable phenotypes of the H_2O_2 response are divided in three categories: (**A**) high basal H_2O_2 level and a slight but fast H_2O_2 increase (Phenotype i), (**B**) low basal H_2O_2 level and rapid H_2O_2 burst (Phenotype ii) and (**C**) no significant H_2O_2 elevation post irradiation (Phenotype iii). For each measurement, the value for the basal and the maximal Δ 488 nm/405 nm ratio as well as the increase from basal to peak value (Max-Basal) are indicated.

In the following analysis, I focus on measurements which belong to category i, since it is the largest monitored subpopulation. In this case, IR triggered an immediate but small increase in the level of H_2O_2 **(Figure 12A**) which superimposed with the high basal H_2O_2 level of the mitochondria. Approximately < 1 min post X-ray exposure the H_2O_2 signal reached its maximal value before it rapidly decreased back to the pre-irradiation level. Different from the cytosolic H_2O_2 signal, the initially increased mitoHyPer signal recovered completely and dropped 20 minutes post-irradiation even below its basal level. Further addition of externally applied 1 mM H_2O_2 (indicated by a red arpanel) evoked only a small increase in the mitoHyPer signal. It can be concluded that the external application of a high H_2O_2 concentration (1 mM) triggers a less pronounced increase in mitochondrial H_2O_2 than irradiation. This suggests that the mitochondrial membrane represents an additional barrier to externally added H_2O_2, which allows less of the second messenger to travel into the mitochondria than into the cytosol.

Analysis of the experiments shows that the mean mitochondrial 488 nm/405 nm ratio increased by 0.1 ± 0.06 after 5 Gy of X-ray irradiation. Based on the calibration curve for mitoHyPer this increase corresponds to the addition of 10-100 µM H_2O_2 to the external solution. Considering that the mitochondrial concentration is 200 times lower than the external concentration the real peak value of mitochondrial H_2O_2 after irradiation with 5 Gy X-ray will be at approximately 250 nM. Since the mitochondrial membrane presents an additional barrier for the diffusion of externally applied H_2O_2, the exact conversion factor may be underestimated.

In summary, the results of these experiments show that irradiation of Jurkat cells with X-ray has an effect not only on the cytosolic but also on the mitochondrial H_2O_2 concentration in about 70% of the monitored cells. For this reason, I analyzed in the follow-up chapter the causal relationships between mitochondrial and cytosolic H_2O_2.

3.1.2.6 The mitochondrial and cytosolic responses in H_2O_2 level post IR show comparable patterns but different kinetics

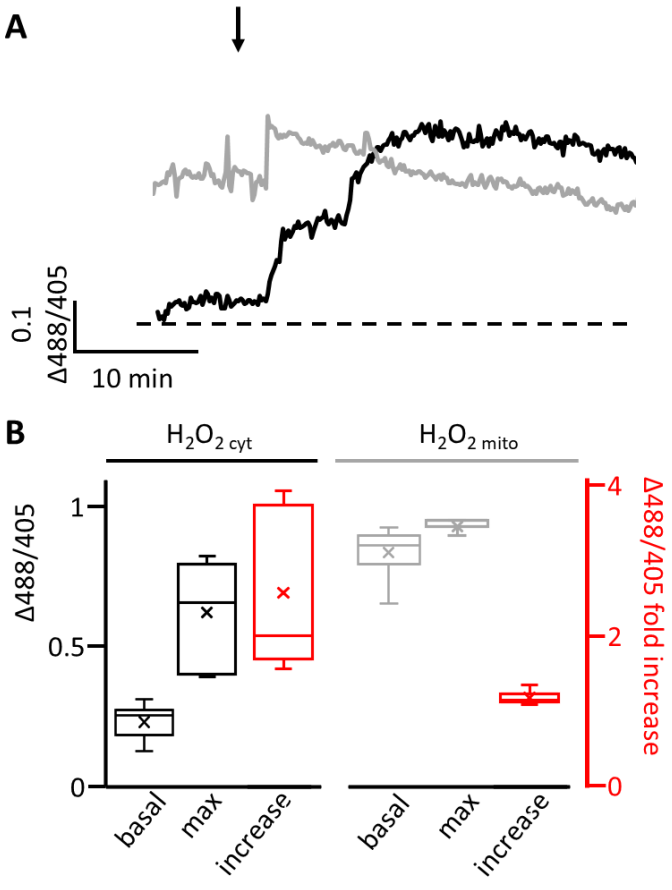

Figure 13: Mean changes of the H_2O_2 concentration in the predominant phenotypes of X-ray responses in the cytosol and mitochondria. Jurkat cells transiently expressing either HyPer or mitoHyPer were irradiated with 5 Gy X-ray and the fluorescence intensity was monitored with a confocal microscope. (**A**) The Δ 488 nm/405 nm ratio of a representative HyPer signal (black) and mitoHyper (gray) reveal different response kinetics in mitochondrial and cytosolic H_2O_2 generation and buffering. The exposure time is indicated by a black arpanel. (**B**) The mean Δ 488 nm/405 ratio for the calculated basal and maximal value and the resulting basal to maximum ratio increase is different for HyPer (n=9) or mitoHyPer (n=25) expressing Jurkat cells. The data reveals that the basal H_2O_2 concentration in the mitochondria is generally higher than in the cytosol.

In **Figure 13A** the two representative live-cell measurements of cytosolic (black) and mitochondrial (grey) H_2O_2 concentrations are plotted together. From the comparison of the two signals it can be concluded that the H_2O_2 concentration-changes in the mitochondria and cytosol respectively differ in their kinetics in response to X-ray irradiation. The amplitude of increase of the cytosolic H_2O_2 level is much higher than in the mitochondria. Additionally, the former rises slowly while the latter changes abruptly with a small amplitude (**Figure 13A)**. The data allows the suggestion that the buffer capacity for H_2O_2 in the cytosol and mitochondria also differs. While the small increase of H_2O_2 concentration in the mitochondria is quickly buffered, the increase in the cytosol returns slowly over approximately 20 min back and even beyond the basal level. Moreover, the data imply that the resting H_2O_2 concentration in the organelles (0.88 ± 0.08) is approximately 3.5 times higher than in the cytosol (0.25 ± 0.07) (**Figure 13B)**. It is consistent with the literature, since the mitochondria generate H_2O_2 as a byproduct in the cell metabolism and therefore have a higher basal oxidative level. However, for an exact indication of the H_2O_2 concentrations, there are so far only relative values of mitochondrial and cytoplasmatic H_2O_2 concentrations or mathematical models that predict the concentration. Depending on the study basal mitochondrial H_2O_2 level ranges from 2-400 nM (Treberg et al. 2015; Stein et al. 2020), and on the contrary the cytoplasmic H_2O_2 concentration, is supposed to be <0.5 nM, which results in a difference of 4-400 fold lower, according to published data (Ng et al. 2007; Sies 2017). Exposing cells with 5 Gy X-ray causes a large (2.4 ± 0.9) increase in cytosolic and a small 1.1 ± 0.08 fold increase in mitochondrial H_2O_2 concentration (**Figure 13A)**. The process of cytoplasmic H_2O_2 increase is rather slow; in 7 cells it requires on average 13 ± 8.7 min for the HyPer sensor to reach a maximal value. The mitochondria respond much faster to X-ray irradiation than the cytosol. In the organelles H_2O_2 reaches already within 2.3 ± 1.4 min after irradiation a peak value.

3.1.3 Conclusion

The results of the present study can be well linked to previous gained knowledge about IR induced H_2O_2 increase observed by Gibhardt (2014), and Fuck (2017). The special aspect of my performed experiments is that they provide information about the generating and buffering dynamics of H_2O_2 in the mitochondria as well as in the whole cytosol as a response of Jurkat cells to IR. The first interesting result is an increase in H_2O_2 concentration within the mitochondria and cytosol, lasting for several minutes. Since H_2O_2 has a short life time of less than one millisecond (Reth 2002) it can be concluded that the elevated H_2O_2 concentration is not a primary effect of IR, but H_2O_2 is generated by the cells as a consequence of radiation exposure. Indeed, the present data are not yet able to provide conclusive evidence for a functional interplay of H_2O_2 signaling between mitochondria and cytosol. Only the temporal dynamics of the H_2O_2 response in the two compartments advocates the following scenario: Irradiation of Jurkat cells with 5 Gy X-rays causes a rapid response of the mitochondria (2.3 ± 1.4 min), with the effect that the H_2O_2 concentration in the organelles increases by several fold. While this peak in H_2O_2 concentration is rapidly cleared in these organelles, it may nonetheless serve as a trigger for a RIRR mechanism, which allows a H_2O_2 influx into the cytosol. The consequent ongoing development of secondary ROS in the cytosol causing a slightly delayed (13 ± 8.7 min), but long-lasting rise of ROS. Notably, *in vitro* experiments with naïve human T-cells and Jurkat cells gained the knowledge that TCR-induced oxidative signals peak in a period between 30 to 120 minutes after activation (Kamiński et al. 2013). This implies that the cytosolic H_2O_2 increase is in a similar time frame as after physiological TCR stimulation. Further, it is possible that the generated H_2O_2 acts as a second messenger similar to its function in TCR activation mechanisms to promote different cellular processes like proliferation or expression of T-cell activation marker e.g. cytokines (Dumont et al. 1999; Reth 2002). This assumption is based on the intracellular H_2O_2 concentration of 400 nM, which fits well to the concentration range known for the mentioned processes (Sies et al. 2017; Sies 2017). While this scenario is still speculative, it is interesting to note that cells reacted very heterogeneously to X-ray irradiation with three distinct patterns of H_2O_2 responses in cytosol and mitochondria. The finding that three different categories of responses with a similar frequency occur in both compartments, underlines a signaling interplay between the two divisions.

3.1.4 Perspectives

The function of mitochondria during T-lymphocyte activation is not limited to the generation of ROS-based second messengers. The simple cation Ca^{2+} is also an essential second messenger, ruling over cell proliferation or cell death. Importantly, the subcellular locations of Ca^{2+} stores and ROS production are in close distance, prominently at the ER-mitochondrial interface and the plasma membrane (Jiang et al. 2011; Guse and Wolf 2016; Phillips and Voeltz 2016; Tafani et al. 2016; Zhang et al. 2019). Therefore, it can be assumed that sublethal changes in both ROS and Ca^{2+} levels fine-tune the cell's signaling cascades. Mitochondria are able to rapidly buffer an increased calcium concentration, so they consequently play an important role in the calcium homeostasis and signaling. For this reason, mitochondria are often found in the proximity of the ER and plasma membrane after stimulation of the TCR, which allows them to ensure an efficient exchange between ROS and calcium in the required organelles. Furthermore, T-cell activation-induced mitochondrial Ca^{2+} uptake stimulates mitochondrial function, e.g. by activating enzymes of the Krebs cycle (Guerini et al. 2005). The expression in turn leads to a positive feedback loop of signal initiation. Additionally, the ER acts as an intracellular calcium storage, whereas the ERs primary purpose is the proper folding of proteins (Braakman et al. 1992; Tu et al. 2000; van Anken and Braakman 2005). Protein folding is highly dependent on posttranslational oxidative modification of e.g. cysteine thiols and subsequent disulfide bond formation (Braakman et al. 1992; Tu et al. 2000). In these processes, the ER provides a more oxidative environment than the cytoplasm and contributes to the production of H_2O_2, as a consequence of the protein folding machinery (Ameziane-El-Hassani et al. 2005; Gross et al. 2006).

In addition, it is demonstrated that an elevation of the Ca^{2+} level in the cytosol via ER-membrane-located calcium conducting IP_3R increases H_2O_2 at the ER-mitochondrial interface (Adam-Vizi and Starkov 2010; Mazars et al. 2010; Decrock et al. 2013; Kamiński et al. 2013; Görlach et al. 2015; Diebold and Chandel 2016; Daiber et al. 2017), resulting in a positive redox feedback on IP_3R activation and consequently a Ca^{2+} influx and H_2O_2 generation. Furthermore, several publications showed an even more complex H_2O_2 interaction between mitochondria, ER and the PM (Khodorov et al. 1999; Cahalan and Chandy 2009; Kam and Banati 2013; Diebold and Chandel 2016). One example is that different PM-bound Ca^{2+} channels like the transient receptor potential (TRP) (Hecquet et al. 2008) or CRAC channels are activated by externally applied H_2O_2 channels (Cahalan 2009; Bogeski and Niemeyer 2014; Simeoni and Bogeski 2015b; Bhardwaj et al. 2016). These findings underscore the complexity of the cellular ROS/ Ca^{2+} signaling network, where Ca^{2+}_{cyt} can not only influence ROS production but also ROS can influence Ca^{2+}_{cyt} concentration. These processes are generally known as ROS-induced-calcium-release (RICR) or calcium-induced-ROS-release (CIRR), respectively. Due to the complex crosstalk of the two second messengers, the next chapter focuses on the investigation of Ca^{2+}_{cyt} levels as a response to irradiation.

3.2 Chapter 2 – IR induces delayed calcium oscillations

Some results in this chapter (**Figure 19**, **Figure 21**) were already published in Voos P, Fuck S, Weipert F, Babel L, Tandl D, Meckel T, Hehlgans S, Fournier C, Moroni A, Rödel F and Thiel G (2018). Ionizing Radiation Induces Morphological Changes and Immunological Modulation of Jurkat Cells. Front. Immunol. 9:922. doi: 10.3389/fimmu.2018.00922

Abstract

Calcium ions (Ca^{2+}) serve as a ubiquitous second messenger in cells and play a key role in the regulation of numerous cellular processes. To orchestra various signaling pathways, cells possess a highly sensitive mechanism, which regulates the intracellular calcium concentration (Ca^{2+}_{cyt}). It is well established that already a minor increase in Ca^{2+}_{cyt} is essential for the mediation of diverse cell functions such as cell activation, proliferation, differentiation, muscle contraction, cytokine production, and also cell death. One major question in the field of calcium signaling is, how can a simple ion control such a broad spectrum of cellular processes?

One phenomenon, which provides a partial answer to this question is that calcium responses can be organized in the form of oscillatory patterns which offer a large spatial and temporal diversity. Different from a continuous increase in Ca^{2+}_{cyt} these oscillations contain additional signal information in the form of signal amplitude and frequency. These distinct parameters can be "decoding" by specific receptor proteins for an interpretation in cell signaling. STIMulus induced Ca^{2+}_{cyt} oscillations are particularly important for T-lymphocyte activation. It is well established that antigens' binding to the T-cell receptor (TCR) induces calcium oscillations with a defined pattern eventually leading to cytokine expression and, consequently immunological response of the stimulated cell.

In the present chapter live-cell microscopy and time-lapse analysis were used to monitor the Ca^{2+}_{cyt} response of Jurkat cells to X-ray irradiation. The data demonstrate that IR can also trigger Ca^{2+}_{cyt} oscillations in Jurkat T-cells comparable to those evoked by physiological activation. The major population of Jurkat cells showed dose-dependent, but frequency (~3 mHz) independent calcium oscillations which started with dose-independent, but very heterogenous delay time of 10 to 80 min post irradiation. The Ca^{2+}_{cyt} response could be prevented by the addition of 1.) 10 mM ROS scavenger N-acetylcysteine (NAC) and 5 mM reductant dithiothreitol (DTT), 2.) 5 mM calcium chelator ethylene glycol-bis(β-aminoethyl ether)-N,N,N',N'-tetraacetic acid (EGTA) and 3.) 5 µM broad calcium channel blocker gadolinium (Gd^{3+}). These results support a model according to which IR induced calcium oscillations are mediated by ROS require an influx of Ca^{2+} via calcium channels in the plasma membrane.

3.2.1 Introduction

3.2.1.1 The intracellular signaling paradox of calcium: combining specificity with universality

A multitude of hormones, neurotransmitters, paracrine, autocrine, and physical stimuli are constantly bombarding the PM of cells (Kahn 1976; Exton 1996). In case that surface receptors for appropriate stimuli are expressed, binding of the agonist elicits a specific cellular response. Many of these external signals alter cell behavior by generating second messengers, which are small and diffusible molecules activating intracellular effectors (Raucher et al. 2000; van BLITTERSWIJK et al. 2003). The latter than trigger distinct intracellular signaling cascades. In this context calcium is one of the most essential and versatile second messenger (Carafoli 1974, 1982; Berridge et al. 2000; Berridge et al. 2003). In addition, not only chemical agonists but also physical cues from the environment like temperature and mechanical stress can result in the activation of Ca^{2+} signals (Hughes-Fulford 2004; Katz et al. 2006). The cytosolic concentration of free Ca^{2+} in resting cells is with about 100 nM very low so that already a small increase in this concentration is essential for the mediation of diverse cell functions. This includes for instance the release of neurotransmitters and hormones by exocytosis, cell differentiation and proliferation, activation of transcription factors, and modification of cellular proteins. Calcium responses also play an important role in physiological processes such as fertilization, muscle contraction and synaptic signal transmission (Amundson and Clapham 1993; Bading et al. 1993; Buxbaum et al. 1998; Clapham 2007; Smedler and Uhlén 2014). In most cases Ca^{2+} mediated signaling involves only short-lasting elevations in the concentration of this second messenger. Specific Ca^{2+} transporters and Ca^{2+} binding proteins are part of a homeostatic system, which brings the Ca^{2+} concentration back to the resting level. In the case of sustained periods of increased Ca^{2+}, cells can undergo apoptosis (Clapham 2007; Fulda et al. 2010). It is remarkable that a simple ion like Ca^{2+} is able to induce such a huge orchestra in cellular responses, which are in some cases even antagonistic. The complexity of Ca^{2+} triggered signaling in cells has fostered for more than 40 years the fundamental question: “how is it possible that so many different stimuli can be mediated by the same second messenger but still generate specific cellular responses? To give an answer to this question, it is necessary to understand the mechanism of calcium homeostasis. Therefore, **Figure 14** illustrates the key players in the regulation of the intracellular calcium concentration in non-excitable cells.

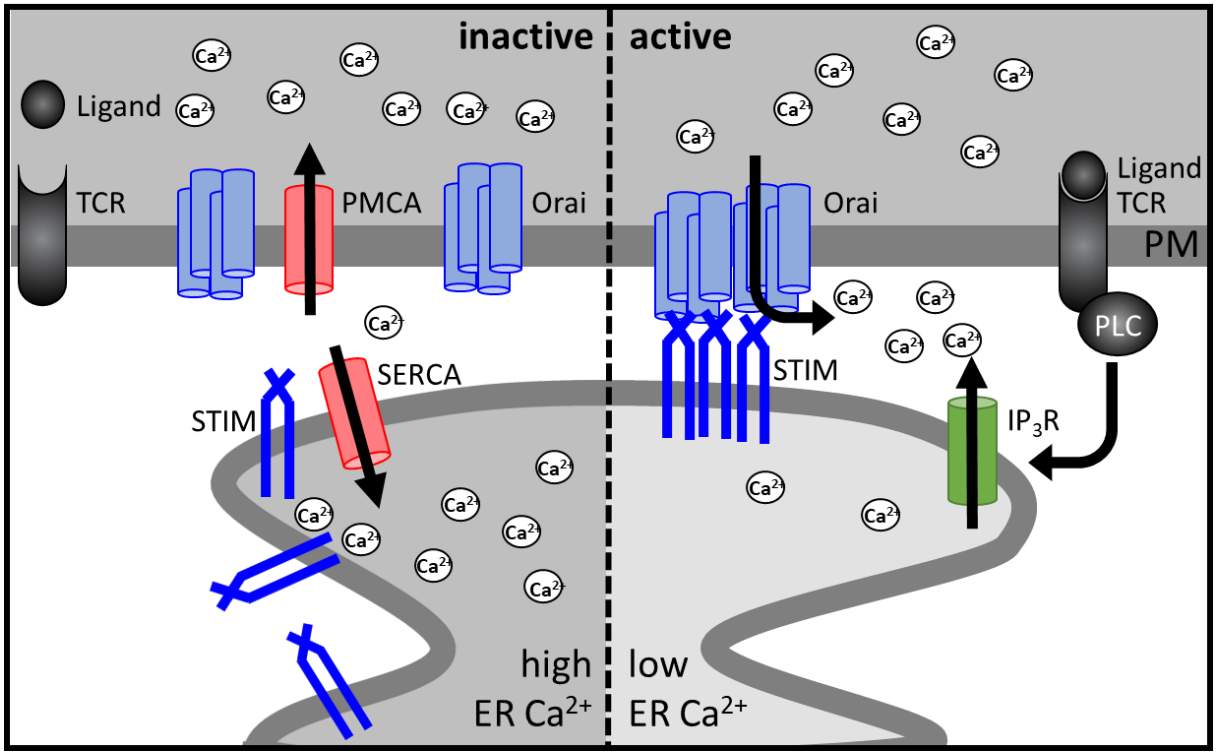

Figure 14: Schematic representation of intracellular calcium homeostasis and calcium signaling regulators. Left: To maintain the basal intracellular, nanomolar calcium concentration, a variety of different proteins are involved. In the absence of an extracellular stimulus in the form of a ligand, sarco-/endoplasmic calcium ATPase (SERCA) pumps calcium from the cytosol into the ER, which acts as an intracellular calcium reservoir, and plasma membrane-bound calcium ATPase (PMCA) pumps calcium into the extracellular space. Right: When a ligand binds to a membrane receptor, a signaling cascade causes an increase of the intracellular calcium level. Thus, the phospholipase C (PLC) bound to the receptor cleaves phosphatidylinositol-4,5-bisphosphate (PIP_2) into the second messengers inositoltriphosphate (IP_3) and diacylglycerol (DAG). The binding of IP_3 to IP_3 receptors (IP_3R) in the ER membrane causes a calcium flow via the IP_3R from the ER into the cytosol. As a result, stromal interaction molecule (STIM) proteins in the ER membrane aggregate into oligomers and activate the plasma membrane Orai channels that conduct calcium from the extracellular space into the cytosol.

3.2.1.2 How is the low basal calcium concentration in quiescent cells maintained?

The distribution of calcium ions in the resting state of non-electrically excitable cells plays a major role in the formation of calcium signals. A high sensitivity for cytoplasmic calcium signals results from large concentration differences between the cell interior and exterior. The concentration of Ca^{2+}_{cyt} in the cytosol is about 10 - 100 nM during the resting state (Berridge et al. 2003) and can increase to a concentration of several micromolar by activating calcium signaling mechanisms in the affected cell (Berridge et al. 2003; Bootman et al. 2013b). In opposite, within the extracellular space is the concentration of Ca^{2+}_{cyt} is about 1-2 mM, which means 10,000 - 20,000 times higher than in the cytoplasm (Amundson and Clapham 1993). As calcium ions cannot diffuse across membranes, specific channels for the maintenance of calcium homeostasis are necessary (Cahalan and Chandy 2009; Feske et al. 2012). These calcium-conducting channels are closed under quiescent conditions. The combination of low Ca^{2+} in the cytosol and a high concentration in the external medium and in some organelles in the cells results in an enormous concentration gradient for the second messenger across the membranes. This gradient determines the high sensitivity of calcium signals due to minimal changes in its intracellular concentration. In order to maintain calcium homeostasis in cells during their resting state, or to lower the increased intracellular concentration after a short-term calcium increase, Ca^{2+}-ATPases actively transfer Ca^{2+} ions from the cytoplasm via the plasma membrane to the

extracellular space mainly proceeded by the plasma membrane Ca^{2+}-ATPase (PMCA). In addition to that, membrane-bound ion exchanger, such as Na^{+}/Ca^{2+} antiporter (NCX) are involved in the transport of calcium ions across the membrane, too (Berridge and Dupont 1994; Berridge et al. 2003). Furthermore, calcium is actively transported via the membranes of calcium-storing cell organelles (Pedersen and Carafoli 1987; Rizzuto et al. 1992; Rizzuto et al. 1993). Here, the mitochondria quickly take up free Ca^{2+} ions from the cytoplasm through calcium uniporters (mitochondrial calcium uniporter, short: MCU) and slowly release them back into the cytosol, to enable other membrane-bound ATPases to keep up with the speed of Ca^{2+} flux. Calcium ions from the mitochondria can also be directly transferred into the ER lumen via MCU, if the proximity of both cell organelles allows this (Rizzuto et al. 1992; Rizzuto et al. 1993; Rizzuto et al. 1998; Berridge et al. 2003). The most important calcium reservoir for intracellular signaling is the endoplasmic reticulum (ER). Its calcium concentration is with 0.5-1 mM much higher than in any other compartment (Demaurex and Poburko 2009). This calcium accumulation is mainly achieved by the sarcoplasmic/endoplasmic Ca^{2+}-ATPase (SERCA), which transports calcium ions against the concentration gradient into the ER lumen (Pozzan et al. 1994; Rizzuto et al. 1998). To sum up, in order to efficiently increase the intracellular calcium concentration after specific external stimuli, a whole orchestra of calcium channels are essential to convert this external stimulus into an intracellular signaling response. In most non-excitable cells, the binding of an agonist to its membrane-bound receptor is the first step of a signaling cascade followed by an activation of receptor-associated kinases (Berridge 1993; Berridge and Dupont 1994; Bito et al. 1996). These kinases in turn activate the phospholipase C, which then hydrolyze the phospholipid phosphatidylinositol-4,5-bisphosphate (PIP_2) in the plasma membrane into the two second messenger inositol-1,4,5-trisphosphate (IP_3) and diacylglycerols (DAG) (Mustelin et al. 1990). While DAG remains in the PM, IP_3 can diffuse in the cytoplasm (Nahorski et al. 2003; Leybaert 2016). The destination of IP_3 is a receptor protein in the membrane of the endoplasmic reticulum (ER). Under resting conditions, the receptor is in an inactive state and waits for free IP_3 to bind. The liaison leads to a conformational change within the IP_3 receptor causing this channel to open (Lock et al. 2019). Since the ER acts as an intracellular calcium storage, calcium ions can now enter the cytosol along their steep concentration gradient via the IP_3 receptor. This process is called store operated calcium entry (SOCE) (Sampieri et al. 2018; Thillaiappan et al. 2019). The increase of the intracellular calcium concentration triggers a calcium-induced-calcium release (CICR), which means that calcium-dependent calcium channels in the plasma membrane open due to the increased intracellular calcium concentration. This leads to an additional calcium influx into the cell (Galione et al. 1991; Miyazaki et al. 1993; Laver et al. 2013). In immune cells, these channels are predominantly the calcium-release-activated (CRAC) channels (Grupe et al. 2010a; Hogan et al. 2010). They consist of two different subdomains, a calcium-regulated subunit (STIM), located in the ER membrane (Carrasco and Meyer 2011) and a pore domain (Orai) (Cai et al. 2018), located in the PM .

However, this scenario does not give an adequate answer to the question “How calcium is able to trigger different physiological processes”. So far, it was found that this complex signaling cascade generates distinct and dynamic patterns of Ca^{2+} signals ranging from Ca^{2+} oscillations with different frequencies to sustained elevations of the Ca^{2+} concentration. It was furthermore shown that the precise spatial and temporal pattern of messenger generation is crucial for the cellular output of a Ca^{2+} signaling cascade (Berridge and Dupont 1994; Dolmetsch and Lewis 1994; Lock et al. 2019).

3.2.1.3 How are different calcium signals organized within a cell?

The remarkable diversity of downstream events, which are triggered by Ca^{2+} signaling cascades depends on the way the signaling system is organized in both time and space (Berridge et al. 2000; Berridge et al. 2003). This means that not an overall increase in Ca^{2+}_{cyt} maintains the cells fate, but an oscillating alternation between the basal and elevated Ca^{2+}_{cyt} level leads to specific cell reactions. By varying the amplitude, frequency, duration, and localization of the calcium signal, a large information spectrum is available, which is interpreted by the cell to transmit signals for different biochemical and physiological processes (Amundson and Clapham 1993; Clapham 2007; Smedler and Uhlén 2014). For example, short, recurring calcium oscillations are responsible for a change in metabolism and the initiation of exocytosis. Long-lasting, constant increase in the intracellular calcium level leads to programmed cell death (Nicotera et al. 1992; Orrenius et al. 1992).

3.2.1.4 Precisely regulated calcium reactions are essential for an immunological activation of T-cells

The interest in stimulus induced Ca^{2+}_{cyt} oscillations has been centered on two main questions: 1. what is the underlying mechanisms and 2. what are their possible consequences for physiological responses? In this context T-lymphocytes turned out to be a most attractive model system for studying these phenomena for several reasons. First, Ca^{2+}_{cyt} oscillations are specifically triggered by stimulation of the TCR (T-cell antigen receptor) (Zweifach and Lewis 1996; Fracchia et al. 2013), a process which will be explained in the next paragraph. Second, Ca^{2+}_{cyt} signals are known to have a critical physiological function in these immune cells by controlling gene expression during the activation of T-cells via antigens (Shaw et al. 1988; Emmel et al. 1989; Feske et al. 2003; Gwack et al. 2007).

3.2.1.5 Calcium oscillations in T-cell activation processes

Oscillations in Ca^{2+}_{cyt} are a manifold but universal signaling tool in eukaryotic cells. This process is enabled by an excellent accomplished concert played by the above mentioned Ca^{2+} transporters and channels (**Figure 14**). Because of this interplay the cytosolic Ca^{2+} concentration can rapidly start to oscillate after a stimulus, much like a radio signal. Specific information can thus be efficiently encoded in the signal and transmitted through the cell via a variety of different calcium decoding proteins (Orrenius et al. 1992; Berridge et al. 1998).

Oscillation can be triggered either by fluctuations in membrane potential, leading to the repetitive opening and closing of voltage-gated Ca^{2+} channels or, more common, through activation of cell-surface receptors that increase the level of IP_3. An oscillatory Ca^{2+} response confers numerous signaling advantages over a sustained increase in Ca^{2+}. First, by increasing Ca^{2+} to high levels only transiently, oscillations avoid the toxic effects that arise from a maintained Ca^{2+} signal (Smedler and Uhlén 2014). Second, oscillatory signals support long-lasting cellular reactions, because they circumvent desensitization of Ca^{2+}-dependent responses that can occur during a prolonged Ca^{2+} signal. Third, oscillations in Ca^{2+} can increase the ability of low-level-stimulation to activate responses (Yissachar et al. 2013a). Therefore, the oscillatory frequency can vary from tens of Hz in neurons to mHz in non-excitable cells (Boulware and Marchant 2008). Occasionally, the frequency and/or amplitude is proportional to the amount of stimulus to which the cell is exposed (Woods et al. 1987; Berridge et al. 1998). However, Ca^{2+} oscillations *in vivo* are barely homogenous, but rather have intrinsic variations in

their frequency and amplitude (Zhu et al. 2011). What is still not known is how calcium oscillation are organized and recognized within a cell.

3.2.1.6 **Reading Ca^{2+} oscillations: the AM and FM catechism**

The amplitude modulation (AM) and frequency modulation (FM) catechism of signals that have sinoidal waveforms are common in electronics. Due to the periodic properties of calcium oscillations, they can be seen as sinoidal waves. Hence, for a simple harmonic oscillator, the voltage output (V) can be described **by Equation 2.**

$$V = Asin2\pi ft$$

Equation 2

where A is the amplitude and f the frequency (Hz).

Also, the oscillatory signal is defined not only by its amplitude and frequency, but also by its period (T), whereby 1/T equates to the frequency and the oscillation duration (d) which is schematically shown in **Figure 15**.

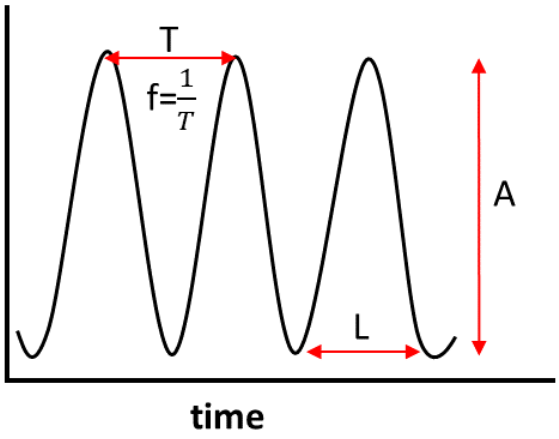

Figure 15: Abbildung 1: Frequency modulated Ca^{2+} oscillations. In silico oscillating waves are characterized by different parameters: Period (T), frequency (f) as 1/T, length (L), amplitude (A) and the total duration. Modified after Smedler 2014.

Waves carry information in form of all of the aforementioned properties: amplitude, frequency, and also their total duration. Extrapolating this to oscillations of Ca^{2+} in biological systems, the conventional view is that information is encrypted in either the amplitude or frequency. For its decryption, cells have a variety of tools to extract the information out of the different Ca^{2+} signaling patterns (Parekh 2011).

Signaling through amplitude modulation is conceptually straightforward, because it is dominated, by the Ca^{2+} affinity of the calcium decoder or sensor. The binding affinity of calcium to a protein is enabled by a highly conserved EF hand motif (Persechini et al. 1989; Grabarek 2006). This motif is a specific amino acid motif in proteins. The motif is a so-called helix-loop-helix motif with charged amino acids that are capable of binding Ca^{2+} ions. Due to the binding of calcium, the conformation of the protein changes and can thus also change its function. If the decoder has a high-affinity Ca^{2+}-binding site, then

it will rapidly respond to small elevations in cytosolic Ca^{2+}; by contrast, a low-affinity Ca^{2+} sensor would require a significantly larger increase in ambient Ca^{2+}. Consequently, Ca^{2+} signals of a different concentration or amplitude respectively, would recruit sensors in a manner proportional to their respective Ca^{2+} affinities. To avoid an accumulated calcium effect, many Ca^{2+} sensors have more than one Ca^{2+}-binding site (Grabarek 2006; Parekh 2011). However, the limitation of a simple amplitude-encoded system is that sensors with different Ca^{2+} affinities will be recruited sequentially, not independently. In more detail, a bulk Ca^{2+} rise, which is needed to activate a low-affinity sensor, stimulates at the same time all sensors with a higher affinity for Ca^{2+}. A possible mechanism to circumvent this is the arrangement of the sensors into discrete subcellular compartments, named the concept of spatially limited signaling (Davidson and Duchen 2006; Peglow et al. 2013). Another possibility to allow the functionality of low-affinity calcium decoder is to determine the kinetics or time-course of the Ca^{2+} signal, which is accomplished by frequency modulation (Parekh 2011). These oscillatory kinetics or temporal properties are detected by downstream Ca^{2+} sensors and translated into distinct cellular responses. In this context decoding of oscillatory properties means the binding of calcium ions, causing a change in the conformation of the sensor. This conformational change influences the proteins functionality, usually from an inactive into an active status. Two such Ca^{2+} sensors are the conventional (Ca^{2+}-dependent) protein kinase C (PKC) (Grumont et al. 2004) and Ca^{2+}/calmodulin dependent protein kinase (CaMK) (Dolmetsch et al. 2001; Vaca and Sampieri 2002; Berchtold and Villalobo 2014).

3.2.1.7 **Calcium decoding: How sensitively can a target protein respond to changes in the frequency of calcium oscillations?**

From the earliest detection of Ca^{2+}oscillations, several speculations focused on their purpose. The observation that the oscillation frequency varies more often than the amplitude gave rise to the popular notion of oscillations as a frequency-encoding system (Hajnóczky et al. 1995; Carafoli 2002; Boulware and Marchant 2008; Di Capite et al. 2009; Smedler and Uhlén 2014). Such a system increases the signaling fidelity by 'filtering out' random or low-amplitude fluctuations in Ca^{2+}_{cyt}. Finally, oscillations enhance signaling specificity by activating frequency-selective pathways in the cell. A major problem in addressing these possibilities experimentally was the generation of controlled Ca^{2+} oscillations. Because following stimulation through cell-surface receptors, oscillation frequency and amplitude often varies between cells in the measured population and also in single cells over time (Prakriya and Lewis 2003). Since 1982, when Tsien and colleagues developed Ca^{2+}-sensitive fluorescent dyes (Tsien et al. 1982), which can enter the cell, more precise calcium oscillation analyses became possible. A milestone was achieved in the combination of improved Ca^{2+} reporters and high-resolution microscopic imaging. It enabled the visualization of changes in Ca^{2+}_{cyt} within living cells at a high spatial and temporal resolution (Russell 2011; Bootman et al. 2013a; Gibhardt et al. 2019).

In the following I used the further developed, membrane-permeant calcium indicator Fluo4 for live-cell confocal measurements. The dye is commonly used as a non-fluorescent acetoxymethyl ester (Fluo4 AM), which is cleaved inside the cell by cellular esterases to receive the free Fluo4 (Russell 2011; Bootman et al. 2013b; Diercks et al. 2017). Fluo4 remains non-fluorescent in a calcium-unbound state and changes conformation upon Ca^{2+} binding resulting in its green fluorescent state.

3.2.2 Results

The strong correlation between ROS and calcium signaling in the physiological T-cell activation has been demonstrated in a variety of studies (Zhou et al. 2009; Adam-Vizi and Starkov 2010; Görlach et al. 2015; Simeoni and Bogeski 2015a). Nevertheless, not much is known about the direct influence of radiation on calcium homeostasis in immune cells. In the **Chapter 1** I was able to show that X-ray exposure triggers a transient increase in cytosolic as well as in mitochondrial H_2O_2 in approximately 50% of the monitored Jurkat T-cells. Nevertheless, it remains unclear if there is a physiological association between this observed IR induced H_2O_2 elevation and a potentially altered calcium homeostasis in the Jurkat cell line. To answer the question on a potential causal relation between H_2O_2 production and Ca^{2+} signaling, Jurkat cells were loaded with the common PM permeant calcium dye Fluo4 and were subsequently monitored after radiation exposure by live-cell analysis using a confocal microscope.

3.2.2.1 **Fluo4 is PM permeant and able to migrate into mitochondria, but not into the ER**

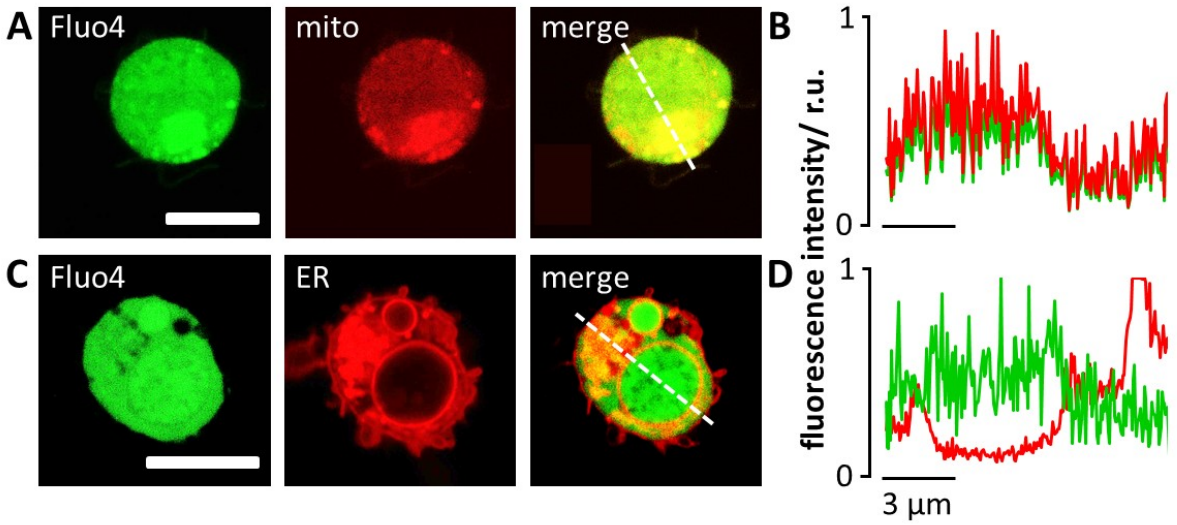

Figure 16: In Jurkat cells Fluo4 is PM permeant and located in the cytoplasm and the mitochondria, but not in the ER. A, C Confocal images of Jurkats stained with Fluo4 (first column) and additional mitoTracker red (A, middle column) or ERTracker red (C middle column) respectively. The last column shows an overlay of the Fluo4 and Tracker fluorescence channels. (**B, D**) Line Plots for each marker were taken in positions indicated with a white dashed line in the merge images. The fluorescence intensity of either (B) Fluo4/mitoTracker or (D) Fluo4/ERTracker were normalized to the highest value of each signal; the color of the line plots corresponds to those in the images. Scale bar = 10 µm.

In order to perform *in vivo* calcium measurements, first of all, I verified the properties of the intentiometric calcium dye Fluo4. For an appropriate experimental use, the PM permeability and the distribution of the calcium indicator in the cell is essential. Therefore, Fluo4 loaded, unstimulated Jurkat cells were additionally loaded with either mitoTracker red (**Figure 16A, B)** or ERTracker red (**Figure 16C, D)** and examined with respect to their colocalization properties. **Figure 16** shows representative confocal images of Jurkat cells, each stained with the different organelle trackers. In

both cells (**Figure 16A, C first column**) it can be clearly seen that Fluo4 is able to diffuse through the PM and bind calcium in the cytosol. The fluorescence intensity is almost evenly distributed throughout the cell. The merged images in **Figure 16A**, on the right show a high fluorescence intensity and a colocalization signal of Fluo4 and mitoTracker red. This indicates that the dye reaches the mitochondria and that the organelles gave a higher calcium concentration. This finding is in good agreement with literature (Hajnóczky et al. 2006; Lemasters et al. 2009). To further quantify this colocalization, a line plot (**Figure 16B**) was taken, which is indicated by a white dotted line in (**Figure 16A, right**). The line plot, normalized to the highest fluorescence intensity value, exhibits the same intensity curves for the Fluo4 and mitoTracker red signals supporting the notion that the reporter enters the mitochondria and that the latter have a high Ca^{2+} concentration. The behavior is completely different with the colocalization of Fluo4 with the ERTracker. Here, the fluorescence images (**Figure 16C**) and the corresponding line plot (**Figure 16D**) show an inverse localization pattern. The Fluo4 signal is low in the area where the ER marker generates a high intensity. This is best seen at the localization of the perinuclear ring, where the ER marker has a high intensity while the Ca^{2+} signal is low. Since it is well accepted that the calcium concentration in the ER is up to 10,000 times higher than in the cytosol the data indicate that Fluo4 is not entering the ER.

3.2.2.2 **Fluo4 is a suitable calcium dye for intentiometric measurements in Jurkat cells**

In a second step I investigated the Fluo4 calcium-binding affinity to test whether the calcium indicator is suitable for physiological examinations in the Jurkat cell line. Because of the low Kd=345 nM value of the dye for Ca^{2+} it is expected that the reporter reaches saturation at 1 mM (Molecular Probes' the Handbook: A Guide to Fluorescent Probes and Labeling Technologies, Tenth Edition (2005)").

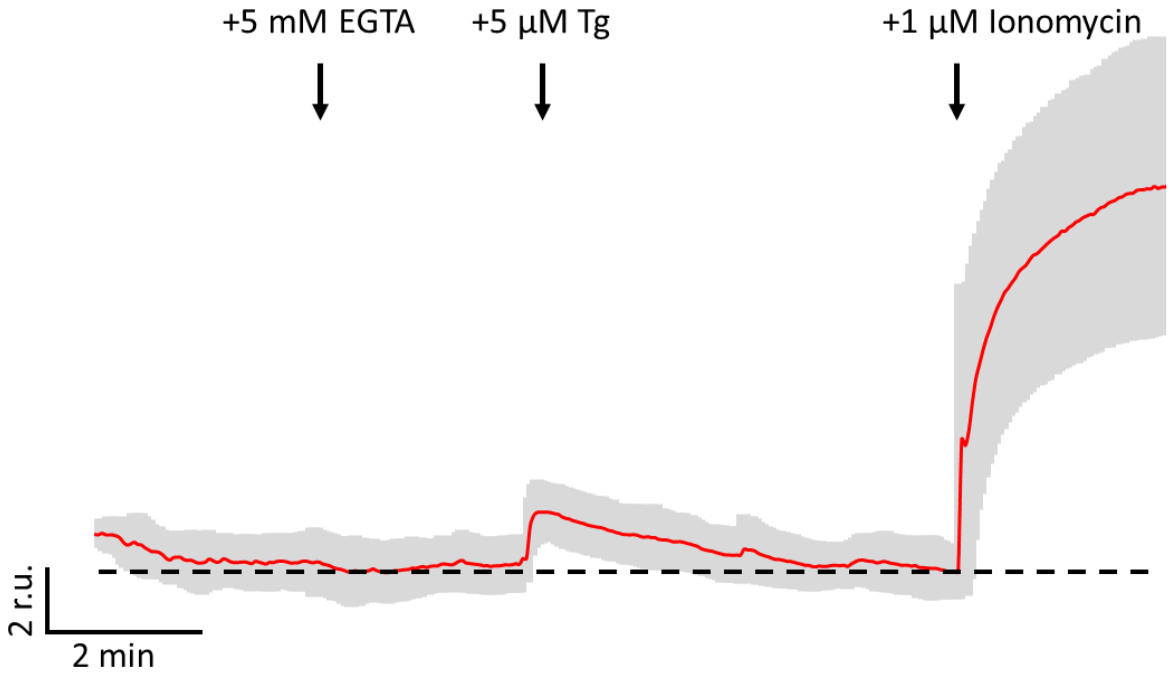

Figure 17: Fluo4 is a suitable plasma membrane permeable calcium dye for intentiometric analysis of the intracellular calcium concentration *in vivo*. Fluo4 loaded Jurkat cells were measured for a period of in total 25 min where every 5 s an image was taken and the external solution was replaced after indicated timepoints with the same solution containing 5 mM EGTA, 5 mM EGTA and additional 5 µM thapsigargin (Tg), or 2 mM Ca^{2+} and additional 1 µM ionomycin in the external solution. Fluorescence intensity of was analyzed and the mean value (red) of n = 108 cells ± SD (gray) is plotted as a function of time (dotted line indicates basal fluorescence level).

The range of excursions in the Fluo4 signal in Jurkat cells in response to different experimental manipulations can be carried out by measuring the fluorescence intensity in these cells in different external solutions with (**Figure 17**):

i.) precisely known free Ca^{2+} concentration,

ii.) Ca^{2+} free solution and additional 5 µM thapsigargin (Tg) for after depletion of internal calcium stores. Tg is in these experiments used as a specific inhibitor of SERCA to study the role of the SERCA in the formation of calcium signals in the cytoplasm. Therefore, Tg binds irreversibly to SERCA, but does not affect PMCA or other calcium-conducting channels (Thastrup et al. 1990; Y Sagara and G Inesi 1991). Thus, the enzyme is specifically retained in its inactive form. Inhibition of SERCA then indirectly leads to a reduced calcium concentration in the ER lumen and causes the release of calcium ions into the cytoplasm (Thastrup et al. 1990; Y Sagara and G Inesi 1991). A subsequent CICR cascade triggered by calcium ions from the extracellular space is prevented by the absence of calcium in the external buffer solution. As a consequence, only the Fluo4 fluorescence intensity increase via SOCE is detectable.

iii.) An external solution with 2 mM Ca^{2+} and 1 µM calcium ionophore, ionomycin will generate a high Ca^{2+} conductance in the plasma membrane. With the high Ca^{2+} concentration in the external buffer this should generate a maximal fluorescence intensity, which fully saturates the Fluo4.

At this point is important to mention that this procedure is not a calibration in the strict sense because it does not provide a value for the Ca^{2+} concentration. These experiments only show if stimulations, which generate different excursions in the Ca^{2+} concentrations are also causing different increases in the fluorescent intensity.

For the experiments Fluo4 loaded Jurkat cells were measured under control conditions (2 mM calcium solution) followed by the aforementioned three specific conditions in 5 min long time series during which every 5 s an image was taken. Afterwards, the fluorescence intensity of more than 100 cells was analyzed and the mean value ± SD was plotted as a function of time in **Figure 17**. It is evident, that the basal calcium concentration in Jurkat cells is constantly low with 2 mM Ca^{2+} external solution over the period of 5 min. This value is maintained after a change to Ca^{2+} free external solution. Addition of thapsigargin induces a slight, transient increase at its maximal value of 1.8±0.6 of fluorescence intensity, which is slowly rebuffered within the 5-minute measurement. This is in good agreement with values described in literature with an 2-4-fold increase in Ca^{2+}_{cyt} to ˜ 400 nM after Tg application (Y Sagara and G Inesi 1991; D Kline and J T Kline 1992). A rapid and long-lasting rise in the Ca^{2+}_{cyt} to a value 14.3±5.7 times higher than the basal level, is induced by addition of ionomycin. Based on these measurements it is possible to determine the dissociations constant K_d with the following **Equation 3**:

$$K_d = \frac{(F - F_{\min})}{(F_{max} - F)}$$

Equation 3

Where F_{min} is the fluorescence intensity of the calcium indicator in the absence of calcium (Ca^{2+} free) and F_{max} the fluorescence intensity of the saturated calcium indicator (2 mM Ca^{2+} + ionomycin), and F the fluorescence intensity of an intermediate calcium level (Ca^{2+} free + Tg). This results in a *in vivo* K_d value of 150 nM, which corresponds very well with the 345 nM of the manufacturer's specifications. According to the received data, I considered that Fluo4 is well suitable for intentiometric, fast kinetic calcium measurements in Jurkat T-lymphocytes.

3.2.2.3 **X-ray does not cause an immediate calcium level alteration in T-cells**

In a study in 2015, Roth and colleagues were able to show that externally applied hydrogen peroxide triggers calcium signals in a large population of A549 lung carcinoma cells (Roth et al. 2015). In subsequent studies it was discovered that irradiation with X-rays leads to an increase in intracellular H_2O_2 in the same cell line (Gibhardt 2014). This fostered the hypothesis that A549 cells elicit a calcium signaling cascade in response to X-ray generated cellular H_2O_2.

The same type of experiment was repeated in Jurkat T-cell (Fuck 2017) using the combined microscopy/X-ray irradiation setup at the GSI. **Figure 18A** shows in the upper trace one exemplary Fluo4 signal from a Jurkat cell, which is low over the entire period of recordings. After 10 min of recording 5 µM ionomycin was added to the external solution (blue arpanel) which leads to an immediate upstroke of the fluorescence signal. The lower trace in **Figure 18A** shows the mean fluorescence intensity of 15 control cells ± SD. These data confirm that the calcium concentration in unstimulated cells is in general constantly low. The upper trace in **Figure 18B** shows a representative

calcium response of a Jurkat cell exposed to either 1 Gy (black dotted line) or 10 Gy (black line) X-ray; the time of irradiation is indicated by a black arpanel. Against all expectations this treatment caused no change in the cytosolic calcium concentration within 10 min of recording neither after irradiation with 1 Gy nor 10 Gy. However, in the representative recordings the intracellular calcium concentration again increased immediately after addition of 5 µM ionomycin. The latter response confirms that the Fluo4 reporter is in principle responding to Ca^{2+} changes in these cells and that as a consequence X-ray irradiation is most likely not causing an immediate Ca^{2+} signal in Jurkat cells.

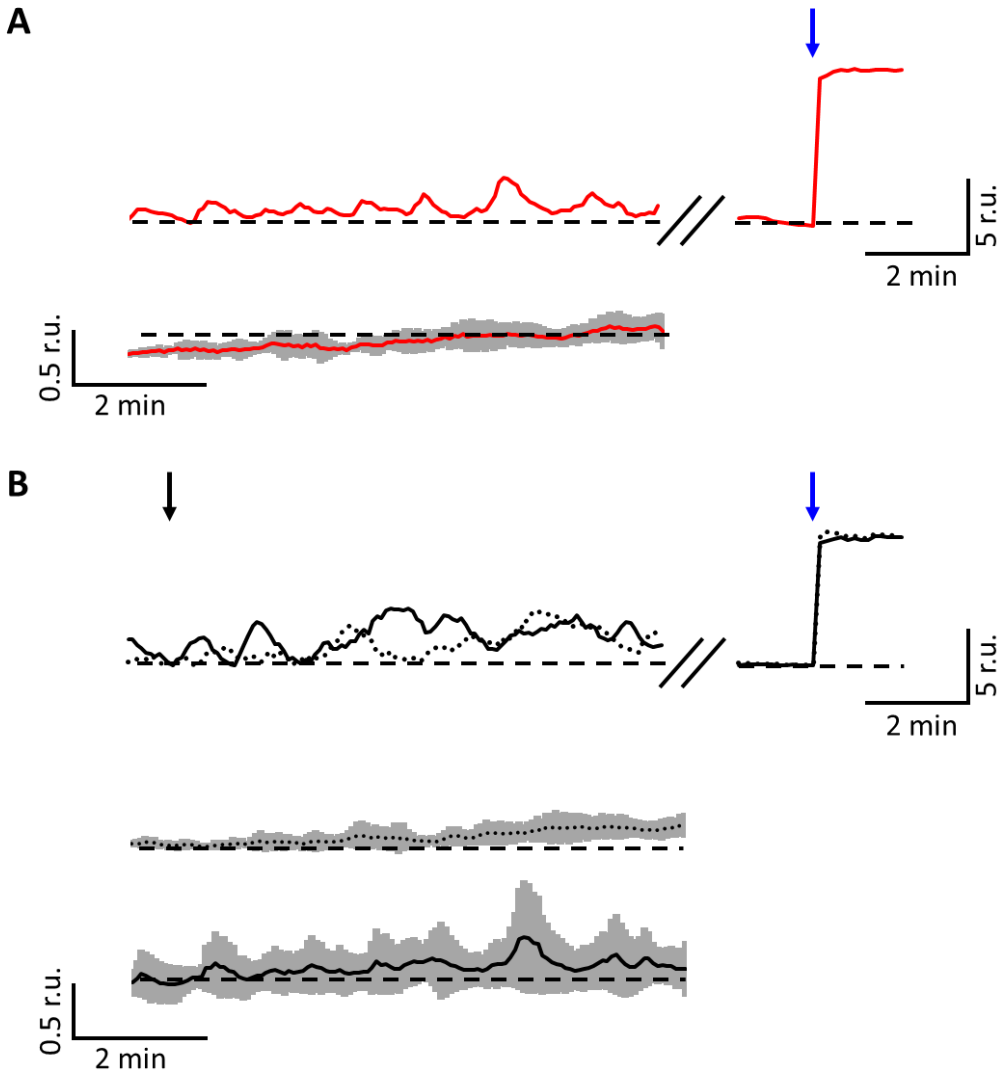

Figure 18: X-ray does not cause immediate calcium level alterations in T-cells. Fluo4 loaded Jurkat cells were monitored for 10 min at a specific microscopic setup at the Helmholtzzentrum für Schwerionenforschung (GSI). All Ca^{2+}_{cyt} measurements were performed in buffer containing 2 mM Ca^{2+}. (**A**) Representative Fluo4 signal as measure of changes in cytosolic Ca^{2+}_{cyt} in an untreated control Jurkat cells; maximal fluorescence increase after addition of 1 µM ionomycin (blue arpanel) (Top). The mean Fluo4 intensity ± SD (grey) from 10 control cells (Bottom). (**B**) Fluorescence was recorded in real time before and after X-ray irradiation with 1 Gy (black dotted) and 10 Gy (black) at times indicated by black arpanels. The same cells responded with a maximal fluorescence increase after addition of 1 µM ionomycin (blue arpanel) (Top). Mean Fluo4 intensity from cells irradiated at arpanel with 1 Gy (middle) or 10 Gy (bottom) X-ray. Data are means ± SD (grey) from 15 cell for each dose. Modified according to Voos 2018, Fuck 2017.

The same conclusions are supported by a statistical analysis of a large number of cells treated in the same manner. The average fluorescence value ± SD (n=12) shown in **Figure 18B mid trace (1 Gy) and lower trace 10 Gy** illustrates that there is no significant effect of X-ray on the intracellular calcium concentration over the first 10 min after irradiation. Taken together the data suggest that IR exposure leads to an increase in cellular H_2O_2 (**Chapter 1**) but this has no immediate impact on Ca^{2+}_{cyt} in Jurkat cells.

3.2.2.4 **Radiation induces dose dependent, long lasting calcium oscillations after several minutes of delay**

Literature reports from experiments by Lewis, Cahalan and Zweifach show that stimulation of immune cells by appropriate stimuli like antigens or immune cell activator may trigger no immediate but delayed Ca^{2+} responses which occur with some 2-20 minutes delay after stimulation (Xia et al. 2018), whereas a fast increase in Ca^{2+} was observed in 1-3 min after addition of Tg, which is in good agreement with the data in figure 4 (Lewis and Cahalan 1989; Zweifach and Lewis 1995, 1996). To test the possibility to X-ray irradiation elicits similar delayed Ca^{2+}_{cyt} signals I monitored the Fluo4 fluorescence in Jurkat cells over an extended time window of up to 3-5 hours; during this monitoring period an image was taken every 5 s The acquired integrated density values of the Fluo4 signal in each of the analyzed cells where than normalized to the first datapoint at the start of the life cell imaging.

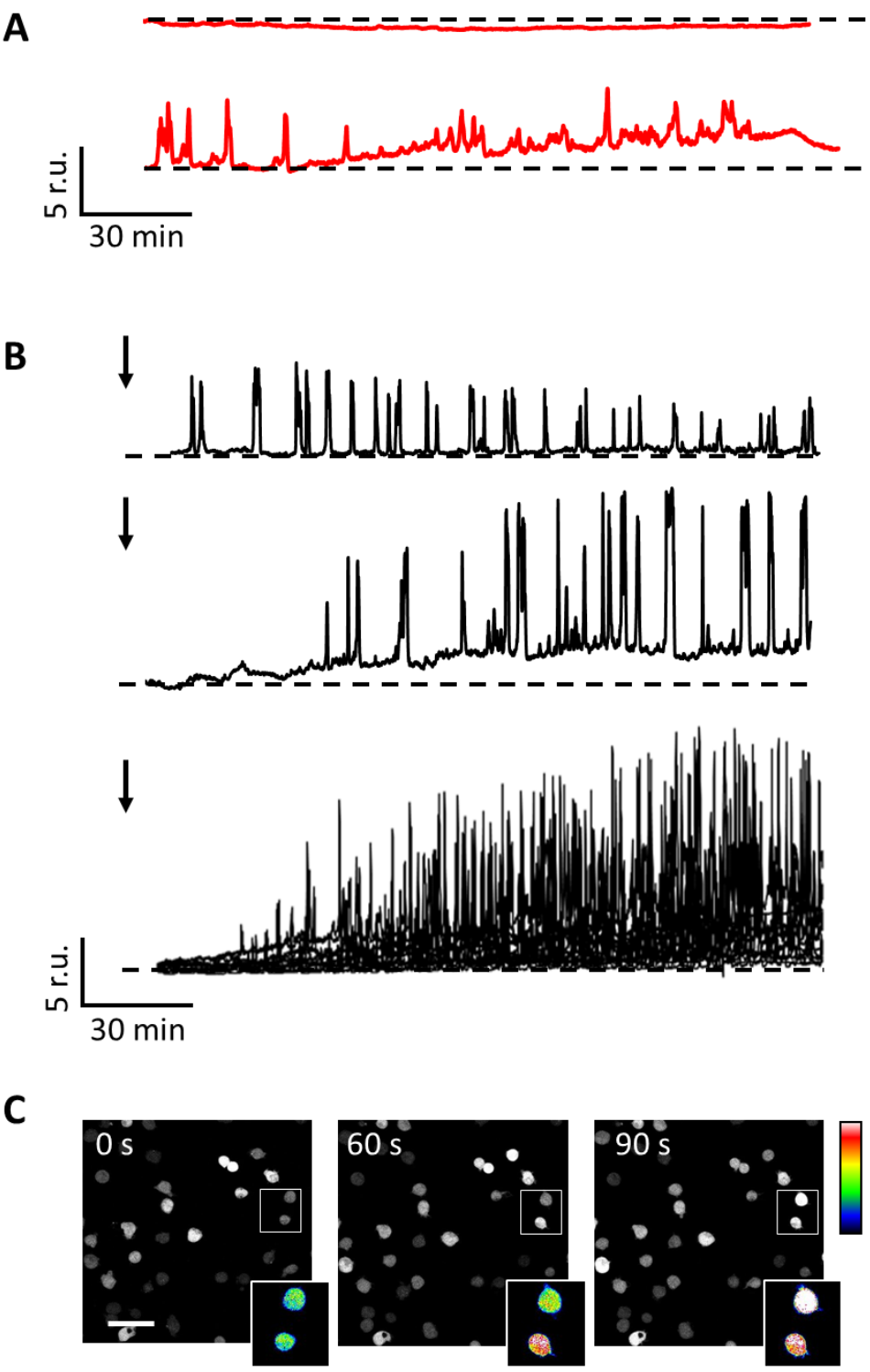

Figure 19: Ionizing irradiation elicits delayed Ca^{2+}_{cyt} oscillations with distinct frequencies and amplitudes. Representative long-term measurements of Fluo4 intensity in Jurkat cells. All Ca^{2+}_{cyt} measurements were performed in buffer containing 2 mM Ca^{2+}. (**A**) Fluo4 intensity traces of non irradiated control cells where one cell has a contantly low signal (upper trace) and one elicits unperiodic, spontanous oscillations (lower trace). (**B**) cells were exposed to a dose of 1.5 Gy (upper trace) or 5 Gy (middle trace). Time of X-ray exposure is indicated by black arpanels. The irradiated cell starts to oscillate after a lag time with a distinct frequency. The lower trace shows an overlay of Fluo4 signals from 15 individual cells after irradiation with 5 Gy; Time of X-ray exposure is indicated by black arpanels. (**C**) Exemplary fluorescence confocal images with an enlarged 16 color pseudocolor section of one oscillatory cell. Scale bar = 10 µm.

Figure 19A shows the representative and normalized Fluo4 fluorescence intensity trace of a single untreated control cell. Typical for untreated cells is that the Ca^{2+}_{cyt} remains constant at a low value through the recording. This phenotype was seen in 105 of 130 (81%) of the untreated control cells (**Figure 19A upper trace**) which all remained at a low level for at least three. In the remaining 25 cells some spontaneous excursions in Ca^{2+}_{cyt} were observed. Characteristic for these Ca^{2+} signals was that they were mostly present already at the start of the imaging and the they exhibited no obvious periodicity (**Figure 19A lower trace**). The visual appearance of a calcium oscillation in Jurkat cells in live-cell confocal microscopic recordings is shown in **Figure 19C.** The black (=1) to white (=16) pseudocolor images illustrate that the basal fluorescence intensity in the cell is low and rises dramatically during an oscillation before it returns back to the basal level.

To determine whether irradiation has any delayed effects on the intracellular calcium concentration over a period of minutes to hours after exposure, Jurkat cells were exposed to 1.5 Gy X-ray. After irradiation approximately half of the cell population (n=42) exhibited well-defined Ca^{2+}_{cyt} oscillations; one representative cell response of an X-ray treated cells is shown in **Figure 19B upper trace**. Similar delayed and long lasting Ca^{2+}_{cyt} oscillations were observed in a large fraction (77%) of in total 87 monitored cells after irradiation with 5 Gy (**Figure 19B middle trace**). The remaining cells, which exhibited no response either maintained a constant low Ca^{2+}_{cyt} like the controls in **Figure 19A upper trace**. This was the case in 20 out of the 87 cells tested (23%). In the remaining cases (18 cells) (21%) unspecific Ca^{2+}_{cyt} excursions with non-periodic signals like those in the control cells (**Figure 19A lower trace**) were observed. For further quantification of radiation induced effects on Ca^{2+}_{cyt} I consider here only Ca^{2+}_{cyt} oscillations, which occurred ≥10 min after start of the imaging with a distinct, periodic frequency. Based on this analysis it occurs that calcium oscillations with these criteria can be recognized in only 10% of the control cells. But after exposure to 5 Gy X-ray the number of cells with this type of oscillations increases to 56%. The overlay (**Figure 19B lower trace)** of the fluorescence intensity of 10 Jurkat cells shows that the cells exhibit after exposure to 5 Gy X-ray after some delay Ca^{2+}_{cyt} oscillations with a comparable frequency and amplitude, which is quantified in more detail in the next paragraphs.

3.2.2.5 **The frequency of radiation induced calcium oscillation is dose independent**

The pattern of X-ray induced Ca^{2+} oscillations is not only determined by the amplitudes of the fluorescence signal but also by the beginning of the oscillation, their duration and the frequency. An analysis of many recordings shows that the onset of the oscillating Ca^{2+}_{cyt} signals varied with the same irradiation dose considerably from one cell to the other. For example, in cells stimulated with 1 Gy the first detectable Ca^{2+}_{cyt} peak occurred between 10 min (fastest) and 72 min (slowest) after X-ray exposure. A plot of the average lag times as a function of X-ray dose shows that this value is not significantly changing with the stimulation dose (**Figure 20A**). The lag times vary from 33.5 ± 4.7 min in 0.5 Gy to 51.5 ± 3.8 min in 5 Gy irradiated cells. With an average lag in the order of > 30 min between irradiation and the onset of Ca^{2+} oscillations it is not surprising that real time imaging experiments reported in failed to detect any Ca^{2+} response to the irradiation stress.

Next, to obtain more information about the calcium oscillations their frequency was examined in more detail. This is particularly interesting since the oscillation frequency is a key code of the oscillatory

responses and can provide information for the downstream signaling pathway in T-Lymphocytes (Dolmetsch et al. 1998; Di Capite et al. 2009; Parekh 2011; Smedler and Uhlén 2014). **Figure 20B** presents the frequency analysis of the oscillation patterns depending on the irradiation dose. The data reveal that Ca^{2+}_{cyt} oscillates in Jurkat cells in response to X-ray with a frequency of 2.1 to 3.8 mHz; this frequency is independent of the irradiation dose. A scrutiny of oscillations in individual cells further shows that they oscillate with a given frequency over several hours (**Figure 20B**). This means that as soon as the calcium signaling is initiated after a lag time, a cell oscillates with a stable frequency. Minor fluctuations within the biological system are negligible.

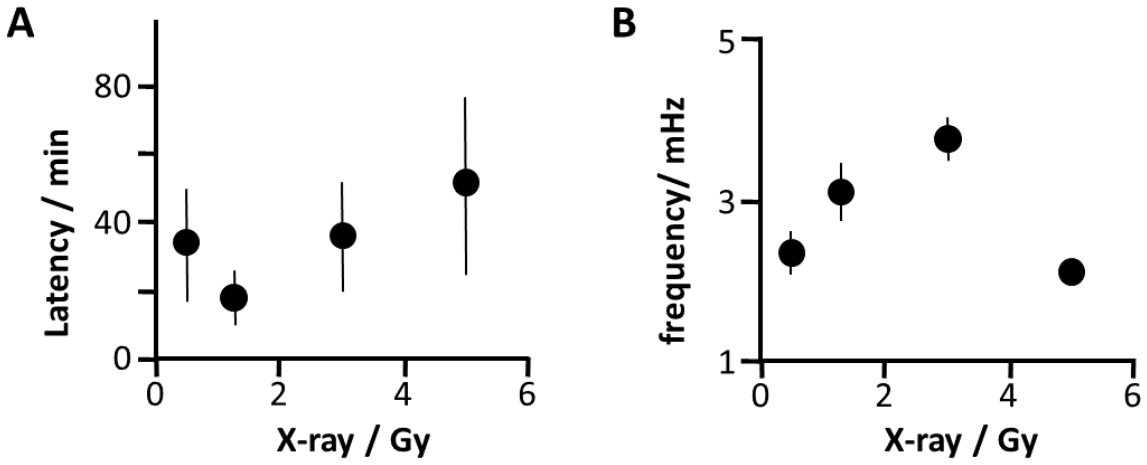

Figure 20: The X-ray induced calcium oscillations are initiated with a dose-independent latency and oscillatory frequency. (**A**) Latency time between onset of Ca^{2+}_{cyt} oscillations after irradiation, (**B**) oscillation frequency. Data are mean values ± SD from >25 cells per dose.

3.2.2.6 The amplitude of X-ray induced calcium oscillations is dose-dependent

It has been mentioned before that Jurkat cells exhibited after X-ray exposure three different categories of Ca^{2+}_{cyt} signals: 1. They generated calcium oscillations with distinct amplitude and frequency, 2. They generated calcium signals with no distinct frequencies and random amplitudes and 3. They generated no effect. **Figure 21A** summarizes the relative probability P of finding cells which exhibited a Ca^{2+} signal of category 1 in, long-term calcium recordings after irradiation over a range of clinically relevant X-ray doses from 0.5 to 5 Gy. The resulting P value is with 0.13 quite low in unstimulated control cells. The P value increases than to values between 0.45 and 0.58 after exposing cells to the previously mentioned doses of X-ray in a dose-independent manner.

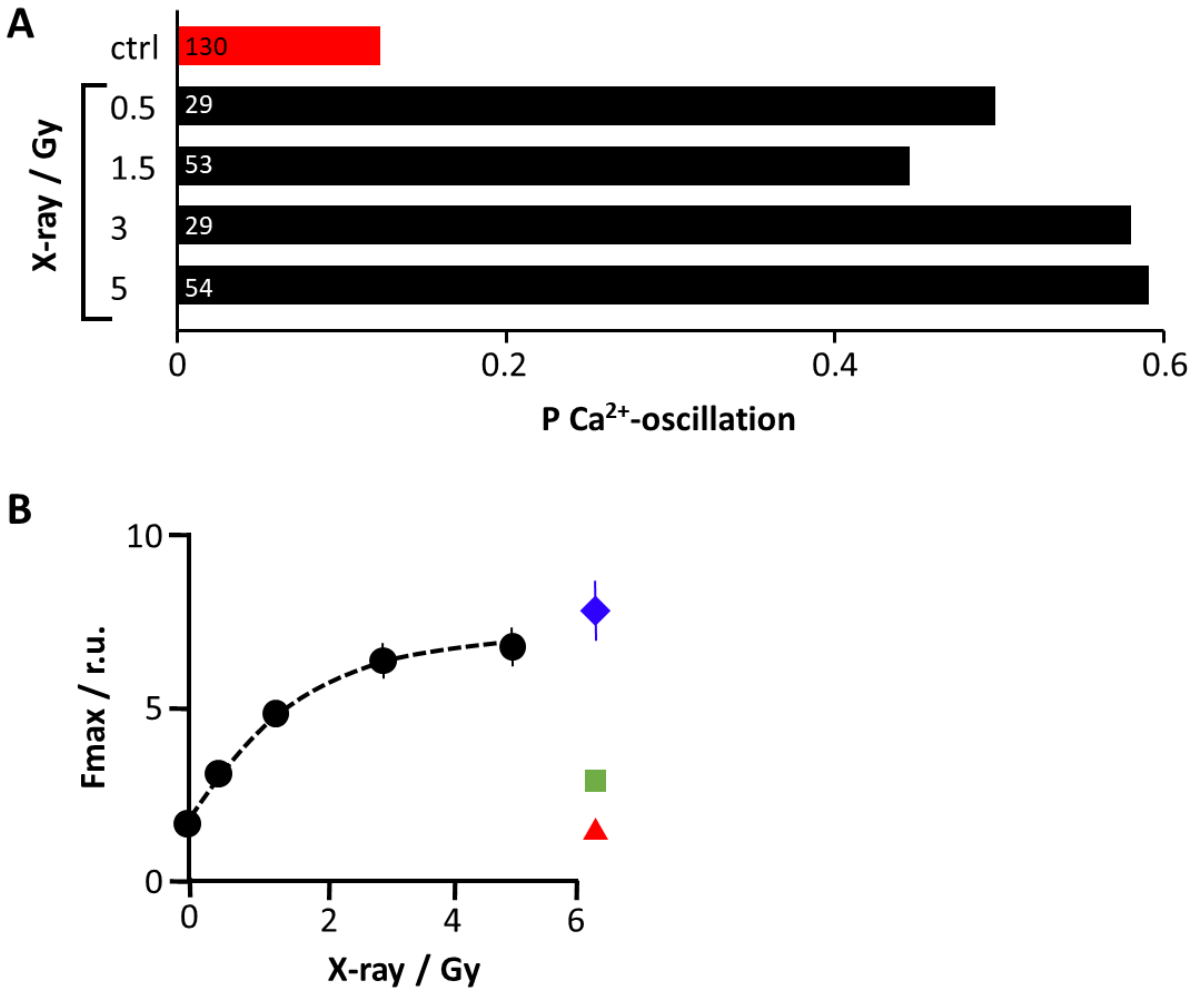

Figure 21: The amplitude of X-ray induced calcium oscillations is dose-dependent. (**A**) Probability for detecting periodic Ca^{2+}_{cyt} oscillations in Jurkat cells. Cells were either non irradiated (ctrl) (red bar) or exposed to X-ray doses between 0.5 and 5 Gy (black bars).). For analysis only cells, which started oscillating ≥10 min after X-ray exposure with periodic frequency were considered. Numbers indicate the number of cells analyzed. (**B**) Maximal amplitude of oscillation as a function of irradiation dose. Data are mean values ± SD from >25 cells per dose. All Ca^{2+}_{cyt} measurements were performed in buffer containing 2 mM Ca^{2+}. The colored symbols show the maximal level of Fluo4 fluorescence intensity obtained in the same buffer by adding 1 µM ionomycin (blue diamond) or by depleting Ca^{2+} stores with 2 µM thapsigargin (green square) or the minimal Fluo4 intensity by adding 5 mM EGTA resulting in a nominally Ca_{2+} free external buffer (red triangle). The half maximal Ca^{2+}_{cyt} peak is achieved by 1.5 Gy.

In a next step I analyzed the peak values of X-ray induced Ca^{2+}_{cyt} excursions by measuring the maximal fluorescence intensity in a single cell. These data were plotted the mean values ±SD of >25 cells as a function of the stimulation dose (**Figure 21B)**. This plot illustrates that the amplitude of the Ca^{2+}_{cyt} excursions increase in a dose-dependent manner with relative fluorescence values reaching from 3.0 ± 0.25 after 0.5 Gy to a maximum of 6.6 ± 0.5 post 5 Gy exposure. For this reason, the data could be fit with a single saturating exponential function (**Equation 4**):

$$Y=F_{max}(1-e-x/k)+F0$$

Equation 4

where F_{max} is the maximal increase in peak fluorescence, F0 the background fluorescence of the control cells and k the dose for half maximal increase in fluorescence. The fit yields a half maximal Ca^{2+}_{cyt} peak for 1.5 Gy X-ray.

As a reference value for the maximal Fluo4 signal the plot in **Figure 21B** also shows the fluorescence value, which was measured in the presence of ionomycin (blue diamond) in a 2 mM Ca^{2+} solution. Because of the affinity of the sensor for Ca^{2+} this value must be considered as the upper limit of Fluo4 fluorescence. Comparison between this value and the X-ray induced increase in Fluo4 fluorescence shows that this upper limit is approached by Ca^{2+} excursions elicited by 5 Gy X-ray (red triangle) (**Figure 21B**).

In case of an antigen-mediated T-cell activation, Ca^{2+}_{cyt} oscillations are mainly the result of store operated Ca^{2+} entry (SOCE), a mechanism, which can be imitated by Tg. The data on the X-ray induced Ca^{2+} excursions (**Figure 21B)** include as a further reference value also the mean maximal fluorescence intensity of > 100 individual cells treated with 2 µM Tg (green square) in a calcium free external solution to validate the increase in cytosolic calcium levels exclusively influenced by SOCE. The fluorescence intensity of these cells increased to a plateau well below that of the maximal amplitude measured in response to X-ray stimulation. This indicates that IR elicits Ca^{2+}_{cyt} excursions to much higher levels than Tg alone, but to levels where the Fluo4 calcium dye presumably approaches saturation; this is at about 1 mM Ca^{2+} (Gee et al. 2000). The fluorescence intensity amplitudes following irradiation with ≥ 2 Gy X-ray are more similar to those elicited by 1 µM ionomycin in buffer with 2 mM Ca^{2+} than to the effect evoked by Tg. This implies that the depletion of the intracellular storages alone does not cause the high oscillation amplitudes post X-ray exposure. The data advocate the importance of Ca^{2+} influx via channels in the plasma membrane.

To test this hypothesis recordings similar to those in **Figure 19** were repeated in a nominally Ca^{2+}_{cyt} free extracellular solution. For this purpose, the buffer contained 5 mM EGTA **Figure 22**. In this nominally Ca^{2+}_{cyt} free solution 5 Gy X-ray reduced the probability of Ca^{2+}_{cyt} oscillations to 10% in 50 tested cells; also, the average fluorescence intensity of the Ca^{2+} sensor was reduced dramatically to a mean value of 1.4 ± 0.09, which is in the range of untreated control cells.

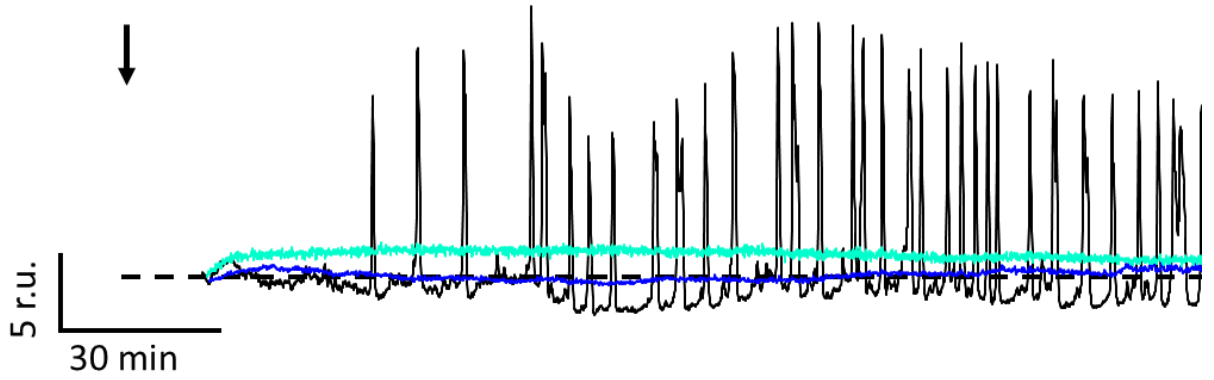

Figure 22: Ca^{2+}_{cyt} oscillations can be suppressed by buffering external Ca^{2+} and by blocking Ca^{2+} influx. Representative long-term measurements of Fluo4 intensity in Jurkat cells, irradiated with either 5 Gy X-ray (black) and additional 5 mM EGTA as a nominally free Ca^{2+} solution (blue) or additional 5 µM Ca^{2+} channel blocker gadolinium (Gd^{3+}) (turquoise). All Ca^{2+}_{cyt} measurements were performed in buffer containing 2 mM Ca^{2+}. Black arpanel indicates irradiation timepoint.

The results of these experiments show that the absence of external Ca^{2+}_{cyt} abolishes radiation induced Ca^{2+}_{cyt} oscillations but still allows some steady increase in Ca^{2+}_{cyt}. The latter value is comparable to the calcium level measured after addition of Tg. These experiments underpin a calcium influx via plasma membrane channels as the main trigger of Ca^{2+}_{cyt} oscillations in irradiated cells. To further test this hypothesis, experiments were repeated in a buffer containing 2 mM Ca^{2+}_{cyt} and 5 µM gadolinium (Gd^{3+}), a broad inhibitor of Ca^{2+}_{cyt} permeable channels in T-cells **Figure 22** (Adding et al. 2001; Biagi und Enyeart 1990). In the presence of the Ca^{2+} channel blocker the probability of radiation-induced Ca^{2+}_{cyt} oscillations is with 15% (n=77) reduced close to that of control cells. Like in the calcium-free EGTA solution also Gd^{3+} does fully prevent an X-ray induced increase in the concentration of Ca^{2+}_{cyt} to a value of 1.7 ± 0.1 above the control level (**Figure 22**). Taken together these data confirm a general impact of radiation on Ca^{2+}_{cyt} in Jurkat cells. They furthermore underline the importance of a Ca^{2+} influx from extracellular space as a part of the radiation induced signaling cascade which eventually results in Ca^{2+}_{cyt} oscillations.

3.2.2.7 **IR induced calcium signaling is caused by ROS and extracellular calcium ions**

The present data imply that the X-ray induced Ca^{2+} oscillations are not an immediate effect of the radiation stress but the downstream response of a signaling cascade which is initiated by radiation. In search for further upstream event, which might also explain the long lack tine between radiation and Ca^{2+} responses, it is interesting to look at the relationship between ROS and Ca^{2+}. It has been shown that X-ray exposure triggers in Jurkat cells an increase in ROS. It is also known, that ROS and Calcium are essential second messenger for the T-cell activation mechanisms. On the background of this information I address the question on a potential direct relationship between IR mediated increase in H_2O_2 and the distinct calcium oscillatory patterns. For this purpose, the time-lapse calcium experiments in Jurkat cells were repeated 10 mM of the ROS scavenger n-acetylcysteine (NAC) and with 5 mM of the reducing agent 1,4-Dithiothreitol (DTT). Both agents were added to the extracellular buffer prior to X-ray irradiation. The first mentioned reagent NAC is a commonly used antioxidant that is broadly effective in the cell. Chemoprotection by NAC frequently results from inactivation of primary toxic or reactive electrophiles which are generated as products of metabolites or from lipid peroxidation (Ezeriņa et al. 2018; Zhitkovich 2019). In addition to its direct antioxidant effect NAC exhibits disulfide breaking activities and acts as a glutathione (GSH) precursor, which in turn is well known as a direct antioxidant (Foyer and Halliwell 1976). On the contrary, DTT protects thiol groups and reduces disulfide bonds to sulfhydryl groups hence, prevents oxidation of the first mentioned (Okuno and Kondelis 1978).

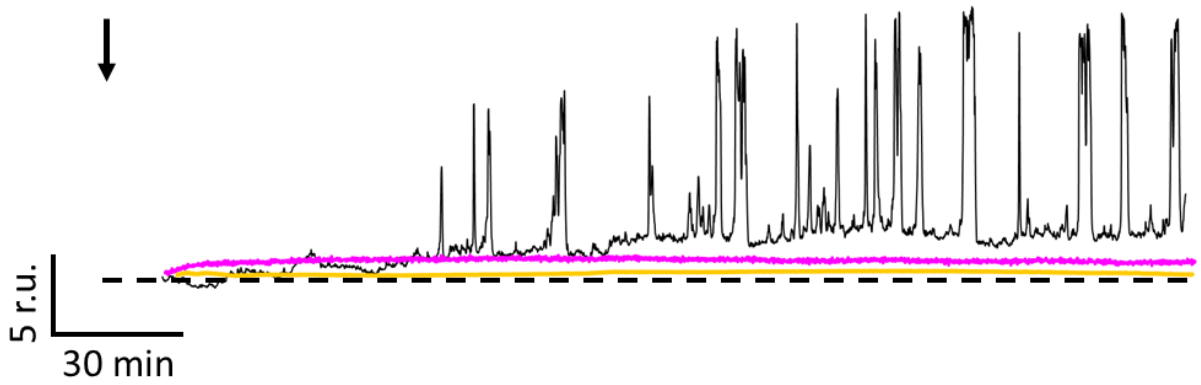

Figure 23: ROS scavenger and reducing agents prevent ionizing irradiation evoked Ca^{2+}_{cyt} oscillations. Representative long-term measurements of Fluo4 intensity in Jurkat cells, irradiated with either 5 Gy X-ray (black) and additional 10 mM ROS scavenger n-acetylcysteine (NAC) (pink) or additional 5 mM reducing agent 1,4-Dithiothreitol (DTT) (orange). All Ca^{2+}_{cyt} measurements were performed in buffer containing 2 mM Ca^{2+}.

Jurkat cells were incubated for 30 min with either NAC or DTT in the same buffer that was also used for loading Fluo4 into the cells. The cells were then irradiated with 5 Gy X-ray and the fluorescence intensity of Fluo4 was monitored over a period of 3 h. The measured fluorescence intensity of a representative cell treated with either NAC or DTT respectively is shown in **Figure 23**. The data show that the presence of NAC or DTT lowered the propensity X-ray stimulated calcium oscillations. The percentage of responsive cells decreased from 58% in the absence to 11%/7% in the presence of the two redox agents. The results of these experiments suggest that X-ray generated ROS molecules are an essential intermediate in a signaling cascade that eventually triggers the downstream calcium

response. Furthermore, the data imply that the transient increase in cytosolic and mitochondrial H_2O_2 concentration, which is elicited by X-ray irradiation, could be the critical event, which elicits this signaling cascade. This assumption is supported by the temporal sequence of events and by the number of reactive cells. Notably the X-ray induced increase in H_2O_2 precedes the onset of Ca^{2+} oscillations and in both cases about 50% of the Jurkat cells exhibit a H_2O_2 increase and Ca^{2+} oscillations.

3.2.3 Conclusion

According to the still unidentified mechanistical effects of radiation on the calcium response of immune cells, the present study takes a particular view on the temporal arrangement of Ca^{2+}_{cyt} events induced upon X-ray exposure.

Using live-cell microscopy analysis, I determined calcium oscillations as an early response after X-ray exposure, showing some minutes of a delay. These calcium events are generally characterized by a dose-independent canonical frequency of 2-4 mHz and a dose-dependent amplitude. The addition of ROS scavenger NAC and DTT, and the inhibition of Ca^{2+} influx with EGTA and the broad calcium channel inhibitor Gd^{3+} abolished calcium oscillations. This leads to two conclusions of IR-induced signaling pathways. First, they are ROS-dependent and second, Ca^{2+} from the extracellular space is needed for the oscillatory signal.

3.2.3.1 **How to translate calcium oscillatory patterns?**

In order to determine how the calcium oscillations are generated and what their cellular function is, it is advisable to analyze the information provided by the oscillations itself in more detail. These oscillation properties can provide information not only about their origin, but also about their destination. Since the construction of an unique signal that is associated with a specific stimulus, calcium oscillations can be seen as an information encoding system. This includes not only amplitude- or dose-dependent discrimination, but also spatial restriction of Ca^{2+} signaling in microdomains (Dolmetsch and Lewis 1994; Politi et al. 2006; Di Capite et al. 2009; Parekh 2011).

In order to have homogeneous, precisely regulated oscillations, which are necessary to test the influence frequency and amplitude on downstream effects within T-cells, Berridge (1993, 1998, 2003 and 2009) developed the calcium clamp method. Experiments with the calcium clamp have shown that the sensitivity of different calcium dependent proteins to Ca^{2+}oscillations is highly frequency dependent in T-lymphocytes (Berridge and Dupont 1994; Dolmetsch and Lewis 1994; Dolmetsch et al. 1998; Tomida et al. 2003; Salazar et al. 2008). Referring to calcium-clamp experiments, **Figure 24** shows that the most prominent transcription factors in T-cells, NFκB, MAP kinases, NFAT, and calmodulin as an important signal mediator, differ markedly in their dependence on frequency. NFAT and MAP kinases and calmodulin require oscillations with frequencies of 2-1000 mHz, whereas NFκB shows activity at even lower frequencies (0.2-20 mHz) (Dolmetsch and Lewis 1994; Dolmetsch et al. 2001; Zhu et al. 2011; Smedler and Uhlén 2014).

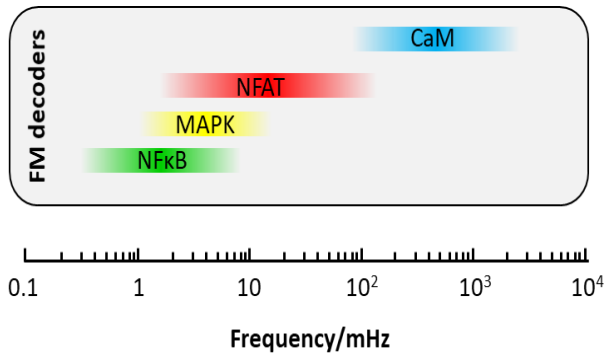

Figure 24: The activity of various calcium-dependent proteins is modulated by the frequency of calcium oscillations. Frequency decoders are modulated by specific oscillatory frequency plotted in a logarithmic scale. Frequency range necessary for appropriate T-cell activation is 0.3-1000 mHz. NFκB=nuclear factor 'kappa-light-chain-enhancer' of activated B-cells, MAPK=mitogen-activated protein kinases, NFAT=nuclear factor of activated T-cells and CaM=calmodulin. Modified according to Smedler, 2014.

However, calcium clamp is not the only method to investigate decoding properties of various calcium-dependent proteins. **Table 1** summarizes results of different studies with the aim to elucidate stimuli induced calcium responses in T-lymphocytes and **Figure 25** illustrates the provided data. The most surprising aspect is the frequency and amplitude range in relation to the basal Ca^{2+}_{cyt} level. Even this small range comprises mitogen (PHA), a well-known as T-cell stimuli (Lewis and Cahalan 1989), antigen (CD3/CD28), and IR induced responses. In addition, the temporal delay of induced calcium-oscillations after IR or antigen treatment are comparable, too. In contrast to this Tg stimulated cells show almost no delay in the generation of Ca^{2+}_{cyt} oscillations. Finally, it needs to be pointed out that all applied treatments have one thing in common; they are able to trigger NFAT activation, a hallmark of the T-lymphocyte activation (Tomida et al. 2003).

Table 1: Cytoplasmic calcium (Ca^{2+}_{cyt}) oscillation characteristics as a response to different stimuli.

	Frequency [mHz]	Amplitude [fold increase]	Delay [min]	NFAT activity	Published by
Calcium clamp	1-80	variable	/	✓	(Berridge and Dupont 1994; Smedler and Uhlén 2014)
PHA	˜ 10	˜ 4	˜ 3	✓	(Lewis and Cahalan 1989; Zweifach and Lewis 1993)
CD3+CD28 antigen	˜ 3.3	˜ 2	2 - 20 Ø=6	✓	(Xia et al. 2018)
Tg	persistent increase	˜ 4	< 1	✓	((D Kline and J T Kline 1992)
5 Gy IR	2- 4	˜ 6.6	10 – 72 Ø=52	?	/

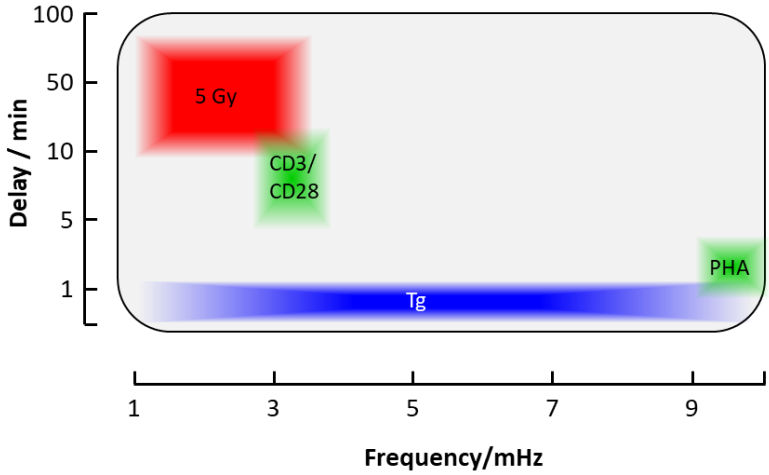

Figure 25: Cytoplasmatic calcium (Ca^{2+}_{cyt}) oscillation characteristics as a response to different stimuli. Data provided in Table 1 are illustrated as oscillation delay time post stimulation and plotted against the oscillation frequency.

Taken together, the investigations of different research groups provide important insights into the Ca^{2+}_{cyt} dynamics as a response to various T-cell activation stimuli. Comparing the frequency range in **Figure 24**, **Figure 25** and **Table 1** with the frequency analysis of my IR induced calcium oscillations, it is conspicuous that they fit perfectly into the perception range of proteins necessary for the T-cell activation machinery. In addition, the similarity in frequency, amplitude and delay time of IR and PHA/antigen treatment, but the difference in the delay time towards Tg treated cells leads to the assumption that IR triggered Ca^{2+}_{cyt} excursions are dependent on processes, which are upstream of ER Ca^{2+} depletion, such as PLC activation. All in all, it is very promising that IR provokes downstream processes, such as NFAT activation. Thus, it is able to stimulate T-cells similar to the physiological activation processes.

3.2.4 Perspectives

The present experiments were designed to determine the effect of X-ray on the behavior of the second messenger Ca^{2+}. The obtained findings of IR-induced oscillations lead to two follow up questions:

1. Which key steps of an IR-induced signaling pathway trigger the increase of calcium in the cell?
2. Which subsequent signal processes are initiated by the calcium oscillations?

From this point of view, based on the current data, there is for me no possibility to give an adequate answer but a hypothesis to the first question. As demonstrated in the previous chapter, IR leads to a transient increase in cytosolic as well as in mitochondrial H_2O_2. The chronologically later generated calcium oscillations can be prevented by the ROS scavengers NAC and DTT (**Figure 23**). This impairs that H_2O_2 is directly linked to the calcium signaling response post IR. Nevertheless, it is still unknown how the observations of a ROS-induced calcium response are causally related. The schematical illustration of **Figure 26** summarizes four different hypothetical possibilities for an RICR, where each option is explained in more detail below.

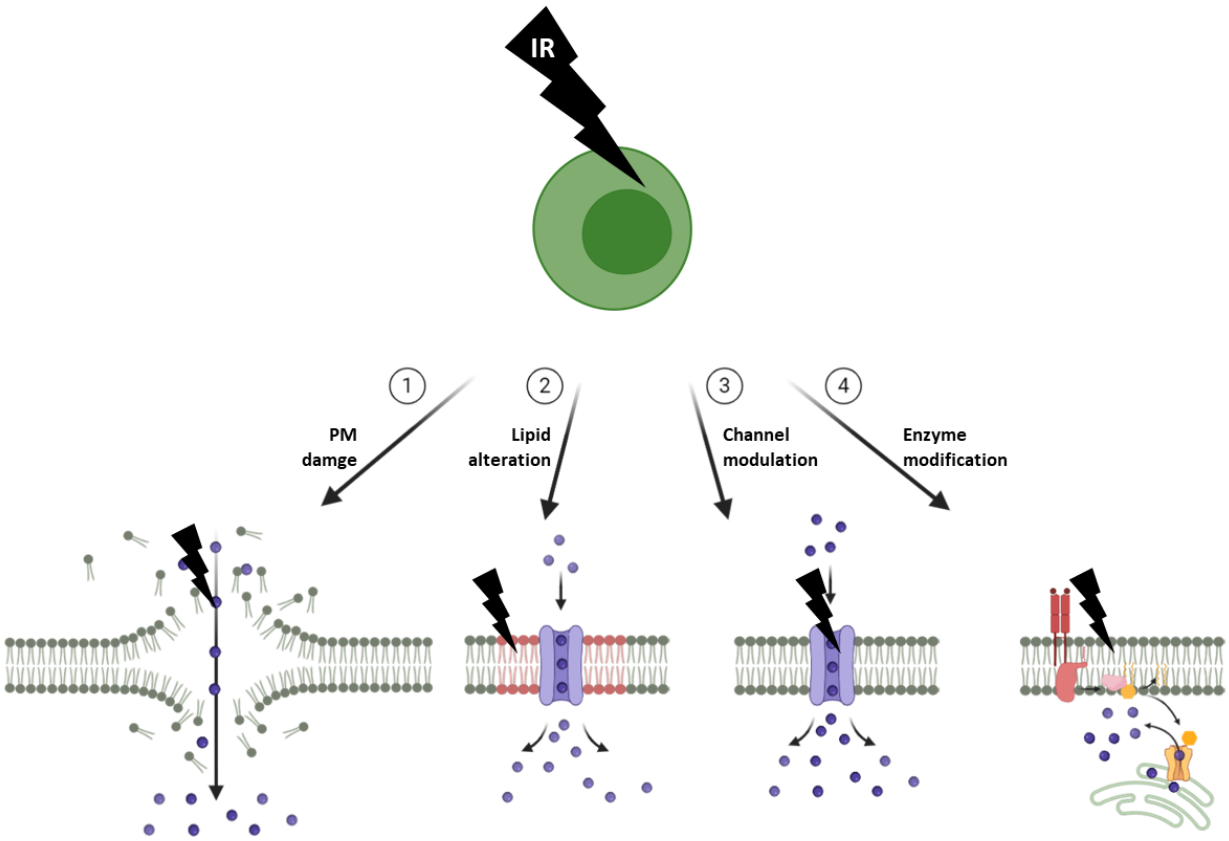

Figure 26: Schematic hypotheses on the effectiveness of IR on components of the plasma membrane (PM). IR could: 1. induce lipid damage, resulting in a defect barrier function of the PM. 2. induce lipid damage resulting in altered function of proteins located in the PM. 3. directly influence ion channel conductance or ion channel composition in the PM. 4. cause alterations in protein activity in the signaling pathway of T-cell activation via PLC and IP_3.

1. IR induces lipid damage, resulting in a defect barrier function of the PM

One possible explanation for ROS dependent Ca^{2+} influx is the interaction of ROS with the PM as it is the first mechanical barrier for X-rays. It is commonly approved that IR leads to lipid damage in the PM (Corre et al. 2010; Tomita et al. 2019; Ferranti et al. 2020). The most prominent damages are alterations in the PM fluidity and permeability. This is caused by IR-induced lipid peroxidation followed by fragmentation leading to the loss of the naturally barrier function of the membrane (Corre et al. 2010). Recently, Ferranti and colleges (2020) were able to show that IR directly induces PM permeability by the formation of lipid nanopores (Ferranti et al. 2020). Hence, it is conceivable that exposing cells to X-ray allows a direct influx of calcium ions into the cell interior through the IR-formed nanopores. A consequence of this scenario is a constant elevation of the calcium concentration. Returning increased calcium concentrations back to the basal low level mainly the calcium pumps SERCA (Odermatt et al. 1996), PMCA (Fresu et al. 1999), and MCU (Khodorov et al. 1999) are responsible. Buffering of the increased calcium concentration seems difficult, because the cells buffer capacity is limited but the calcium concentration gradient between the cells interior and exterior is extremely high. For this reason, directly IR-induced PM damage seems to be no satisfactory explanation for the precisely defined and regulated calcium excursions within the exposed cell.

2. IR is able to induce lipid damage resulting in altered function of proteins located in the PM

Besides its barrier function, the PM creates an environment that is crucial for the functionality of transmembrane proteins or PM-related proteins. Thus, ROS-induced alterations in the lipid composition can foster changes in the mentioned protein structures and functions. For example, it is demonstrated that PIP_2, the most important phospholipid for T-cell activation, which is located in the inner leaflet of the PM and target of PLC, can be directly influenced by oxidative conditions (Exton 1996). Therefore, the hydrolysis of PIP_2 into the two second messengers DAG and IP_3 occurs directly through the interaction of ROS, independent of the cleavage by the PLC. As a consequence, released IP_3 can maintain Ca^{2+} flux from the ER into the cytosol through the binding to its IP_3R. This described process confirms the idea of an association between irradiation and a regulated Ca^{2+} signaling mechanism.

3. IR is able to directly influence ion channel conductance and/or composition in the PM

Recent studies identified PM-related ion channels as novel targets of IR. The reported data support a direct effect of X-ray exposure, modifying electrical properties in Jurkat cells and PBMCs (Ghanshani et al. 2000; Cahalan and Chandy 2009; Roth et al. 2015). This phenomenon is caused by either a radiation induced elevation of the expression of different ion channels or an altered open probability of oxidized ion channels. In this context, an interesting finding is that the expression of calcium-dependent potassium channels KCa2.2. and KCa3.1 is upregulated 24 hours post IR, leading to a modified electrophysiological phenotype. This change is similar to the electrophysiological changes in T-cells during immunological activation, where the enhanced KCa3.1 expression is a direct marker for an immunological activation (Ghanshani et al. 2000; Voos et al. 2018). Consequently, it is conceivable that IR initiates the canonical calcium oscillatory pattern via direct modulation of ion channels in the exposed cells independent of the physiological T-cell activation pathway via TCR and PLC.

4. Alterations in protein activity in the common signaling pathway of T-cell activation via PLC and IP_3

Another possible explanation for an IR induced Ca^{2+} response is the direct modulation of key proteins in the common T-cell activation pathway. Different scientists demonstrated that many proteins in the T-cell activation cascade were influenced in their activity by X-rays, including IP_3R (Renard-Rooney et al. 1995), PLC (L Legendre et al. 1993) and calcineurin (Zhang et al. 1999). However, these studies do not fully explain which downstream signaling cascades could be initiated with the activation of the mentioned proteins. This highlights the still existing knowledge gap in the current radiation research and reflects the significance of my present work. Based on the publications mentioned above, it can be assumed that IR directly regulates the activity of the enzymes necessary for the immunological activation of T-cells. For instance, it is conceivable that radiation triggers a TCR-independent activation of PLC, leading to the initiation of the calcium signaling cascade with the canonical frequency and dose-dependent amplitude I observed.

All of the above mentioned IR-induced lipid or protein modulations highlight the huge complexity of possible non-nuclear IR targets and their mutual influence. Taken together, it is imaginable that radiation not only induces direct oxidative modulations of lipases, kinases or ion channels, but also indirect by changes of the lipid environment. One cellular key player in mediating calcium responses in T-cells that is thought to combine both, direct and indirect modulations caused by IR, is the CRAC channel. This channel has a crucial function in calcium signal transduction as it connects the SOCE with the calcium influx from the extracellular space. For this reason, the investigation of CRAC channel properties after irradiation is the subject of the following chapter.

3.3 Chapter 3 – IR induces CRAC channel formation

In this chapter, I designed the experiments for measurements with heterologous expressed STIM and Orai constructs and performed the analysis of endogenous channel components. Dr. Stephanie Hehlgans (Goethe University Frankfurt) provided support in handling peripheral blood mononuclear cells (PBMCs). Tim Sponagel mainly performed the experiments as part of his master thesis.

Abstract

In T-lymphocytes, the spatial and temporal regulation of cellular calcium signals is mainly initiated by a receptor-mediated release of calcium from cell-internal calcium stores, which is known as store-operated Ca^{2+} entry (SOCE). Key steps in the activation of immune cells are the generation of the second messenger inositol trisphosphate (IP_3) and the subsequent calcium efflux from the endoplasmatic reticulum (ER) into the cytosol via the IP_3 receptor (IP_3R). The following depletion of Ca^{2+} from internal stores evokes in a next step the functional interaction between stromal interaction molecule (STIM) in the ER and a Ca^{2+} pore forming protein (Orai) in the plasma membrane. The resulting functional Ca^{2+} release-activated Ca^{2+} (CRAC) channel is then mediating Ca^{2+} influx across the plasma membrane. This mechanism is described as Ca^{2+}-induced Ca^{2+}-release (CICR) and plays a major role in stimulus induced Ca^{2+} oscillations in immune cells. By using confocal microscopy, I monitored the cellular distribution of endogenous STIM and Orai after X-ray irradiation. These studies show in combination with live-cell imaging of heterologous expressed STIM-YFP and Orai-CFP, that X-ray exposure of Jurkat cells and PBMCs evokes in 50% of the monitored cells the formation of STIM/Orai clusters in the plasma membrane within 15 min post irradiation. This cluster formation is similar albeit approx. 3-5 times slower than that elicited by canonical T-cell activators. In terms of the temporal dynamics of the X-ray triggered formation of CRAC channels, falls roughly together with the IR induced calcium oscillations. The hypothesis that X-ray evoked CRAC channel formation is causally related to the Ca^{2+} oscillations is supported by experiments in which the latter were abolished by specific CRAC channel blocker Synta (10 µM).

3.3.1 Introduction

3.3.1.1 Store-operated Ca^{2+} entry (SOCE) – a main regulatory mechanism in T-cell activation

In non-electrical excitable cells, such as cells of the immune system, calcium signals are mainly generated by receptor-mediated release of calcium from cell-internal stores, for example by binding of the second messenger inositol triphosphate (IP_3) to its receptor in the ER membrane (Berridge et al. 2003; Decrock et al. 2013). However, in order to amplify this initially small calcium signal in the cytoplasm in response to receptor activation, it is necessary that calcium ions are additionally transported from the extracellular space through plasma membrane channels into the cell interior. Putney (1986) suspected early on that the calcium influx from the extracellular space is elicited and controlled by the initial emptying of intracellular Ca^{2+} stores in the ER (Putney 1986). Because of this causal relationship between store depletion and Ca^{2+} influx via plasma membrane channels this mechanism was described as store-operated Ca^{2+} entry or short SOCE.

3.3.1.2 SOCE is mediated by Ca^{2+} release-activated Ca^{2+} (CRAC) channels

Calcium fluxes across the plasma membrane caused by SOCE were measured in patch-clamp recordings and the current was coined since the early 90th as I_{CRAC} (Ca^{2+} release-activated Ca^{2+}) (Hoth and Penner 1992). It took several decades to identify the two molecules responsible which are responsible for the conductance of the respective calcium current and, which connect both calcium influxes at the plasma membrane and the filling status of the intracellular calcium stores. With the establishment of fluorescent dyes and high-resolution microscopy in the early 2000s the two proteins STIM and Orai could be identified as key components for conducting I_{CRAC}. It was found that the respective Ca^{2+} conducting channel is dynamically constructed by the interactions calcium sensor stromal interaction molecule (STIM) in the ER membrane with the plasma membrane-localized pore subunit Orai. Formation of this complex generates the functional Ca^{2+} release-activated Ca^{2+} (CRAC) channels, which conducts the influx of calcium into the cytoplasm along its concentration gradient (Feske et al. 2003; Gwack et al. 2007; Feske et al. 2012)

How is it possible, that two proteins, which are located in membranes of two different cellular organelles form together one functional calcium channel? To answer this question, it is important to consider the general structure of ion channels. In a very simplified view ion channels are composed of a modular structure that can be divided into a pore-forming domain and a regulatory-domain (Kawasaki et al. 2009). The aforementioned pore-forming subunit Orai is highly conserved throughout different ion channels. This general architecture of a channel is responsible for the appropriate ion selectivity and conductivity of the functional channels (Prakriya and Lewis 2003; Park et al. 2009). Regulatory domains of ion channels on the contrary are able to sense diverse stimuli including voltage, temperature, mechanical stretch or pressure, other ions, small molecules, pH, or other ligands (Berrier et al. 1996; Waldmann and Lazdunski 1998; Sampieri et al. 2018). If a particular stimulus generates a conformational change in the regulatory domain this structural information is directly transferred to the pore domain where it promotes opening or closing of the ion permeation pathway (Mangialavori et al. 2013). In other words, a structural alteration of the regulatory domain has a direct influence on the channel gating properties. This general scheme of ion channels can also be applied to the CRAC

channels in which Orai serves as the pore domain in the PM and STIM as a calcium-dependent regulatory domain in the ER membrane.

3.3.1.3 **The calcium sensing subunit: STIM**

Under resting conditions, the homodimer STIM consists of two single-pass transmembrane domains and the proteins are evenly distributed throughout the ER membrane. In this orientation the N-terminus of STIM is located in the ER lumen and the C-terminus in the cytoplasm (**Figure 27**). Importantly, the STIM N-terminus has two major functional domains: it contains high-affinity EF hand domains and a sterile α-motif (SAM) domain (Stathopulos et al. 2008; Ma et al. 2017). The EF hand domains of STIM bind luminal calcium ions in the ER with a dissociation constant (Kd) of about 200 µM. Thus, at physiologically high Ca^{2+} concentrations of approximately 600 µM in the ER the Ca^{2+} binding sites of STIM are saturated by Ca^{2+} ions. On the contrary the SAM domain functions as an oligomerizing subunit. Its main function is to activate the STIM protein by conformational change, which leads to translocation and oligomerization of the STIM homodimers. Therefore, the N-terminus of the molecule is responsible for both, its self-association sequence as well as its function as a calcium sensor (Park et al. 2009; Hogan et al. 2010; Soboloff et al. 2012).

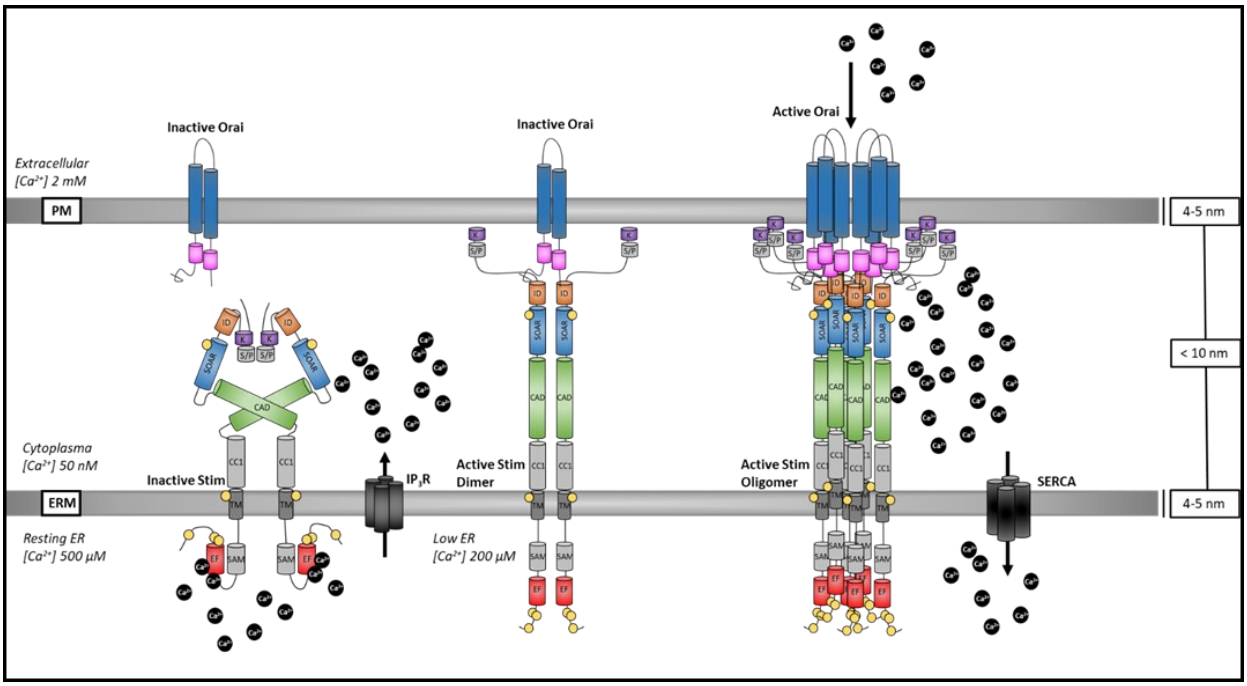

Figure 27: Schematic representation of the Stim/Orai interaction. Inactive Orai molecules in the plasma membrane (PM) and Stim molecules in the membrane of the endoplasmic reticulum (ERM) are present as dimers. If the calcium concentration in the ER decreases, due to calcium efflux through the inositol triphosphate receptor (IP3R), the conformation of the stim dimers changes, causing them to combine into oligomers. As oligomers, these bind to Orai oligomers and thus form a functional calcium channel. K= lysine rich region, S/P= serine/proline rich region, ID= inactivation domain, SOAR= STIM/Orai activating region, CAD= channel activating domain, CC1= coiled-coil domain, TM= transmembrane domain, SAM= sterile alpha motif, EF= EF-hand calcium sensing domain

The cytosolic C-terminus of STIM contains three coiled-coil domains (CC1-3), the STIM/Orai activation region (SOAR), which is also known as CRAC activation domain (CAD) and a highly polybasic tail. All C-terminal domains are involved in establishing physical contact to the PM and the PM located Orai pore-domain (Hogan et al. 2010; Nwokonko et al. 2018).

3.3.1.4 **The pore domain: Orai**

An Orai subunit comprises four transmembrane domains (TM1-4) where both, the C- and N-terminus, are localized in the cytoplasm of the cell allowing an interaction with the STIM-C-terminus. In TM1, the amino acid glutamic acid at position 106 (E106), probably serves as a pore-forming calcium binding site in the CRAC channel and is therefore essential for its calcium selectivity. It is assumed that in total six E106 are involved in the formation of the pore ring, serving as a selectivity filter for calcium in functional CRAC channels (Cai et al. 2018). For this reason, it is thought that the functional CRAC channel consists of six Orai1 subunits and forms a hexameric calcium channel (**Figure 27**) (Nguyen et al. 2018). Nevertheless, much about the exact structure of the CRAC channels is still unknown.

3.3.1.5 **How are CRAC channels sufficiently activated?**

A drop in the calcium concentration inside the ER lumen which is triggered by the binding of IP_3 to its ER located calcium conducting receptor, evokes a dissociation of calcium ions from the EF hand domain in the STIM protein (Stathopulos et al. 2008; Ma et al. 2017). This is accompanied by a conformational change of the whole molecule involving interactions of both SAM domains in a dimer. As a result, the protein changes from a bended into a stretched form whereby the coiled-coil domains protrude even more into the cytoplasm. This STIM dimer activation induces the oligomerization of several STIM-dimers to stable multimers.

The emerging multimers further translocate to constriction sides between ER- and plasma membrane, which is enabled by the interaction of the polybasic C-terminal tail with the lipids of the PM (Stathopulos et al. 2008; Ma et al. 2017). In these constrictions sites, in which both membranes are separated by only 10-15 nm SOAR domain of STIM and the C terminus of Orai physically interact (Barr et al. 2009; Park et al. 2009; Covington et al. 2010). One SOAR dimer interacts with one Orai protein to build a functional CRAC channel. These clusters of functional STIM/Orai are typically visible as so-called *puncta* in microscopic images in the plasma membrane of cells. As a result of the physical interaction of the two protein components the CRAC channels open by movements in the transmembrane helices TM1 and TM4 (Shim et al. 2015) and Ca^{2+} ions are able to flow inside the cell down of the steep electrochemical gradient. In addition, it was also shown that dimers of two SOAR domains alone are capable opening CRAC channels. This probably represent an essential component in the activation of the channels (Lee et al. 2009). Another interesting finding, which is important in the context of the present study is that STIM proteins can not only be activated by empty ER stores but by many cellular stress reactions. Recent studies have shown that STIM is activated by oxidative stress, temperature changes or a decreasing pH. All these stimuli are able to initiate relevant calcium signaling cascades in the affected cell (Soboloff et al. 2011).

3.3.1.6 **How is an inactivation of CRAC channels achieved?**

Not only the activation but also the inactivation of SOCE must be precisely regulated to prevent long-term increase of Ca^{2+} and subsequent apoptosis signals or excessive activation of downstream signaling cascades. If has been shown that this deactivation or decoupling of STIM and Orai is mainly achieved by negative feedback through two inactivation mechanisms. First, a rapid Ca^{2+} dependent inactivation (CDI) of the hexameric Orai subunit prevents further calcium influx into the cell (Zweifach and Lewis

1995). Second, a slow dissociation of the STIM-Orai complex takes place with high Ca^{2+}-concentrations, which is accompanied by a disaggregation of STIM multimers. Presumably, an increasing luminal calcium concentration in the ER initiates the separation of the two interaction partners (Wang et al. 2009; Wang et al. 2014). Furthermore, also other cellular proteins seem to be involved in the regulation of CRAC channels: The cytoplasmic CRAC regulatory protein 2A (CRACR2A) serves to stabilize STIM-Orai interactions during SOCE. As soon as the Ca^{2+}_{cyt} at intracellular ER/ PM constriction sides increases, calcium binds to the EF hand motifs in CRACR2A and promotes dissociation of the protein from the STIM-Orai complex and subsequent to the destabilization of their interaction (Wang et al. 2014; Zheng et al. 2018; Zhou et al. 2018).

In addition, calmodulin, a Ca^{2+}-binding regulatory protein, has been shown to be an important mediator of the Orai CDI; it causes inactivation by its direct binding to Orai. Calmodulin binding occurs at the N-terminus of Orai1 near the STIM1 interaction region where it partially inhibits further calcium influx through CRAC channels (Park et al. 2009). However, the exact regulatory mechanism of STIM and Orai is still subject of ongoing research.

3.3.2 Results

3.3.2.1 CRAC channels are essential for IR induced calcium signaling

Data in chapter 2 have suggested that may CICR also play an essential role in an IR induced calcium signaling pathway in Jurkat cells. The experiment in which the Ca^{2+} channel blocker Gd^{3+} abolished IR induced calcium oscillations already underlines that the initiation of this signaling cascade requires a channel mediated influx of Ca^{2+} from the extracellular space into the cytosol.

In a next step I tested whether the CRAC channels are involved in IR induced calcium oscillations (**Chapter 2**). Previous experiments shown in **Figure 19** were therefore repeated in the presence of 5 µM of the specific CRAC channel inhibitor, Synta (Derler et al. 2013). Like in the protocol used for experiments in in chapter 2 Jurkat cells were loaded with Fluo4 and exposed to 5 Gy X-ray. The exemplary data from a continuous monitoring of Fluo4 fluorescence (**Figure 28**) shows that inhibition of the CRAC channels prevents the occurrence of calcium oscillations. This result was confirmed in a monitoring of 26 cells, which were treated in the same manner. The probability of observing Ca^{2+}_{cyt} oscillations in response to IR treatment decreases from 58% in the absence of the CRAC channel blocker to 30% in its presence. While the typical oscillations disappear in the presence of the CRAC channel blocker the mean value of baseline fluorescence still increases after IR treatment (see base line in **Figure 28**). This indicates that radiation is still causing some elevation of Ca^{2+}_{cyt} in Jurkat cells, which may enter via other types of Ca^{2+} channels in these cells (**Figure 28**).

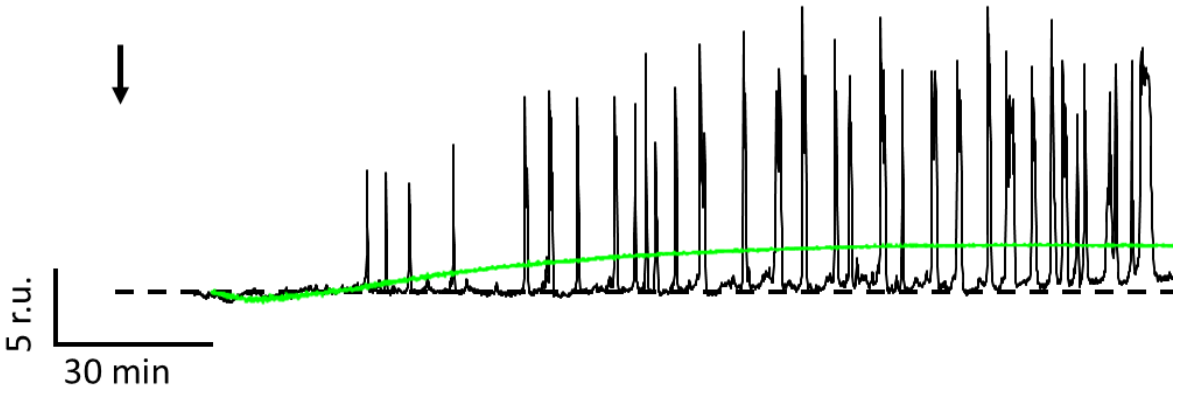

Figure 28: Ca^{2+}_{cyt} oscillations can be suppressed by the inhibition of CRAC channels. Representative long-term measurements of Fluo4 intensity as measure of changes in cytosolic Ca^{2+}_{cyt} in Jurkat cells, irradiated with either 5 Gy X-ray (black) or additionally treated with 10 µM CRAC channel inhibitor Synta (green) 30 min prior to exposure. All Ca^{2+}_{cyt} measurements were performed in buffer containing 2 mM Ca^{2+}.

The results of this experiment show that the prevention of Ca^{2+} influx via CRAC channels also prevent Ca^{2+}_{cyt} oscillations per se in a subpopulation of Jurkat cells. Hence, in comparison to the measurements with calcium-free EGTA solution (**Figure 22**) there is still a higher steady increase in Ca^{2+}_{cyt}. Due to the fact that the IR induced oscillations are largely prevented by the CRAC channel inhibitor, I suggest that this calcium channel is mainly responsible for either; the initiation of the oscillations or the persistence of the calcium oscillations.

3.3.2.2 In resting Jurkat cells endogenous STIM is located in the ER and Orai in the PM

In order to further characterize the function of CRAC channels during the calcium response of irradiated cells, I imaged in Jurkat cells, which were fixed in their resting state, STIM and Orai labeled with an Alexa (Alx) fluorescent antibody. This provides information on the cellular distribution of the two channel forming subdomains.

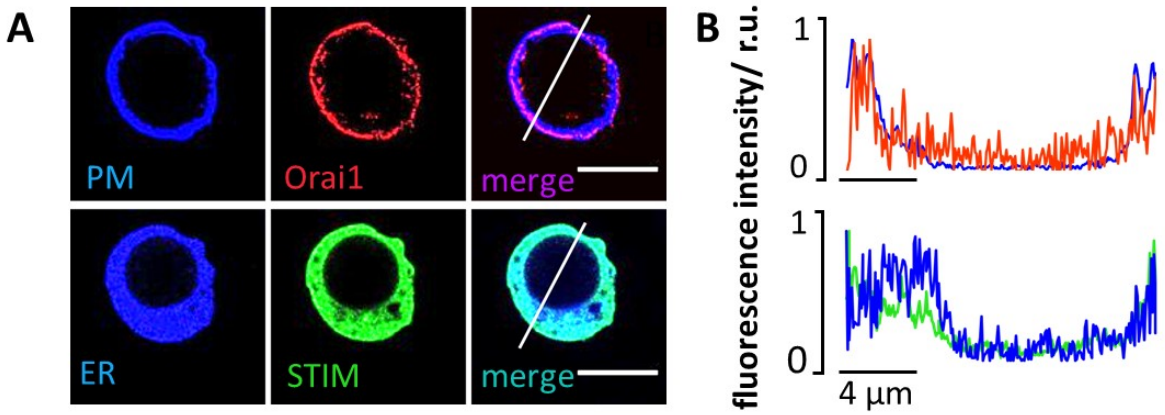

Figure 29: In resting Jurkat cells STIM is located in the ER and Orai in the PM. (**A**) Confocal images of cellular distribution of endogenous Orai (upper panel) and STIM (lower panel) in unstimulated control Jurkat cells. Immunofluorescence was obtained by staining fixed Alx488 or Alx647 secondary antibody respectively (central column). Additionally, the plasma membrane was visualized with the plasma membrane tracker CellMaskOrange and the ER with ER-tracker red (left column). An overlay of both channels is shown in right column. (**B**) Line Plots for each marker were taken in positions report in merge images. Fluorescence intensity of either Orai1/PM (upper panel) or STIM1/ER (lower panel) were normalized to the highest value of each signal; the colors of line plots correspond to those in images. Scale bar = 10 µm.

The representative confocal images in **Figure 29A** show the typical distribution of the two CRAC channel forming components in these unstimulated cells. The Orai domain is evenly distributed in the cell periphery (**Figure 29A upper trace**) while the STIM protein generates a diffuse signal throughout the cytosol (**Figure 29A lower trace**). For a localization of the two proteins the cells were also staining with CellMaskOrange or ER-Tracker red to label the plasma membrane and the ER respectively. The images in **Figure 29A** show that Orai colocalizes with the PM marker and STIM with the ER marker. This positive colocalization between the protein and the organelle markers is furthermore conformed by the intensity plots **Figure 29B.** The Line Plots for each marker were taken in positions report in the merge images. The fluorescence intensity of either Orai1/PM (**Figure 29** upper trace) or STIM1/ER (**Figure 29** lower trace) were normalized to the highest value of each signal. The data illustrate again the visual impression form the images in that the CRAC channel subdomains colocalize with the plasma membrane (Orai) and the ER (STIM).

3.3.2.3 Endogenous STIM and Orai accumulate and form distinct *puncta* post X-ray exposure

It is well established that ER store depletion triggers the interaction between STIM and Orai, which becomes evident in the form of clusters in the plasma membrane. This process can be imitated by addition of the SERCA inhibitor thapsigargin (Thastrup et al. 1990; Y Sagara and G Inesi 1991).

Figure 30A shows the cellular distribution of endogenous STIM and Orai again stained with Alx fluophors. The images are from cells which were fixed in the unstimulated state or from cells fixed 15 min after treatment with 2 µM Tg. While the cellular distribution of STIM and Orai appears as expected diffuse in the resting Jurkat cells a stimulation with Tg leads to a translocation of STIM proteins from the ER to the plasma membrane. There the proteins colocalize with the Orai domains in distinct clusters in 76% of the treated cells.

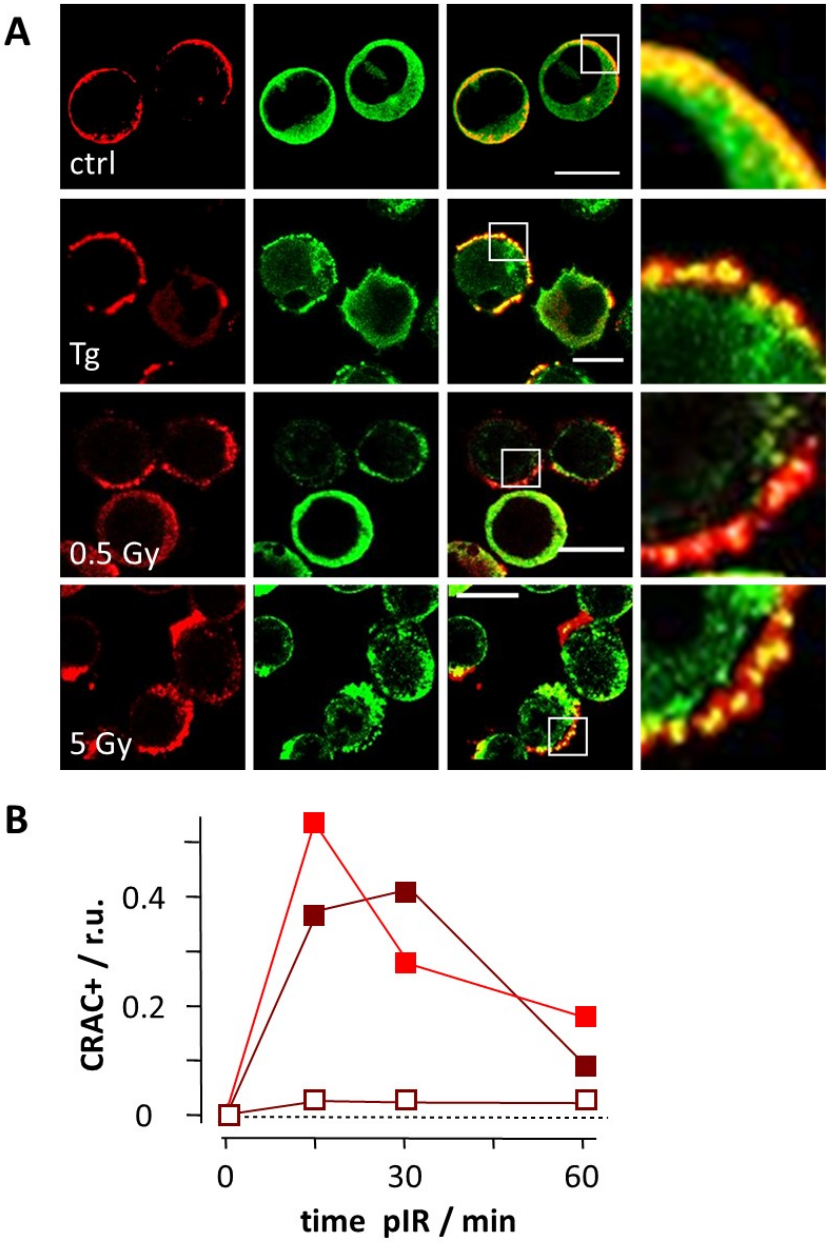

Figure 30: Ionizing radiation triggers Ca^{2+} regulated endogenous STIM/ORAI CRAC channel formation. (**A**) Distribution of auf endogenous STIM1 (green 1st column) and ORAI1 (red 2nd column) in Jurkat cells immunostained with Alx488 and Alx647, respectively. An overlay of green and red channel with blow up of indicated area are shown in (3rd and 4th columns). Fixed cells were obtained from untreated cells (ctrl) (top row), cell treated for 15 min with 2 µM thapsigargin (2nd row) or from cells 15 min after X-ray exposure to 0.5 Gy (third row) or 5 Gy (bottom row). (**B**) Relative number of monitored Jurkat cells with positive clustering of STIM/Orai fixed 15, 30 or 60 min after irradiation with 0.5 Gy (unfilled, dark red), 1,5 Gy (dark red) or 5 Gy X-ray (light red). Dotted line indicates level of non-reacting cells. For each condition ≥ 282 cells were analyzed. Scale bar = 10 µm.

In further experiments Jurkat cells were exposed to X-ray irradiation and the formation of CRAC channel clusters monitored in the same manner. Therefore, cells were fixed 15, 30, 60 min respectively after exposure to X-ray irradiation from 0.5 to 5 Gy before immunostaining at different timepoints. **Figure 30A** shows that this treatment triggers the same type of STIM and Orai clustering in plasma membrane as the positive control Tg. A quantitative analysis shows that the number of cells which exhibit clustering after stimulation varies significantly with the X-ray doses. Important to note that even a low dose of 0.5 Gy is albeit in a low number of cells, still able to induce clustering. The relative number of stimulated cells showing distinct STIM/Orai puncta are reported in **Figure 30B** as a function of time. Already 15 minutes after irradiation a maximal clustering of both proteins was observed in 51% of the analyzed cells exposed to 5 Gy X-ray before the signal gradually decreased (**Figure 30B**). A similar transient clustering of STIM and Orai was evident after 1.5 Gy X-ray exposure. In experiments with 0.5 Gy it was still possible to detect individual cells with a clear clustering of the two proteins (**Figure 30B**). The numbers however were too low for a robust statistical analysis.

The results of these experiments confirm that X-ray exposure enables dose-dependent STIM/ Orai aggregation in Jurkat cells almost identical to the artificial induced SOCE by Tg. Immunostaining of endogenous STIM/Orai proteins indicates that irradiation with X-rays leads to clustering and presumably to activation of CRAC channels. This process occurs in a dose-dependent manner several minutes after X-ray irradiation. To better describe the kinetics of CRAC channel assembly, I employed in a further experiments Jurkat cells transiently expressing STIM1::eYFP and Orai1::eCFP. The advantage of this experimental approach is that the cells do not have to be fixed, so that live-cell confocal imaging can be used to monitor the dynamics of STIM/Orai clustering in real time.

3.3.2.4 In resting Jurkat cells transient expressed STIM-YFP is located in the ER and Orai-CFP in the PM

For a better understanding of the X-ray triggered CRAC channel assembly kinetics described in the previous section, co-expression of STIM1::eYFP and Orai1::eCFP in Jurkat cells allows cellular localization of the two subunits by live-cell real-time confocal microscopy. In a first step I verified the cellular distribution of STIM-YFP or Orai-CFP within unstimulated control cells. Representative images in **Figure 31A** illustrate that the distribution of the CRAC channel subunits in these cells similar to that of the endogenous proteins (**Figure 29**). This visual impression is supported by the perfect colocalization of Orai/PM and STIM/ER markers in line plots (**Figure 31B**.)

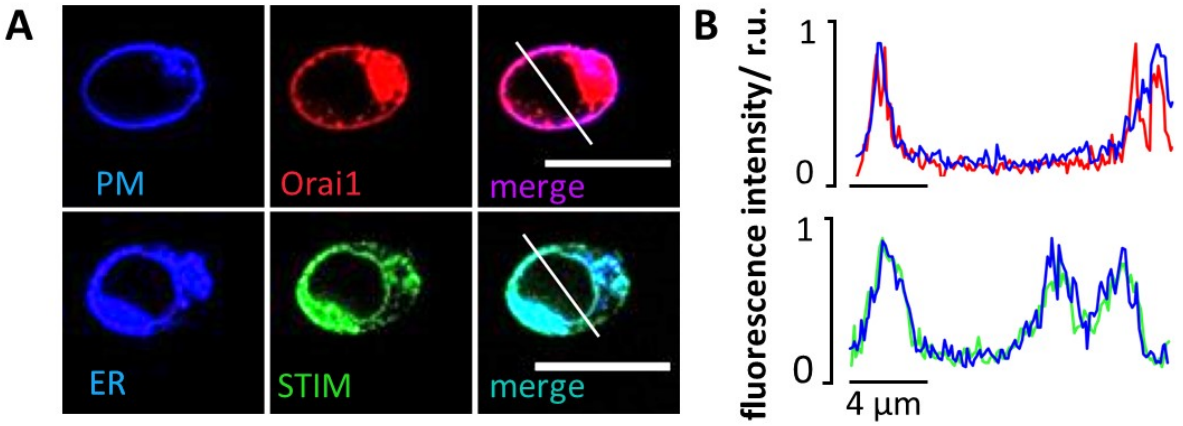

Figure 31: Heterologous expressed STIM-YFP is located in the ER and Orai-CFP in the PM in Jurkat cells. (**A**) Confocal images of cellular distribution of heterologous expressed Orai-CFP (upper panel) and STIM-YFP (lower panel) in unstimulated control cells. Additionally, the plasma membrane was visualized with the plasma membrane tracker CellMaskOrange and the ER with ER-tracker red (left column). An overlay of both channels is shown in right column. (**B**) Line Plots for each marker were taken in positions report in merge images. Fluorescence intensity of either Orai/PM (upper panel) or STIM/ER (lower panel) were normalized to the highest value of each signal; the colors of line plots correspond to those in images. Scale bar = 10 µm.

3.3.2.5 IR induces CRAC channel formation of heterologous expressed STIM-YFP and Orai-CFP

Next, I monitored STIM-YFP and Orai-CFP expressing control cells for a total of 30 min in which an image was taken every 30 s. The experiments were repeated with either addition of 2 µM Tg or 25 µL/mL ImmunoCult human CD3/CD28/CD2 T-cell activator (T-Act). Both stimuli were added immediately before the measurement started.

To quantify the physical interaction of STIM and Orai is to use the excitation spectrum of STIM and the emission spectrum of Orai for measuring protein/protein interactions by FRET (Förster resonance energy transfer). **Figure 32** summarizes the results of the live-cell imaging on the STIM/Orai distribution kinetics. Representative images of either the Orai subdomain (left panel), STIM (central panel) or the resulting heat map of the FRET value (right panel) in response to the aforementioned treatments are shown in **Figure 32A**. The images report the corresponding time point of maximal colocalization of STIM and Orai, which is given by the largest FRET value. The calculated FRETc value is then plotted as an average ± SD of ≥ 5 individual cells in **Figure 32B**.

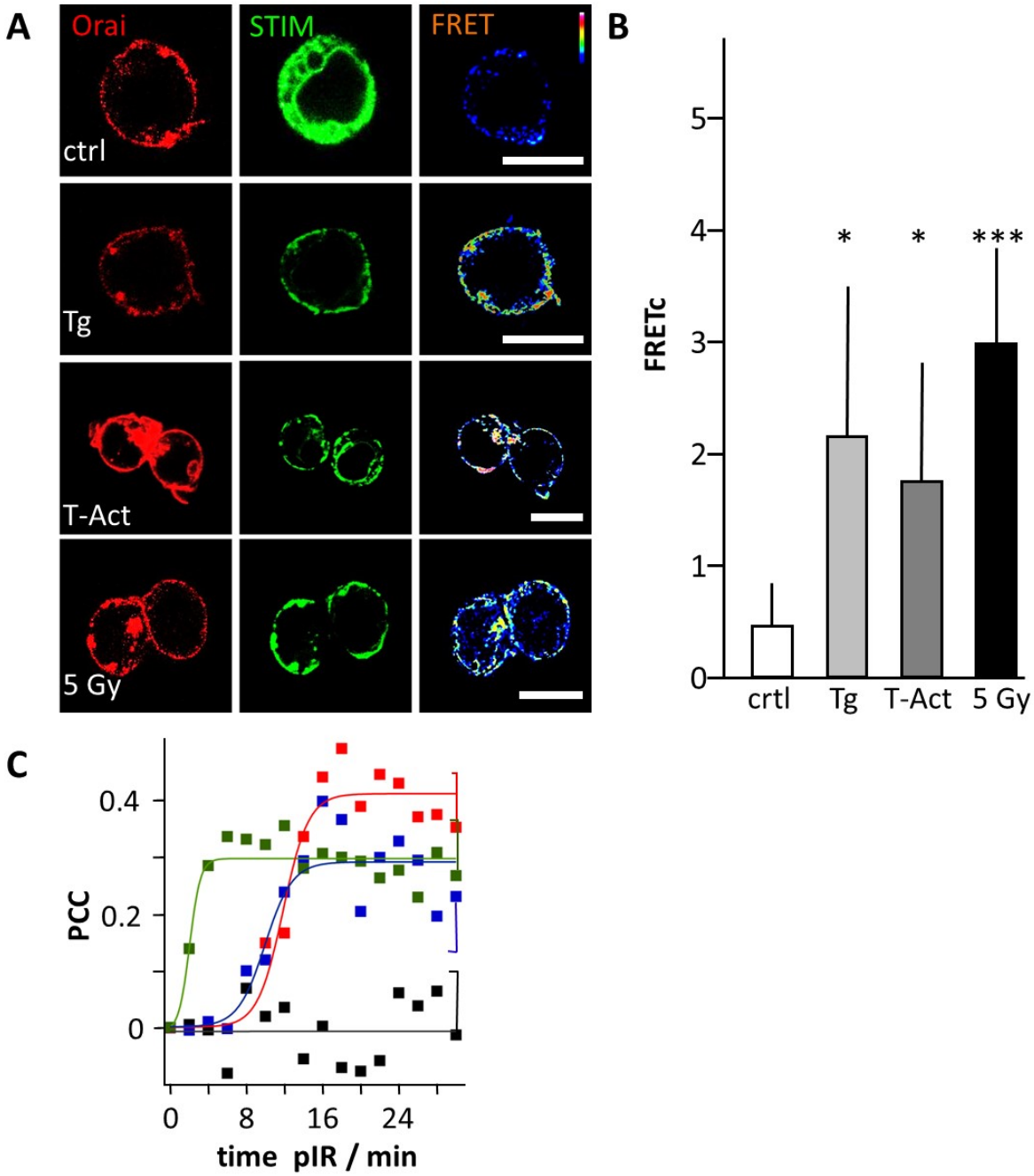

Figure 32: Live-cell analysis revealed an IR-triggered, Ca^{2+}-regulated CRAC channel formation of heterologous expressed STIM/Orai. (**A**) Representative confocal images of same cells with fluorescent donor molecule Orai1-eCFP (red, 1st column), acceptor molecule STIM1-eYFP (green, 2nd column) and heat maps of the resulting FRET signals (3rd column). Images are from untreated cells (ctrl), or cells incubated with 2 µM thapsigargin, 25 µL/mL activator (T-Act) or irradiated with 5 Gy X-ray. Scale bar = 10 µm. (**B**) Average of maximal FRET signal (± SD, n≥5 cells) from plasma membrane of cells treated as in A. The FRET signal from treated cells is significantly higher than the control value (*P < 0.05, ***P < 0.001 from Student-test) (**C**) Pearson correlation coefficient (PC) for colocalization of STIM1-eYFP and Orai1-eCFP. Data obtained from confocal live-cell real-time acquisition of Jurkat cells heterologous expressing the two proteins. After normalizing the start value of all treatments, the PC value remains in control cells (black) but increases with different kinetics in cells stimulated with 2 µM thapsigargin (green), 25 µL/mL T-Act (blue) or 5 Gy X-rays (red). The data were fitted with logistic equation (solid lines) yielding the following times for maximal increase in STIM/Orai colocalization: 2 min Tg, 10 min T-Act, 12 min 5 Gy X-ray. Data are mean values ±SD from ≥ 5 independent experiments. The mean SD is shown on the last data points.

Similar to the fluorescence analyses of endogenous STIM and Orai subunits (**Figure 30**), the heterologous expressed constructs are in unstimulated cells also distributed in PM (Orai) and ER (STIM). The CRAC channel subdomains colocalize only very weakly in control cells, which is illustrated by a low FRET signal (0.57 ± 0.47). The positive stimulus Tg, triggers moment of STIM towards the PM and colocalization with Orai. Accessorily, individual clusters can be recognized. The heat map of the FRET channel (2.18 ± 1.56) underpins that this pattern is due to a strong superposition of STIM and Orai. Comparable phenomena are also obtained after treatment of the cells with T-Act or 5 Gy X-ray. In the first scenario the energy transfer between both proteins increased significantly to a value of 1.87 ± 1.27. Remarkably, an even larger energy transfer of 3.47 ± 0.98 was measured in response to cells irradiated with 5 Gy X-ray. Taken together the FRET measurements confirm that stimulation of Jurkats cells not only with known stimuli like Tg, and T-Act but also with X-ray triggers an interaction between STIM and Orai over a distance <than 10 nm. Collectively the data suggest that the same interaction between the channel components, which is already well established for stimulation with Tg is also occurring after X-ray irradiation.

At this point the data confirm a physical interaction between STIM and Orai after different stimuli including X-ray irradiation. The data however provide no information on the kinetics of this process. To obtain information on the dynamics of CRAC channel formation the time course for stimulus-induced STIM/Orai clustering in Jurkat cells was monitored in cells coexpressing both proteins. For quantification of their colocalization the Pearson correlation coefficient (PCC) was employed. This parameter calculates the linear dependence between two variables, here the fluorescence intensity of STIM and Orai. The PCC can have values between -1 and +1. A value of +1 (or -1) results in a completely positive (or negative) linear relationship between the two parameters of interest. If the correlation coefficient approaches the value 0, the two parameters are not linearly dependent or in other words not correlated at all. The mean PCC values of STIM/Orai colocalization ± SD was estimated at different time points for > 8 cells. The values are s expressed as a function of time in **Figure 32C**. The mean colocalization values in unstimulated cells are as expected low (PCC=0.3 ± 0.08); they remain low in unstimulated cells over a time period of 30 min (**Figure 32C**). After stimulation the PCC value increased rapidly within ~2 min in response to Tg (PCC=0.76 ± 0.05) and slower ~12 min after adding T-Act (PCC=0.79 ± 0.04). The X-ray induced increase in STIM1/Orai1 cluster formation progressed with the same slow kinetics of the activator to a maximal PCC value of 0.79 ± 0.06. The kinetics of changes in the PCC values of Tg, T-Ac or radiation stimulated cells could be fitted by a logistic **Equation 5**:

$$Y = \frac{a}{(1 + e - k^{(x-xo)})}$$

Equation 5

where a is the maximal PCC value, k the rate of increase and xo the time of maximal PCC value increase. Worth noting is that the time point of maximal increase in STIM-YFP or Orai-CFP colocalization at about ~12 min after exposing Jurkats to 5 Gy X-ray, is in good agreement with data from cells which were fixed for the analysis (**Figure 30**). Also, in these experiments X-ray stimulation had already triggered a major clustering of endogenous STIM and Orai 15 min after irradiation (**Figure 30**). Another important finding it that CRAC channel formation, which is evident from *puncta* formation, is visible in a time

window between 10-20 min post irradiation. This time window corresponds well to the onset of Ca^{2+} oscillations after irradiation further suggesting that the formation of CRAC channels is responsible for the Ca^{2+} signaling. This conclusion is in good agreement with the data that show that the CRAC channel inhibitor Synta abolishes these IR induced calcium oscillation (**Figure 28**).

3.3.2.6 **CRAC channel formation post irradiation is a canonical effect in T-Lymphocytes**

The Jurkat cell line are a leukemic T-cell line, serving as a model system for uncovering basic signaling events engaged in T-cell activation (Abraham and Weiss 2004). Because of their tumor cell nature, they are unlike naïve T-cells continuously proliferating. This bears the possibility that they respond differently to naïve T-lymphocytes. To test whether the radiation triggered Ca^{2+} signaling cascade in Jurkat cells also occurs in naïve T-cells the immunofluorescence staining experiments of endogenous STIM and Orai were repeated in peripheral blood mononuclear cells (PBMC).

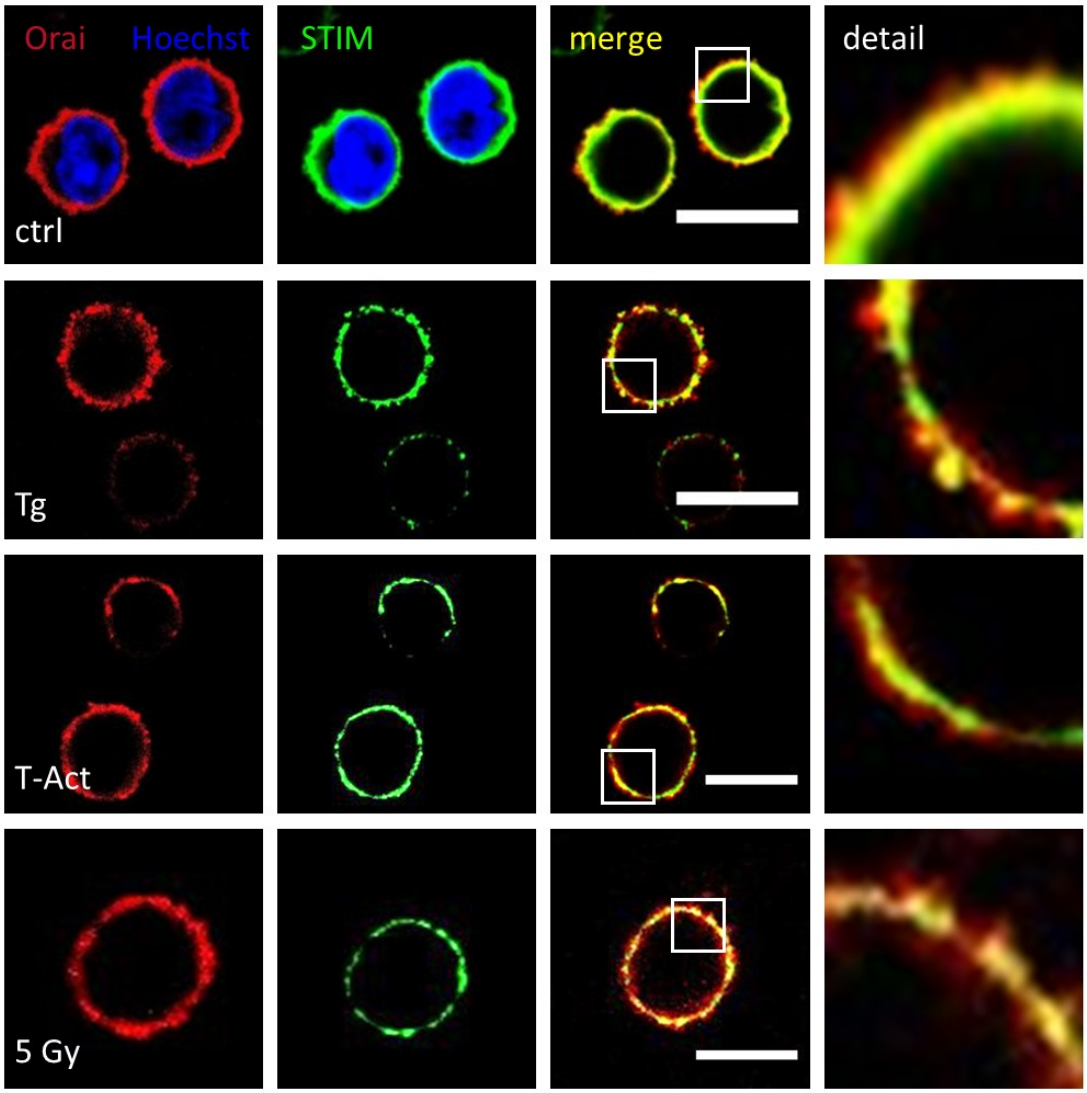

Figure 33: IR induced SOCE pathway is also initiated in naïve T-lymphocytes. Distribution auf endogenous Orai (red, left column) and STIM1 (green, 2nd column) in fixed PBMCs immuno-stained with Alx488 and Alx647 respectively. A merged composition of the two channels is shown in the 3rd column with a higher magnification of the marked area in the right column. In control cells (ctrl) also the nucleus is additionally stained with Hoechst dye (blue). Cells were fixed either 15 min after treatment with 2 µM thapsigargin (Top), 25 µl/ml T-cell activator cocktail (T-Act), or 15 min after exposing cells to 5 Gy X-ray. Scale bar = 10 µm.

The representative images in **Figure 33** indicate that the cytosol volume of non-stimulated lymphocytes is even smaller than that of Jurkat cells, because of their huge nucleus. This makes it even more difficult to detect a translocation of STIM from the ER to the plasma membrane. A comparative analysis nonetheless shows that the Orai and STIM distribution remain uniform in unstimulated control cells while they exhibit a distinct clustering after stimulation with 2 µM Tg in 75% of the treated cells. The same clustering of both proteins is also evident in 48% PBMCs after exposing them to 5 Gy X-ray. This underscores that the IR induced Ca^{2+} signaling cascade is a general response of resting T-cells.

3.3.3 Conclusion

In this chapter I wanted to determine if the CRAC channels, being responsible for the SOCE, are also involved in eliciting IR-induced calcium oscillation. The data showed that the X-ray triggered signal response depends critically on Ca^{2+} influx across the plasma membrane, as they terminated immediately upon the removal of extracellular Ca^{2+} by the addition of 5 µM EGTA, 5 µM Gd^{3+} or 10 µM CRAC channel inhibitor Synta. Further colocalization studies based on immunofluorescence staining of endogenous STIM and Orai subunits as well as live-cell analysis of the transiently expressed STIM-YFP and Orai-CFP proteins, confirm the assumption of IR induced activation of CRAC channels in Jurkat cells as well as in PBMCs. Both methods showed similar kinetics of CRAC channel assembly. Furthermore, an important finding is that Tg elicits a fast *puncta* formation (< 4min) whereas *puncta* formation after stimulation with T-Act or X-ray is rather slow (>10 min). This dynamic range of CRAC channel formation is in good agreement with data from the literature. Formina and colleagues (2000) demonstrated that a treatment of Jurkat cells with either IP_3 or Tg results in an I_{CRAC} 1-6 min post treatment (Fomina et al. 2000), which perfectly fits to the data I collected. This Tg-triggered current increases 2.7-4.7 times compared to the basal level (Lioudyno et al. 2008), which is also in the same range I monitored during FRET measurements. Stimulation of the TCR, by cross-linking antibodies (CD3/CD28) or mitogenic lectins (PHA) can also elicit CRAC channel formation 3-6 min post addition (Fomina et al. 2000; Lioudyno et al. 2008). Taken these studies into account I support the idea of IR triggered CRAC channel assembly, which takes place at a very similar time frame as under physiological conditions. This also accords with earlier observations showing that calcium oscillations are not instantaneously generated post exposition but with 10-60 min of delay. Not only the temporal component of CRAC channel activation and the beginning of calcium oscillations coincide, but also the number of reacting cells. Thus, irradiation leads to the above mentioned effects in 50% of the analyzed cells. Finally, these results provide further support for the hypothesis that CRAC channels play an elementary role in the calcium response of exposed cells. Furthermore, this combination of findings provides support for the conceptual premise that X-ray leads to an activation process in a subpopulation of irradiated T-lymphocytes comparable to an antigen-mediated response.

3.3.4 Perspectives

The present work provides new insights into the complex relationship between radiation as a stimulus to induce an increase in the intracellular H_2O_2 concentration, resulting in an altered CRAC channel function, which is followed by precisely regulated oscillatory calcium signals. However, it is still unknown which mechanism triggers IR-induced CRAC channel activation. To answer this question, three different hypotheses are conceivable. First, as described in the previous chapter IR can cause lipid damage through oxidation resulting in an altered lipid environment and function of Orai. Consequently, the pore domain opens due to a change of its conformation and a calcium influx is created. Second, a direct influence on IP_3R, SERCA, PMCA, STIM or/and Orai properties through oxidation is possible, which would lead to CRAC channel assembly and a calcium response with almost no delay between exposure and the signal. Third, the oxidative environment can lead to alterations in protein activity in the common T-cell activation pathway via PLC and IP_3. According to the literature and the present data a Tg triggered CRAC channel assembly and a resulting calcium influx occurs approximately 5-10 times faster than upon cross-linking antibodies, mitogenic lectins, and radiation (Lioudyno et al. 2008; Xia et al. 2018). These temporal similarities of TCR stimulated and IR stimulated effects support that comparable mechanisms upstream of Tg intervention for the CRAC channel formation including PLC activation take place. Despite these promising assumption, further studies with the focus on IR induced PLC activation can contribute to the explanation of the mentioned effects.

In order to further validate the above mentioned suggestions, the following describes in more detail how proteins essential for physiological T-cell activation can be influenced in their functional state by X-ray exposure.

3.3.4.1 **Cysteine residues – How can IR influence the structure and function of a protein?**

Several amino acid residues have a higher tendency to react with oxidants, including thiolate anions of cysteine residues as one of the most important redox signaling targets. Hence, the thiolate is rapidly oxidized to sulfenic acid in the presence of oxidizing stress including H_2O_2. This oxidation causes different modifications within the amino acid structure of the protein like disulfide bond formation with other thiols, either intra- or intermolecular (Buhrman et al. 2005; Dröse and Brandt 2012). Subsequently, the newly formed disulfide bonds can manipulate not only the proteins structure, but also its entire activation state. In this context, it is already confirmed, that high levels of oxidative stress can induce cytoplasmic Ca^{2+} elevation through oxidized channels located in the PM (Hempel and Trebak 2017).

3.3.4.2 **STIM and Orai are redox sensitive**

Several studies demonstrated that the calcium-dependent STIM is susceptible to oxidation and protein modifications by redox regulation of its cysteines (C49 and C56) (Grupe et al. 2010a; Bhardwaj et al. 2016). Redox modification of cysteine 56 was shown to lead to glutathionylation, which resulted in a decreased STIM Ca^{2+} binding affinity, thereby mediating STIM oligomerization and activation of SOCE, independent of Ca^{2+} ER store depletion (Grupe et al. 2010a; Bhardwaj et al. 2016). It is also already established that redox-dependent modifications of Orai play a role in the regulation of SOCE (Grupe et al. 2010a; Bhardwaj et al. 2016). Clearly, the source of ROS as well as the level and duration of its redox signal will determine the impact on SOCE. For example, domains in the close proximity of ROS

production sites at the ER or mitochondria may exclusively affect SOCE via redox activation of STIM and hence lead to Ca^{2+} signaling, while exogenous redox stress sensed by plasma membrane localized Orai channels may influence CICR. On the contrary, it is also possible that ROS mediated STIM translocation is generated indirectly, through redox activation of ER Ca^{2+} regulator IP_3R and RyR (Renard-Rooney et al. 1995; Hempel and Trebak 2017). In this scenario, it has been demonstrated that oxidation of ER luminal cysteines (C2496, C2504, or C2527) within the IP_3R influence its activity and hence alter the level of Ca^{2+} within the ER. For example, activation of IP_3R by externally applied H_2O_2 results in a consequential ER Ca^{2+} store depletion, which was shown to contribute to the further activation of CRAC channels (Sampieri et al. 2018; Lock et al. 2019).

3.3.4.3 **Oxidative stress reveals an inhibitory effect on calcium pumps**

In contrast to the activating effects of oxidative stress on channels, which are responsible for an intracellular calcium increase, it was shown that the same stimulus induces exactly the opposite effect in calcium pumps like PMCA or SERCA which extrudes Ca^{2+} out of the cell (Patwardhan et al. 2015; Hempel and Trebak 2017). To summarize the most important inhibitory and activating effects of ROS on key molecules of the T-cell activation cascade, **Figure 34** illustrates them schematically.

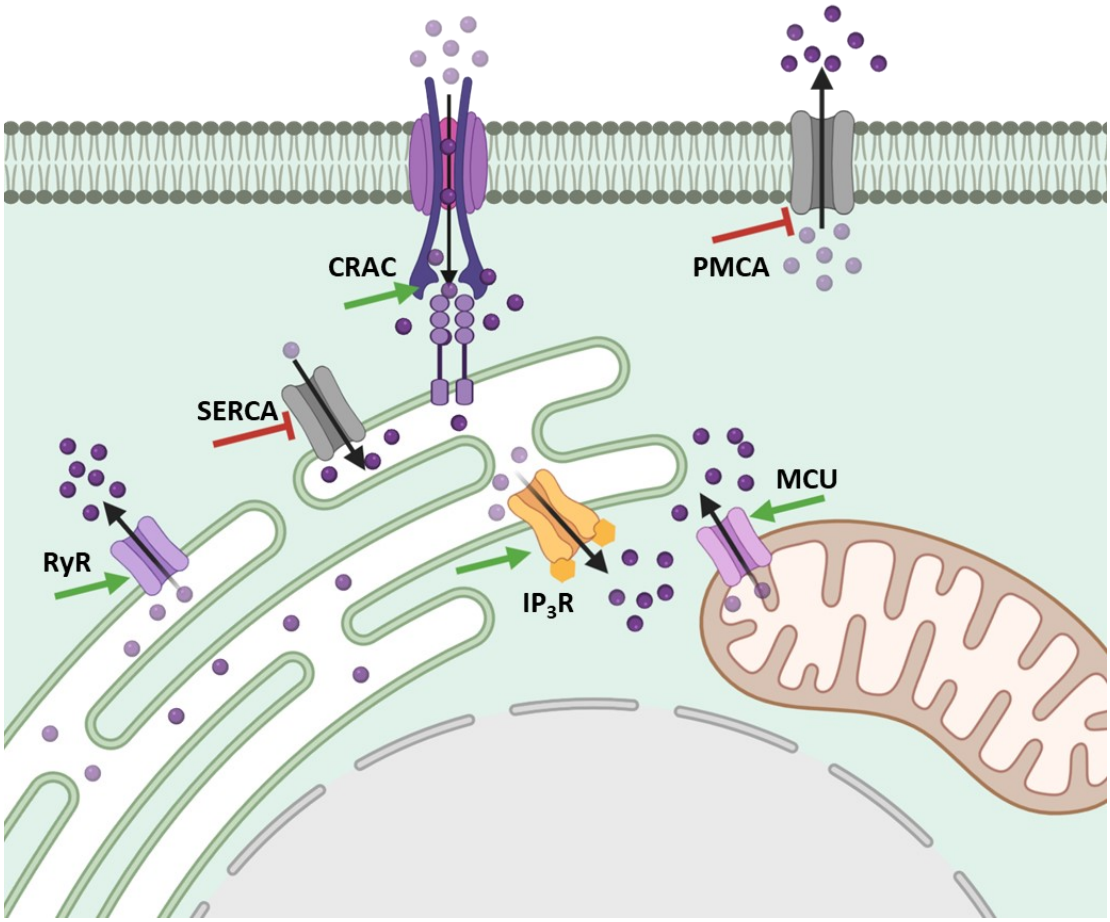

Figure 34: Effects of ROS on channels for maintenance of cellular calcium homeostasis. Activating effects (green) on calcium channels and inhibitory effects (red) on calcium pumps initiate an elevation of the cytosolic calcium concentration. SERCA=Sarcoplasmic/endoplasmic reticulum calcium ATPase, PMCA=plasma membrane Ca^{2+} ATPase, IP_3R=Inositol trisphosphate receptor, RyR= ryanodine receptor, ROS=reactive oxygen species. Created with BioRender.com.

Worth noting is, that an ROS triggered conformational and activation change of a protein is not limited to ion channels, but is also observed in enzymes like kinases and phosphatases (L Legendre et al. 1993; Zhang et al. 1998). This suggests that a global increase in the oxidative state could cause a large enhancement of cytosolic Ca^{2+} levels due to both, its activating effect on calcium concentration increasing channels and its inhibitory effect on calcium concentration decreasing calcium channels/pumps and other proteins, which are necessary for the initiation or duration of the cellular processes.

3.4 Chapter 4 – IR induces NFAT nuclear translocation

In the activation of T-cells by antigens the initially triggered calcium (Ca^{2+}) signaling cascade is sufficient to evoke all downstream events including the activation of the transcription factor nuclear factor of activated T-cells (NFAT). NFAT activation via multi-dephosphorylation by calcineurin is a central step in generating an appropriate immune response in various multicellular organisms. The present chapter examines whether the same signaling cascade is also activated by the X-ray triggered ROS/Ca^{2+} signaling cascade. By using live-cell confocal imaging I monitored the distribution of endogenous and fluorescent tagged NFAT in response to X-ray exposure. The data show that NFAT is prior to irradiation homogenously distributed throughout the cytosol. After exposure to 5 Gy X-ray NFAT is progressively translocating into the nucleus; 50% of the protein are found in nucleus 70 min after irradiation. This translocation is similar but slower than that evoked by canonical T-cell activators. Indeed, in presence of an antigen cocktail for T-cell receptor (TCR) activation or stimulation by thapsigargin (Tg) it takes 21 min and 8 minutes respectively for translocating 50% of the transcription factor into the nucleus. The application of a CRAC channel blocker, Synta (10 µM), underlines that all three stimuli induced NFAT nuclear migrations are mediated by calcium influx via Ca^{2+} release-activated Ca^{2+} (CRAC) channels; where inhibiting CRAC channels abolished NFAT translocation after addition of all three stimuli. Taken together the data imply that an X-ray stimulated cytosolic/nuclear transfer of NFAT may also stimulate an immune response in T- cells.

3.4.1 Introduction

3.4.1.1 NFATS way from cytoplasm towards the nucleus

A stimulus-induced change in the metabolism or even the activity status of a cell is necessarily regulated by an altered gene expression. In this context, the most prominent transcription factor in T-lymphocytes is the nuclear factor of activated T-cells (NFAT). Gene transcription under control of NFAT is one of the cellular responses downstream of CICR generated calcium oscillations (Feske et al. 2003; Grumont et al. 2004; Gwack et al. 2007). In this scenario the message for an activation of NFAT is not simply encoded by an increase in Ca^{2+}_{cyt} but also by the frequency of the Ca^{2+} oscillations (Gwack et al. 2007; Smedler and Uhlén 2014; Hogan 2017). In unstimulated cells NFAT remains highly phosphorylated in the cytoplasm. Additional key molecules in the CICR mediated signaling pathway in T-cells is the regulatory but enzymatically inactive protein calmodulin (CaM) and the calcium-dependent phosphatase calcineurin. Similar to NFAT both proteins remain inactive in the cytosol of unstimulated cells (Macian 2005; Lodygin et al. 2013). Following a stimulus induced increase in the Ca^{2+}_{cyt} concentration these cations bind to the EF-hand binding motives of CaM and calcineurin resulting in a conformational change of both proteins (Salazar et al. 2008; Zhu et al. 2011). As a consequence, CaM binds to calcineurin, which results in an activation of the latter. In a next step calcineurin actively dephosphorylates NFAT in its resting state in the cytoplasm. Prior to its activation phosphoserines appear to mask nuclear localization signals of the transcription factor; following dephosphorylation the nuclear localization signals of NFAT becomes unmasked and the transcription factor is transported into the nucleus. There NFAT assembles with specific DNA promotor elements either alone or in combination with binding partners resulting in the regulation of numerous T-cell activation genes. These include genes for IL-2, IFNγ, CD25 and Integrinβ1 which are essential for an adequate immune response to an appropriate stimulus (Dolmetsch et al. 1998; Tomida et al. 2003; Yissachar et al. 2013b).

3.4.1.2 Structure of the NFAT family

The structure of the NFAT transcription factor family consist of five members, including four calcium-regulated isoforms, NFAT1 (NFATc2 or NFATp), NFAT2 (NFATc1 or NFATc), NFAT3 (NFATc4), and NFAT4 (NFATc3 or NFATx) and a tonicity-responsive enhancer-binding protein (TonEBP or NFAT5). Because in the current study only calcium dependent transcription factors are of interest, I focus here only on the calcium-responsive NFAT members, NFAT1–NFAT4. These are all structural closely related with the NFAT1 isoform primarily present in T-lymphocytes. All NFAT proteins consist mainly of 3 functional units: The N-terminal NFAT homology domain (NHD), a highly conserved Rel homology domain (RHD), and a C-terminal domain (Beals et al. 1997; Macián et al. 2001; Macian 2005). The first mentioned NHD, possesses a potent transactivation domain and a calcineurin docking site. Hence, the NHD also contains both important translocation sequences; the nuclear localization sequence (NLS) and the nuclear export sequence (NES), which control NFATs subcellular localization through phosphorylation and dephosphorylation of the NFAT proteins. In addition, the RHD is known as the DNA-binding domain (DBD) of the NFAT family. Another important well-known aspect for the activity of NFAT in cellular responses is that NFAT1 is expressed constitutively within the cell. This means that exclusively NFATs phosphorylation status and not its expression level is relevant for the transcriptional activity. (Shaw et al. 1988; Emmel et al. 1989; Flanagan et al. 1991).

3.4.1.3 **Targeted nuclear export of NFAT is as important as its nuclear import**

As soon as NFAT is localized in the nucleus after an immunological activation stimulus, the signaling cascade is still not completed. In order, to avoid a hyperactivation of T-lymphocytes it is necessary not only to import NFAT into the nucleus, but also to export it again into the cytoplasm. Otherwise genes for immunological activation would be transcribed continuously leading to a chronical inflammation. Several studies show that different kinases including glycogen synthase kinase (GSK3), c-Jun amino-terminal kinase (JNK), p38 and MAP kinase (Beals et al. 1997; Dolmetsch et al. 2001; Alam et al. 2018) could be responsible for the re-phosphorylation of NFATs NES which consequently causes the deactivation of the transcription factor followed by its active transport back into the cytoplasm.

3.4.1.4 **The crucial role of CRAC channels in the NFAT activation pathway**

It is well established that the initial release of Ca^{2+} from ER store, which is triggered by IP3, is not sufficient to activate NFAT target genes. This initial signal needs to be amplified, which is achieved by an activation of CRAC channels and the consequent influx of Ca^{2+} from the external medium (Putney 1986). Serafini et al. (1995) demonstrated, that a defect in CICR due to a mutation in CRAC channels fails to promote the appropriate calcium signals for NFAT activation *in vivo*. Indeed, the affected cells were not able to produce the proteins needed for the immune response including IL-2, IFNγ and CD40.

The data presented in chapters 1, 2 and 3 show that X-ray irradiation is able to generate the effective signaling components upstream of NFAT. This suggests, that also ionizing irradiation activates via ROS production and Ca^{2+} oscillations a transfer of NFAT from the cytosol into the nucleus. The following experiments support this hypothesis.

3.4.2 Results

To test the hypothesis of IR induced NFAT activation I monitored the cellular distribution of the transcription factor before and after ionizing irradiation. The data in chapter 2 and 3 have shown that X-ray exposure leads to a calcium signaling pathway via an activation of CRAC channels in Jurkat T-cells. This calcium signal reveals the distinct frequency and amplitude modulated oscillations that were described previously (**Chapter 2** – IR induces delayed calcium oscillations, **Figure 19** and **Figure 20**). In this context it is important to note that the frequency of the IR induced Ca^{2+} oscillations in Jurkat cells is typical for a signaling cascade, which elicits the activation of the NFAT pathway (Lewis and Cahalan 1989; Dolmetsch et al. 1998; Smedler and Uhlén 2014).

3.4.2.1 **IR induces nuclear translocation of calcium-dependent endogenous NFAT**

To determine whether IR has an activating effect on the nuclear transfer of NFAT, I performed immunofluorescence staining in fixed cells with a secondary Alx488 nm antibody and monitored the endogenous NFAT proteins by confocal microscopy. First, I analyzed the NFAT localization in untreated Jurkat cells. As a positive control the cytoplasmic-nuclear translocation of the transcription factor was triggered by addition of 2 µM thapsigargin. In the same type of experiments the translocation of NFAT was followed after irradiation of cells with 5 Gy X-ray. To obtain information on the time course of NFAT translocation irradiated Jurkat cells were fixed 15, 30 and 60 minutes after X-ray exposure.

Figure 35 shows representative confocal images of the three treatments in which control cells were immediately fixed while Tg treated cells were fixed 15 minutes after addition of stimulus. The irradiated cells were fixed for microscopic analysis at the three time points mentioned before. The representative images in which the nucleus stained with Hoechst (**Figure 35** first column) show that the transcription factor is primarily located in the cytosol in non-stimulated Jurkat cells (**Figure 35** top panel). Stimulation with 2 µM Tg favors the expected translocation of NFAT into the nucleus in a population of 92% cells tested. In some of the analyzed cells the fluorescence signal of Alx488 stained NFAT was distributed throughout the whole cell. This implies that fixation of these cells occurred while NFAT translocation into the nucleus had started but was not yet finalized. Analysis of X-ray irradiated cells shows that also this stimulus is triggering a nuclear transfer of NFAT. This translocation from the cytosol to the nucleus was observed in > 65% of cells 15 min to 30 min post irradiation with 5 Gy X-ray; for these analysis ≥ 200 cells were monitored for each time point and treatment (**Figure 35**).

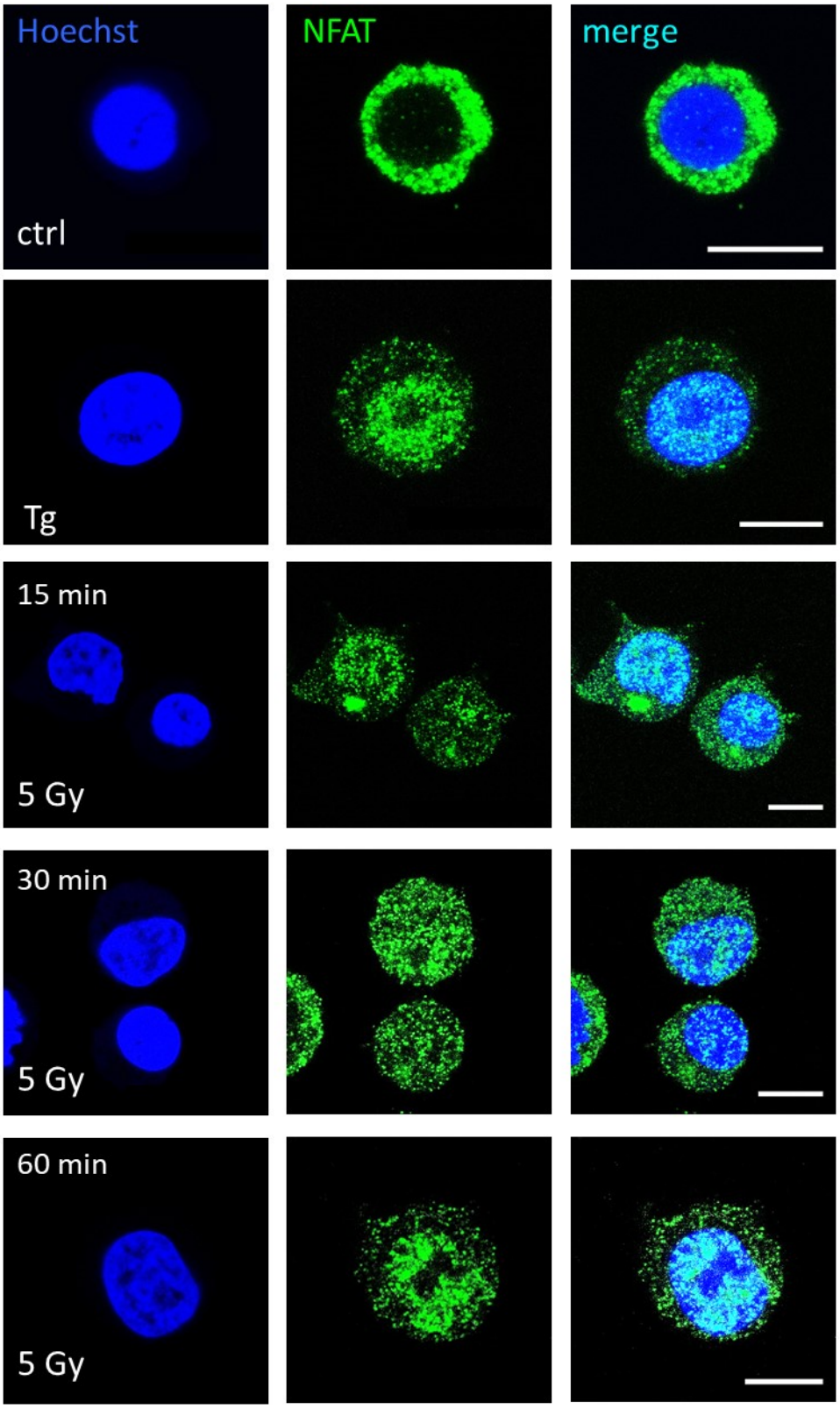

Figure 35: IR causes a nuclear translocation of Ca^{2+}-dependent NFAT in Jurkat cells (**A**) Confocal images of endogenous NFAT immunostained with green fluorescent Alx488 (left panel) and blue fluorescent Hoechst DNA dye (second panel) in Jurkat cells. The third panel shows a merge of the blue and green channels. Cells were fixed immediately in control cells (Top), 15 min after 2 µM thapsigargin Ca^{2+} store depletion (second panel) or 15, 30 or 60 min after X-ray exposure with 5 Gy (three bottom panels). Scale bar = 10 µm.

These data conform the role of IR as a trigger of for an immunological activation in T-cells via activation of NFAT. In the majority of untreated control cells NFAT is as, as expected, located in the cytosol. Activation and subsequent translocation into the nucleus is a fast mechanism in Tg treated cells and requires less than 15 min. The same translocation of NFAT is also evident after X-ray stimulation but it takes at least 30 to 60 minutes for completing this action.

3.4.2.2 **PBMC reveal a nuclear translocation of NFAT after irradiation**

The immunofluorescence staining experiments of endogenous NFAT were repeated in PBMCs to determine if the IR induced NFAT translocation is a canonical response in T-lymphocytes. Representative images of unstimulated PBMCs and PBMCs treated with either Tg or 5 Gy X-ray are shown in **Figure 36**. The data confirm that Tg as well as X-ray irradiation stimulate nuclear translocation of NFAT in 89%/47% of PBMCs in the same manner an in Jurkat cells. In summary, the results indicate that IR initiates a canonical signaling pathway in T-lymphocytes.

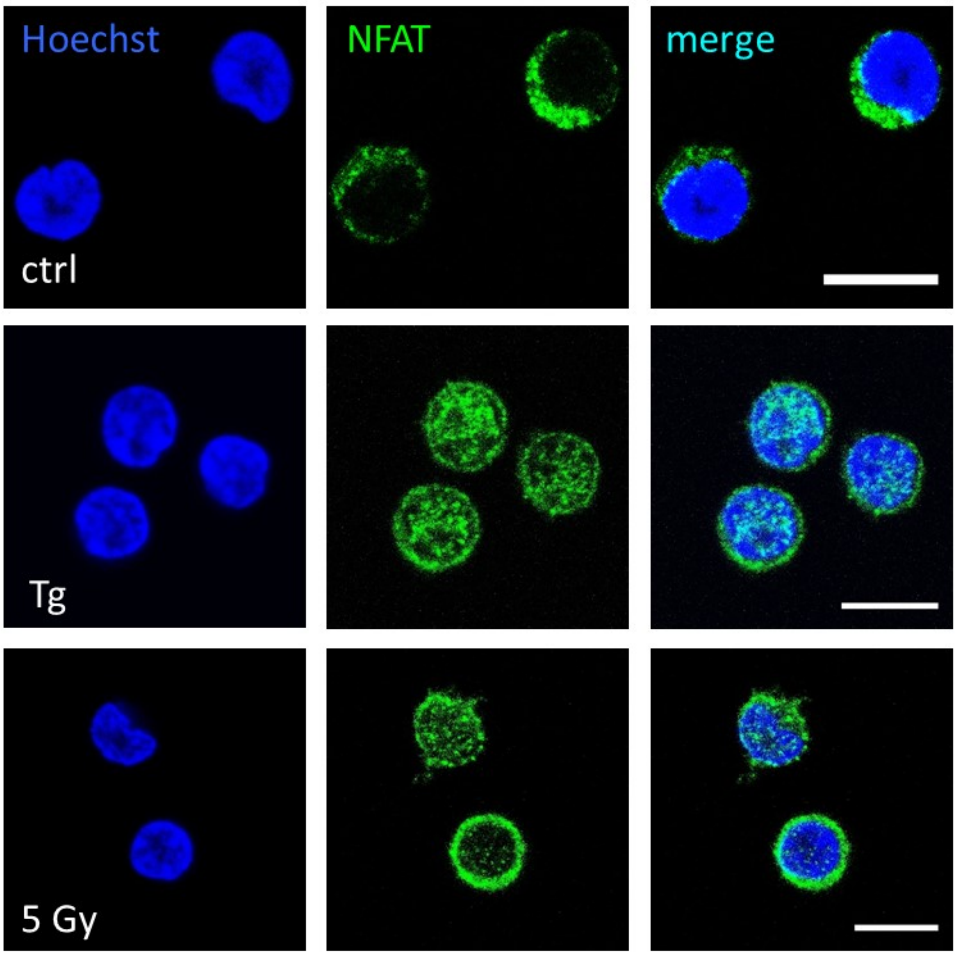

Figure 36: Ca^{2+}-dependent NFAT pathway is activated in naive T-lymphocytes by IR. (**A**) Confocal images of endogenous NFAT stained with green fluorescent Alx488 antibody (left column) and blue fluorescent Hoechst DNA dye (second column) in PBMC. Overlay of both columns is shown in the third panel. Cells were fixed immediately (control, top), 15 min after 2 µM thapsigargin induced Ca^{2+} store depletion (middle) or 60 min after X-ray exposure with 5 Gy (Bottom). Scale bars = 10 µm.

The dynamics of a stimulus induced nuclear translocation of NFAT from the cytosol into the nucleus is an important step for the understanding of an IR induced signaling pathway in immune cells. Since immunofluorescence staining is performed exclusively with fixed cells, it is not possible to track the NFAT translocation in a single cell. This can however be achieved by imaging the cellular localization of heterologous expressed GFP-tagged NFAT.

3.4.2.3 **CRAC channels are essential for a nuclear translocation of NFAT triggered by IR**

In resolve the dynamics of NFAT-GFP translocation in Jurkat cells in life cell imaging I added 2 µM Tg to the cells and tracked the localization of the fluorescent transcription factor over a time period of 100 min. **Figure 37A** shows the cytosolic distribution of the transient-expressed NFAT-GFP in unstimulated control cells prior to Tg stimulation. The distribution is similar to that of the endogenous NFAT seen in **Figure 35**. Following Tg stimulation the heterologous expressed NFAT-GFP is rapidly translocating into the nucleus. In an intermediate phase NFAT-GFP appears homogeneously distributed through the cell very much like the endogenous immune-stained NFAT (**Figure 35**). The same experimental procedure of NFAT-GFP monitoring was repeated with the CD3/CD28/CD2 T-cell activator (T-Act) and 5 Gy X-ray. Both stimuli again emerged as a suitable trigger for the nuclear translocation of NFAT similar to that observed after Tg treatment.

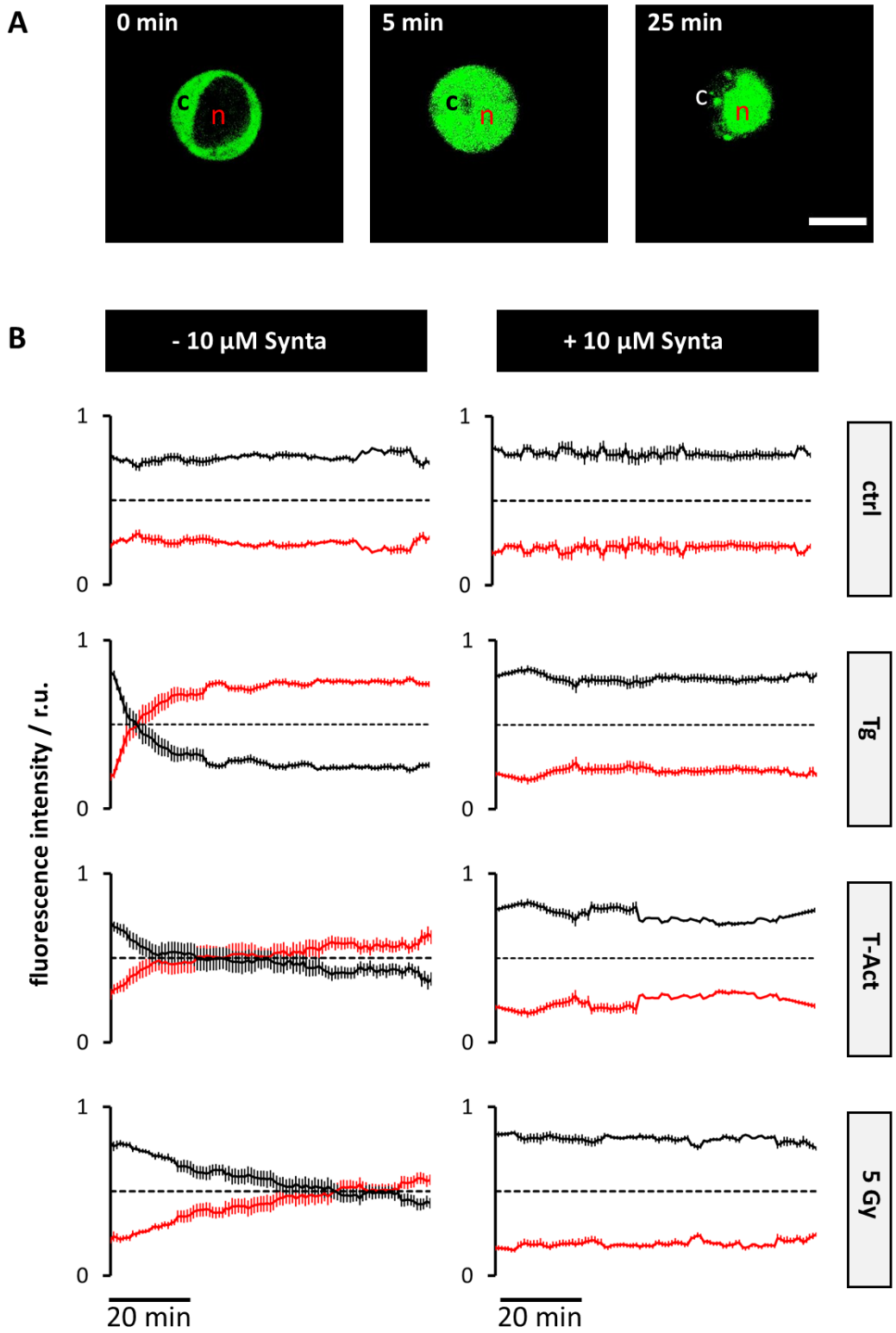

Figure 37: Nuclear translocation kinetics of Ca^{2+}-dependent heterologous expressed NFAT-GFP in Jurkat cells. (**A**) Representative images of life-cell confocal measurements of transiently expressed NFAT-GFP from cytosol (c) to nucleus (n) translocation in Jurkat cells after stimulation with 2 µM thapsigargin. Time post Tg addition is indicated. (**B**) Kinetic analysis of NFAT-GFP nuclear import reactions (nucleus red, cytosol black) of confocal time series in Jurkat cells according to control condition (ctrl), addition of 2 µM thapsigargin (Tg) or 25 µL/mL activator antigen cocktail (T-Act), or after 5 Gy X-ray exposure. Data were obtained without (left) and with 10 µM CRAC channel inhibitor Synta (right). Each time course diagram is the mean ± S.E. of ≥ 12 individually measured cells.

The time course of cytosolic-nuclear translocation of NFAT in Jurkat cells in response to Tg, T-Act or 5 Gy X-ray treatment is summarized in **Figure 37** left column. For comparison also the NFAT distribution in control cells is shown over the same time period. In this analysis the intensity of NFAT-GFP fluorescence was measured in both; the cytosol and the nucleus. The relative values are plotted as mean average ± SD as a function of time. In control cells the fluorescence intensities in either the cytosol (~70%) as well as the nucleus (~30%) remain constant over the 100 min time period in 94% of the monitored cells. In contrast to control cells 2 µM Tg triggered a fast rearrangement of the fluorescent signal in the cells which is evident from the decrease of signal in the cytosolic and the concomitant increase in the nucleus. The same phenomenon was also observed in response to stimulation with T-Act and 5 Gy X-ray. A comparison in the kinetics of this translocation highlights some distinct differences in the response times between stimuli. Tg stimulation causes in 97% of the cells already after 8 ± 1.5 min a 50% nuclear translocation of NFAT, which is indicated by the crossing of the cytoplasmic and nuclear relative fluorescence lines. In T-Act stimulated cells it takes more than 21 ± 6.5 minutes for the same response in 89% of the cells. After stimulation with 5 Gy X-ray it takes even 70 ± 5 minutes before 50% of NFAT is translocated to the nucleus and this effect is only seen in a cell population of 67% (**Figure 37** left column). It is worth noting that similar kinetic and population differences were already seen in **chapter 3** (**Figure 32**) in the context of stimulus triggered activation of CRAC channels. In these experiments Tg induced a rapid aggregation of CRAC channels while the same process required more time after T-Act and 5 Gy stimulation. This finding is in good agreement with the fact that NFAT translocation into the nucleus is a downstream event in the signaling cascade following CRAC channel activation and Ca^{2+} oscillations. To further examine the causal relationship between CRAC channel activity and NFAT translocation the experiments in **Figure 37** left column were repeated in the presence and absence of Synta, a specific inhibitor of CRAC channels. In **chapter 3** it was already demonstrated that Synta works as an appropriate CRAC channel inhibitor and prevents IR-induced calcium oscillations (**Figure 28**). In the presence of the channel blocker all cells behave after treatment with the three stimuli like untreated control cells (**Figure 37**). Over 100 min of recording there was no visible cytoplasmic-nuclear translocation of NFAT. Collectively the data underpin that the nuclear translocation of NFAT is in all three stimuli causally related to the activation of CRAC channels.

3.4.3 Conclusion

The results of the last 3 chapters show that irradiation causes both; a transient increase in the second messenger H_2O_2 and CRAC channel dependent calcium oscillations in Jurkat cells. Under physiological stimulation of the TCR, these steps are essential for the activation of the transcription factor NFAT, which causes the expression of different target genes and thus enables an immune response of the cell and consequently the whole organism. Indeed, the present chapter focused on the elucidation if the successive characterization of the mentioned key molecules, also contribute to the activation of NFAT in a similar manner to its physiological activation.

In general, there are two established methods for the verification of the NFAT activity. First, analyzing the expression of its target genes and second, monitoring its location. By use of live-cell real-time imaging I was able to visualize the translocation of the transcription factor NFAT from the cytoplasm into the nucleus of Jurkat cells either after Tg, T-Act stimulation or irradiation with 5 Gy X-ray. This cytoplasmic-nuclear migration was prevented by applying the CRAC channel inhibitor Synta. Consequently, IR leads to a ROS/Ca^{2+} dependent activation of the most important transcription factor for the immunological activation of T-lymphocytes. However, the observed difference in the translocation dynamics between the treatments are significant. These data can be supported by similar results in the literature (Patwardhan et al. 2015; Loh et al. 1996; Kar et al. 2016; Garrity et al. 1994; Sharma et al. 2011; Berridge und Dupont 1994; Tomida et al. 2003). **Figure 38** provides a compilation of NFAT EC50 values after the addition of different stimuli.

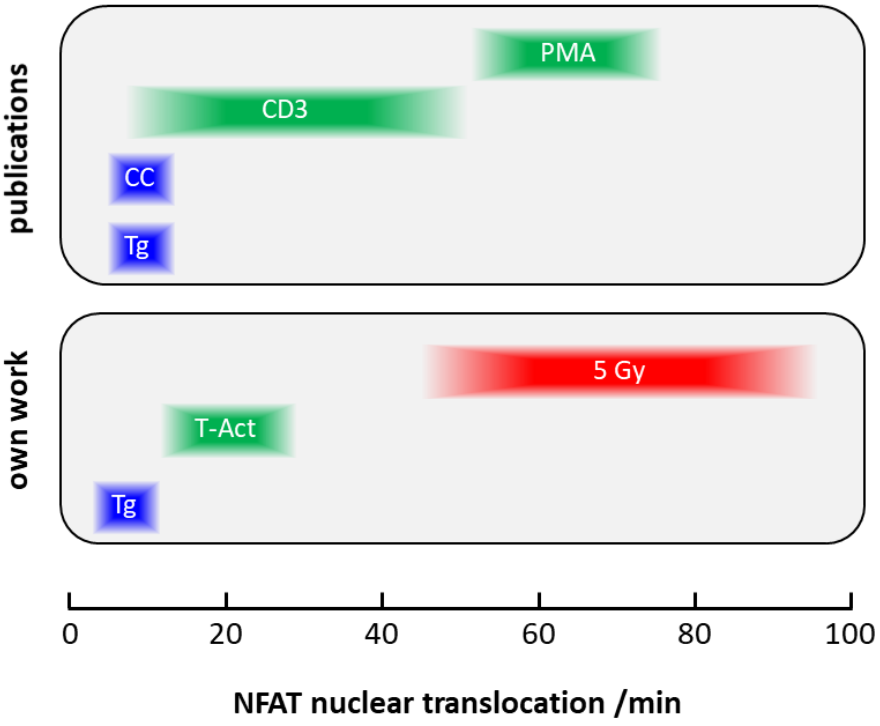

Figure 38: Nuclear translocation time of NFAT as a response to different stimuli. Tg = 2 µM thapsigargin, T-Act = 25 µl/ml CD3/CD28/CD2 antibody mix, CC = calcium-clamp method with a frequency of 10 mHz, CD3 = CD3 antibody, PMA = phorbol myristate acetate. Modified according to (Berridge and Dupont 1994; Garrity et al. 1994; Loh et al. 1996; Tomida et al. 2003; Sharma et al. 2011; Patwardhan et al. 2015; Kar et al. 2016).

The lower half of the illustration depicts data of the present study, the upper half data from literature. What is striking is that the NFAT translocation after Tg addition takes place after approximately 8 minutes in experiments I performed as well as in published attempts (Loh et al. 1996; Sharma et al. 2011). In the same time frame, nuclear NFAT migration also occurs according to the artificial 10 mHz calcium clamp (CC) method (Berridge and Dupont 1994; Tomida et al. 2003). In addition, the same translocation process occurs with the addition of CD3 antibodies (Garrity et al. 1994; Loh et al. 1996) and T-Act (present study), which also contains the CD3 antibody, 20-40 min, which is slightly slower than after Tg addition. Surprisingly, the nuclear translocation process of NFAT after irradiation with 5 Gy X-ray, as well as after addition of the mitogen PMA (Loh et al. 1996) is with 60 min in the same slow timeframe. which does not differ significantly from the kinetics after CD3 addition. However, the reason for different NFAT dynamics between different stimuli remain unexplained where it is assumed that both; the beginning as well as the frequency of calcium oscillations play an important regulatory role. Nevertheless, it can be concluded that the nuclear translocation of the transcription factor after irradiation proceeds in the same time frame as after physiological activation.

3.4.4 Perspectives

3.4.4.1 Understanding the Ca^{2+}-dependency of NFATs translocation dynamics

Model predictions are useful to bring the obtained data of the present work into an overall context of Ca^{2+}-dependency of NFATs translocation dynamics and thus gain new perspectives in the establishment of the IR-triggered signaling mechanism in T-lymphocytes.

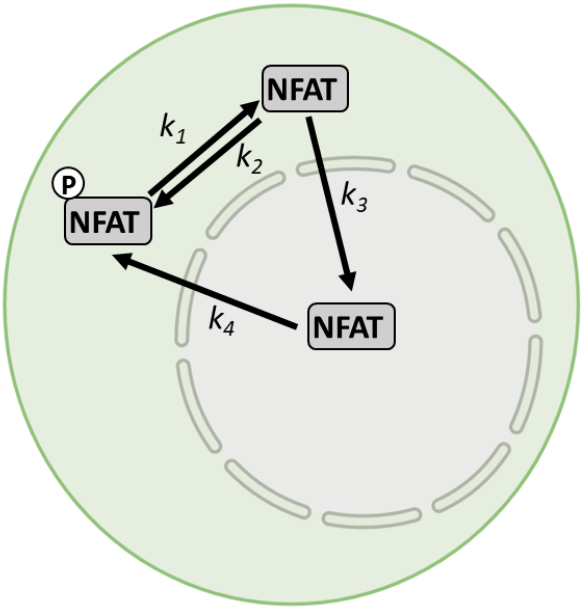

Figure 39: Model of Ca^{2+}-dependent nuclear translocation of NFAT. The schematic illustration of a model of NFAT translocation assumes that NFAT determines in one of the three states: cytoplasmic phosphorylated (inactive), cytoplasmic dephosphorylated (intermediate) or nuclear transported (active). Rate constants (k_1 to k_4) are defined as indicated. The dephosphorylation rate constant (k_1) is assumed to be regulated by Ca^{2+}. Modified according to Tomida et al. 2003. Created with BioRender.com.

A simplified model according to Tomida et al. (2003) is schematically illustrated in **Figure *39*** where it is assumed that NFAT is present in three different states within the cell: cytoplasmic phosphorylated (inactive), cytoplasmic dephosphorylated (intermediate) and nuclear dephosphorylated (active). NFAT could transit between the three states as indicated by arpanels. In this model the transition rate constants for the active nuclear import/export (k_3 and k_4) were assumed to be definite. Only the (de-) phosphorylation rate constants k_1 and k_2 are considered to be variable due to NFATs calcium/calmodulin dependency.

The **Figure 39** implies that the active NFAT states is present if $k_1 < k_2$. Conversely, NFAT is in its inactive, dephosphorylated state followed by its nuclear export if $k_1 > k_2$. On the cellular level this means that the frequency of generated calcium oscillations, which activate CaM, must be higher than the velocity of the NFAT rephosphorylation process. This kinetic model is in agreement with *in vivo* studies, where the dephosphorylation of NFAT is a fast process < 1 min (Kubis et al. 2002; Sharma et al. 2011; Kar et al. 2016), whereas the phosphorylation of nuclear NFAT is with > 15 min rather slow (Garrity et al. 1994; Loh et al. 1996).

The most interesting part is to examine the behavior of the model when a calcium oscillatory change is applied. As a result, Tomida *et al.* were able to demonstrate that a high-frequency oscillation of

0.5 mHz maintains constant NFAT dephosphorylation. Since k1 and k3 are much smaller than k4 NFAT is repetitively dephosphorylated before the rephosphorylation of NFAT could take place. This is why NFAT persists in the nucleus. Furthermore, the scientists tested the model predictions with Ca^{2+} stimulation at intervals varying between 1 and 11 mHz, which include the physiological range of Ca^{2+} oscillation intervals observed in activated T-cells (Lewis and Cahalan 1989; Dolmetsch and Lewis 1994; Dolmetsch et al. 1998). Furthermore, the results of the same studies provided evidence that a low-frequency Ca^{2+} oscillation of <1 mHz induces an intermittent dephosphorylation of NFAT leading to its nuclear export. The discontinuation of dephosphorylation is characterized by the fact that NFAT is present in the nucleus after calcium stimulation and before the next calcium spike occurs, it is rephosphorylated and therefore migrates back to the cytosol. In the cytosol the transcription factor is dephosphorylated again according to the next calcium signal. Therefore, the experiments as well as the model succeed in decoding Ca^{2+}oscillation frequency for NFAT activation processes. Taken together, the Ca^{2+} oscillations induce the nuclear translocation of NFAT in a frequency-dependent manner. The extent of steady-state nuclear translocation NFAT increased with increasing stimulation interval, in other words, with increasing Ca^{2+} oscillation frequency (Salazar et al. 2008). Relating the assumptions of the model to the NFAT translocations kinetic in the present work, I confirm that the IR induced calcium oscillation frequency is sufficiently high that NFAT undergoes permanent dephosphorylation and therefore persist in the nucleus.

3.4.4.2 **Limitations of microscopic translocation analysis**

So far, the reliability of determining the activity of the transcription factor due to its localization is limited. The circumstance that NFAT migrates from the cytosol into the nucleus does not mean that it necessarily reflects its function as a promoter. Indeed, it is still unknown if the nuclear translocation also initiates the expression of appropriate target genes, which are crucial for the immunological response of the cell. In order to verify whether IR-induced nuclear NFAT also initiates the transcription of certain target genes, I examined the expression level of some T-cell activation markers in the following chapter.

3.5 Chapter 5 – IR induces Cytokine expression

Results from this chapter in **Figure 40** and **Figure 41** have already been published in Voos P, Fuck S, Weipert F, Babel L, **Tandl D**, Meckel T, Hehlgans S, Fournier C, Moroni A, Rödel F and Thiel G (2018). Ionizing Radiation Induces Morphological Changes and Immunological Modulation of Jurkat Cells. Front. Immunol. 9:922. doi: 10.3389/fimmu.2018.00922

In this chapter, I designed and performed the cell diameter analysis as well as the analysis of gene and protein expression levels of T-cell activation marker. Dr. Stephanie Hehlgans and Jeannie Peifer (Goethe University Frankfurt) provided support in handling the peripheral blood mononuclear cells (PBMCs) and with the implementation of quantitative PCR and FACS analyses of the cytokines.

Abstract

Activated T-lymphocytes are characterized by increased metabolism, consequently an enhanced proliferation rate, and the secretion of cytokines, chemokines and other messenger substances to attract additional immune cells. A quantity for an increased metabolism in T-cells is their cell diameter. In this chapter, I tested whether X-ray exposure triggers similar morphological and immunological changes of the T-lymphocytes. Indeed, I could determine that in the radiation-induced signaling cascade all important key players for a canonical T-cell receptor (TCR) triggered activation are involved including phospholipase C (PLC), the inositol trisphosphate receptor (IP_3R) as well as calcium-release activated calcium (CRAC) channel mediated calcium response and the calmodulin mediated transcription factor nuclear factor of activated T-cells (NFAT). Furthermore, I could show by quantitative PCR and FACS analysis that this signaling cascade leads to a dose-dependent expression of the cytokines interleukin-2 (IL2) and interferon-γ (IFNγ), as well as the IL2 receptor subunit CD25 in Jurkat cells, 24 h post irradiation, which is comparable to the expression rate after an established TCR activator. Taken together the data imply that X-ray is able to stimulate an immune response in T-cells similar to the canonical antigen-triggered pathway. Thus, the immune response of T-cells can extend to a more global reaction in the affected organism by the recruitment of further immune cell subtypes. For this reason, utilizing the beneficial effects of irradiation on the immune system for radiotherapy, can foster the therapy response of tumor patients.

3.5.1 Introduction

3.5.1.1 Morphological changes in T-cell activation

Under resting conditions naïve T-lymphocytes are in an inactive (G0) state. In this G0 phase the cells do not proliferate and have only a very low metabolic activity to maintain their essential cellular processes. The cells preserve this reduced metabolism in order to keep their volume to a minimum, which eases their traveling within the bloodstream, always prepared to bind to antigens presented by APCs. That is why inactive T-lymphocytes have a typically small cell diameter and consist almost completely of their nucleus with only a limited cytoplasmatic space (Rosenbluth et al. 2006; MacIver et al. 2013; Alwarawrah et al. 2018; Voos et al. 2018). After contact of the T-cell specific cell-surface receptors with antigens, an intracellular signaling cascade is initiated which triggers the change of their activation state. Soon, they start to enlarge their reaction space, since they have to increase in mass and volume for cell division and further proliferation. In addition, they need reaction space for the expression of proteins that are needed for the immunological response (MacIver et al. 2013). For this reason, the cell diameter (Rosenbluth et al. 2006; Voos et al. 2018), as well as the expression levels of T-cell activation markers (Diehn et al. 2002) can be used as a quantifiable parameter for the T-cell activation state.

3.5.1.2 NFAT-dependent gene transcription

It is well established that T-lymphocyte activation is a well-defined orchestra of protein complexes interacting to regulate the transcriptional activity of specific activation targets (Malek 2008; Fracchia et al. 2013; Shaw et al. 2013). The output of this interplay is a highly choreographed series of gene regulations that activate and/or inactivate estimated 4000 genes, based on transcript array studies by Diehn et al. 2002. It has to be considered that most of this variety of genes are not directly involved in the immune response but are required for the transition from the metabolically inactive, non-dividing state into the highly active, proliferating T-cell state.

In the context of a stimulus generated immunological response the most interesting NFAT-dependent classes of genes are those, which code for products that are dedicated to communicating with other cells in their environment. The gene products of these groups include proteins like cytokines, which are secreted and can serve as co-stimuli to receptors on the surface of further immune cells (Diehn et al. 2002; Dranoff 2004; Malek 2008). Also, T-cell activation genes regulating activation processes in adjacent cells, like the CD40 or Fas ligand, which are surface bound proteins, play a major role in the global immune response (Brusko et al. 2009; Triplett et al. 2012).

3.5.1.3 The function of important cytokines in immune response

Cytokines are a broad category of ~5–20 kDa small proteins, which act as multipliers of various stimuli. They have been shown to be involved in autocrine, paracrine, and endocrine signaling as immunomodulating agents (Dranoff 2004). This large group of stimulating molecules include chemokines, interferons, interleukins, lymphokines, and tumor necrosis factors (Turner et al. 2014).

They all act via their corresponding cell surface receptors, with which cytokines especially modulate the balance between humoral and cell-based immune responses. Some cytokines enhance or inhibit the action of other cytokines in complex ways even across different cell types. Binding of cytokines causes downstream cascades of intracellular signaling, including the upregulation and/or downregulation of several genes and transcription factors, resulting in the production of other cytokines, an increase in the number of surface receptors for other molecules, or the suppression of their own effect by a negative feedback loop (Lin et al. 2003; MacIver et al. 2013; Turner et al. 2014).

In the present work, I focused on the analysis of the expression rate of two essential T-cell cytokines mediating immunological reactions: interleukin-2 (IL2) and interferon-γ (IFNγ) in response to X-ray exposure. IL2 is the most important lymphokine which induces proliferation and differentiation of responsive T-cells. In addition, it acts also on B-cells as a gpanelth factor and antibody production stimulant and thus promotes the adaptive immune response within an organism (Cerretti et al. 1986). Because of its pro inflammatory properties IL2 is also used in clinical immunotherapy to treat cancer (Pouget et al. 2015). The second analyzed cytokine in the present study is IFNγ, which is critical for innate and adaptive immunity against different infections. IFNγ is an important immunostimulatory and immunomodulatory effector once it has been secreted by activated T-cells or natural killer cells. Its primary role is to foster the change of a T-cell from its inactive G0 Phase to an immunological active state, representing a positive feedback loop. On the contrary, aberrant IFNγ expression is associated with a number of autoinflammatory and autoimmune diseases (Kiani et al. 2001).

In addition to the cytokine expression levels I analyzed the cell-surface expression of the IL2 receptor alpha chain (IL2RA), which is also called CD25 and forms together with the beta (IL2RB) and gamma (IL2RG) chain a high-affinity IL2 receptor. The latter two IL2 receptor subunits are constitutively expressed in G0 T-lymphocytes at their surface, whereas the CD25 subunit is produced only after appropriate activation of the cell (Brusko et al. 2009; Osinalde et al. 2011). Therefore, CD25 expression is a good marker for T-cell activation to investigate the immunological state of a cell after certain stimuli.

3.5.2 Results

This chapter focuses on morphological and immunological changes of T-lymphocytes induced by X-ray irradiation. In a recent publication by Voos (2018) it was already shown that irradiation of cells with X-ray leads to a dose-dependent enlargement of Jurkat cells and PBMCs. I have taken advantage of this stimulus-dependent cell enlargement and used it as an assay to identify additional key molecules of the T-cell activation pathway. For this purpose, I inhibited certain proteins which I assumed play a crucial role in the IR-induced signaling pathway and analyzed whether or not IR-induced cell enlargement still occurs.

3.5.2.1 **IR triggers dose-dependent cell diameter increase which can be abolished by inhibition of the NFAT signaling cascade**

Jurkat cells exhibit without additional stimuli a narpanel size distribution with a mean value of 10.1 ± 0.2 µm (Voos et al. 2018), which was analyzed using the automated cell counter EVE^{TM}. Forty-eight hours after 5 Gy X-ray exposure the cell volume distribution widens and the mean value increases to 12.5 ± 0.5 µm. A Comparable cell enlargement was observed following irradiation with doses ranging between 0.1 and 10 Gy, confirming a dose-dependent increase in the mean cell diameter (**Figure 40A, B**). A fit of the plot with a logistic equation resulted in a half-maximal enlargement (ED50) after 1.3 Gy and a maximum cell enlargement of 23.5%. In addition, PBMCs showed similar characteristics after irradiation (Voos et al. 2018).

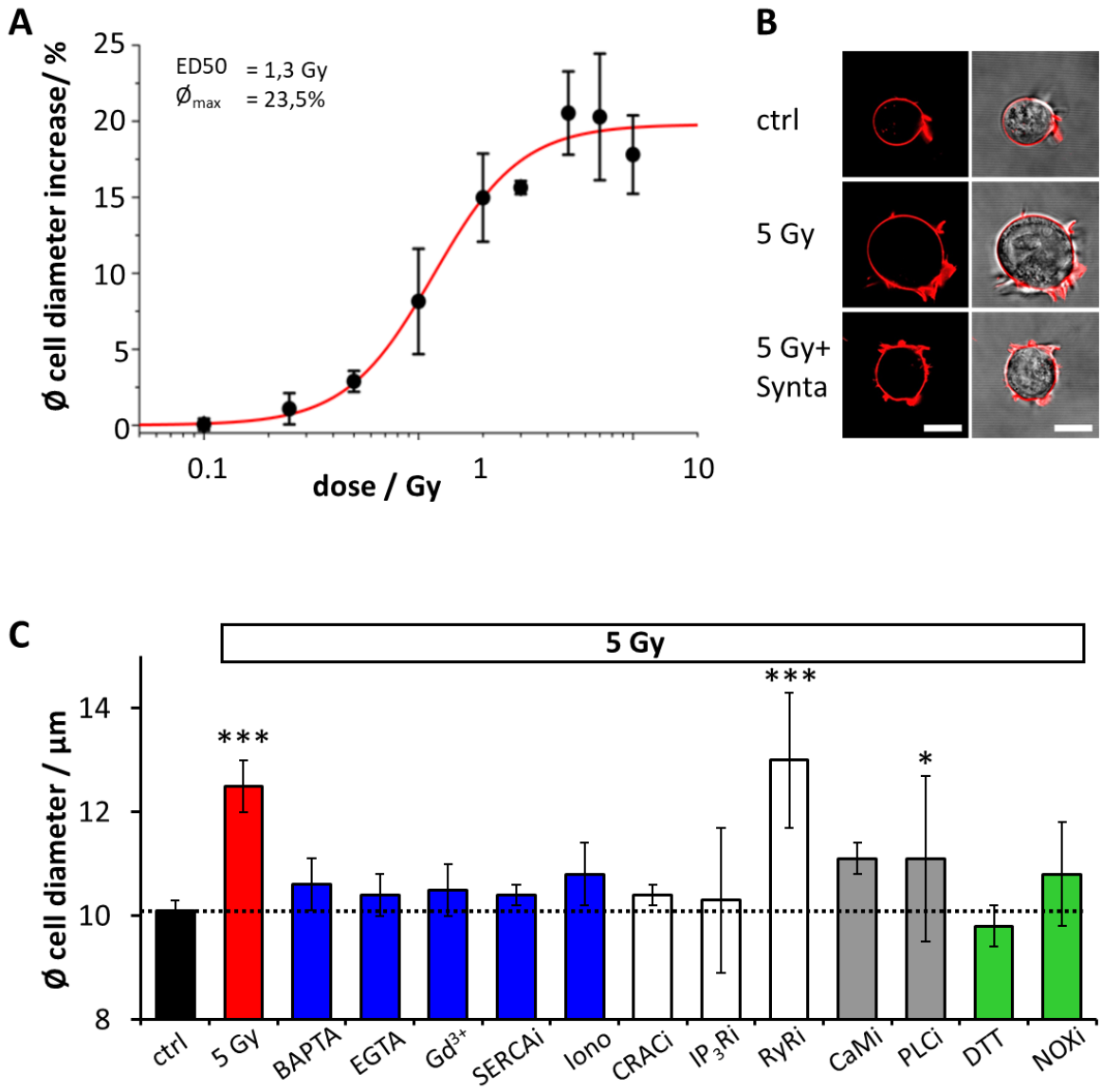

Figure 40: Ionizing irradiation causes an increase in diameter of T-lymphocytes. Using the automated cell counter EVE™ the cell diameter of Jurkat cells was measured 48 h post irradiation without and with additional treatments. (**A**) dose-response curve of Jurkat cells irradiated with X-ray over a dose range from 0.1 to 5 Gy X-ray. A fit of the does response curve yields an ED50 value of 1.18 Gy and a maximal relative increase in cell size ($Ø_{max}$) of 19.8% (modified after Voos, 2018). (**B**) Representative confocal images (left, confocal image of fluorescent stained plasma membrane (red) and overlay of fluorescent and bright field image) of individual Jurkat cells. Control cells (ctrll, top panel) exhibit a small diameter and cells 48 h after 5 Gy irradiation (5 Gy, central panel) increase in cell diameter. This increase can be abolished by addition of 10 µM Synta (5 Gy+Synta, bottom panel). Scale bar = 10 µm. (**C**) Mean diameters ± SD of > 300 cells per treatment measured 48 h after esposure to 5 Gy X-ray. The cell diameter of control cells is indicated by dotted line. Treatments are as follow: ctrl = control, 50 µM BAPTA (Voos, 2018), 5 mM EGTA, 5 µM gadolinium (Gd^{3+}), SERCAi = 2 µM thapsigargin, Iono = 1µM ionomycin, CRACi = 10 µM Synta, IP_3Ri = 100 µM 2-aminoethyldipehnylborinat, RyRi = 50 µM ryanodine, CaMi = 1 µM cyclosporin A (CsA), PLCi = 10 µM U73122, 5 mM DTT and NOXi = 10 µM GKT136901. Statistical significance for differences between irradaiated and non-irradiated cells was tested with Student's t-test; *P < 0.05, **P < 0.01, ***P < 0.001.

Next, the experiment was repeated with cells either untreated (control) or irradiated with 5 Gy, as well as co-treated with different inhibitors for key molecules of the T-cell activation pathway. I reasoned that immune suppression or blocking parts of the Ca^{2+} signaling cascades might abolish the radiation-induced increase in cell diameter. This would indicate an involvement of this signaling cascade in the morphological change of the cells. **Figure 40** summarizes the results of the cell diameters using different inhibitors for proteins which are expresed under control of the NFAT signaling pathway. To better illustrate the change in cell diameter, (**Figure 40B**) representative confocal images of cells are shown: i. before irradiation (top panel), ii. 48 h after 5 Gy irradiation (central panel) and iii. 48 h after irradiation treated with an inhibitor (10 µM Synta,bottom panel). It is evident that the control cell is small and the diameter is enlarged 48 h after irradiation. With inhibition of important componants of the IR-triggered signaling cascade such an IR-induced cell volume increase does not occur.

Comparable experiments using the automated cell counter EVE^{TM} were made with other inhibitors and the results are shown in **Figure 40C** as mean value of the measured cell diameter ± SD. A lot of treatments decreased the effect of the irradiation triggered increase in cell diameter. For example the aforementioned inhibition of CRAC channels during 5 Gy X-ray exposure abolished any significant increase in the mean cell diameter. The diameter of X-ray treated cells in the presence of the CRAC channel blocker was 10.4 ± 0.2 µm compared to 10.1 ± 0.1 µm in the untreated controls. In cells treated with 5 Gy alone the diamter increased to 12.5 ± 0.5 µm. This yields in a relative cell size increase of 19,2% in 5 Gy irradiated cells, which is reduced to only 2,9% in the presence of the CRAC channel blocker. Moreover, also other intervention of the IR-triggered calcium signals with different strategies greatly reduce the irradiation triggered increase in cell diameter. This includes: i. the general buffering of Ca^{2+}_{cyt} by 50 µM of the calcium chelator BAPTA-AM (10.6 ± 0.5 µm; 4.7% increase), ii. the removal of external calcium by addition of 5 mM EGTA (10.4 ± 0.4 µm; 2.9% increase), iii. an artificial increase in the cytoplasmic calcium concentration initiated by 5 µM of the SERCA inhibitor Tg (10.4 ± 0.2 µm; 2.9% increase) and also iv. an artificially increased calcium influx with 1 µM of the calciumionophore ionomycin (10.8 ± 0.6 µm; 6.5% increase). Based on these data I suggested that the sensitivity of the irradiation triggered morphological response of Jurkat cells is highly Ca^{2+}- dependent and requires a very precise regulatory mechanism to generate calcium signals that lead to the morphological change. Neither a too low nor a too high cytoplasmic calcium concentration leads to this phenomenon.

To further investigate whether the CRAC channels are solely responsible for the IR-induced calcium influx into the cell and thus cause cell enlargement, I also considered the influence of the IP_3 receptor (IP_3R) and the ryanodine receptor (RyR) on the cellular diameter. The result of these experiments with specific inhibitors is shown in **Figure 40C**. The data indicates that the inhibition of the IP_3R with 100 µM 2-aminoethyldipehnylborinat (Maruyama et al. 1997) also prevents the enlargement of the cells; after irradiation with 5 Gy X-ray they maintain a control cell-like diameter of 10.3 ± 1.4 (1.9%). The importance of IP_3 in the signaling cascade is further supported by experiments using an inhibitor of phospholipase C, the enyzme which generates IP_3. The presence of 10 µM of the specific inhibitor U73122 (Mogami et al. 1997) largely prevented an IR induced cell increase to a mean diameter of 11.1 ± 1.6 µm (9%), which strengthened the notion that the IP_3 pathway is essential for an X-ray triggered signaling cascade.

In contrast, when cells were treated with 50 µM ryanodine, which functions as a RyR inhibitor (Marban and Wier 1985), they enlarged after irradtion with 5 Gy to a diameter that is not different from that measured in the absence of the inhibitor (13.0 ± 1.3; 22.3%). Based on these data it can be concluded that the calcium influx from the ER into the cytosol through IP_3 activated IP_3R plays a significant role in triggering a Ca^{2+} signaling cascade. The contribution of RyR seems negligible in the IR-triggered immune response.

To further test the causal realtionship betweenn the Ca^{2+} signaling and further downstrem events, additional experiments were perfomed with inhibitors that prevent the dephosphorylation of NFAT. This can be achived by blocking calcineurin with the well-established and clinical relevant inhibitor cyclosporin A (CsA) (Emmel et al. 1989). When cells were pretreated before exposure to 5 Gy X-ray with 1 µM of this inhibitor, IR-induced only a marginal morphological enlargement of jurkat cells. With the above treatments the measured cell diameters are 11.1 ± 0.3 µm (9%). In further experiments the presumed role of ROS in the signaling cascade was tested. Data in **Figure 40C** show, that 5 mM of the reducing agent DTT in the buffer prevents the IR induced cell size increase. The diameter remains at a control-like value of 9.8 ± 0.4 µm (-3.1%). This result is in good agreement with data from chapter 1 on the IR induced generation of H_2O_2. This step seems to be essential for the initiation of the subsequent calcium oscillations. A particularly prominent role in the ROS-signaling seems to be played by NOX, since inhibition of this H_2O_2 generating oxidase with 10 µM of its specific inhibitor GKT136901 (Laleu et al. 2010) also diminishes the RIRR process within the cell. In the presence of this blocker only a 6.5% enlargement of the cell diameter (10.8 ± 1.0) occures 48 h post X-ray exposure.

Collectively, the results of these experiments suggest that the morphological change in Jurkat cells in response to X-ray stimulation is an endpoint of this signal transduction cascade. Based on the inhibitor studies, the cascade involves IR generated H_2O_2 and further RIRR elicited processes most likely induced by mitochondria and NOX. This probably leads to an activation of the PLC, followed by SOCE via IP_3R and STIM/Orai clustering with subsequent calcineurin-dependent NFAT activation.

3.5.2.2 **IR causes NFAT-dependent expression of cytokines**

The data so far indicate that X-ray exposure activates in T-cells all key steps which are required for a successful immune stimulation. The next question to answer is if this cascade also triggers the expression of relevant immunological target genes. To address this question, I have investigated the cytokine expression of IL2 and IFNγ on the RNA level by quantitative real-time PCR. I have furthermore examined the surface expression of the IL2 receptor subunit CD25 on a protein level by FACS analyses after X-ray doses of 1.25, 2 and 5 Gy. As a positive control, the established CD3/CD28/CD2 T-cell activator was used. The corresponding relative levels of each analyzed RNA/protein for either Jurkat cells or PBMCs are shown as an average + SD in **Figure 41**.

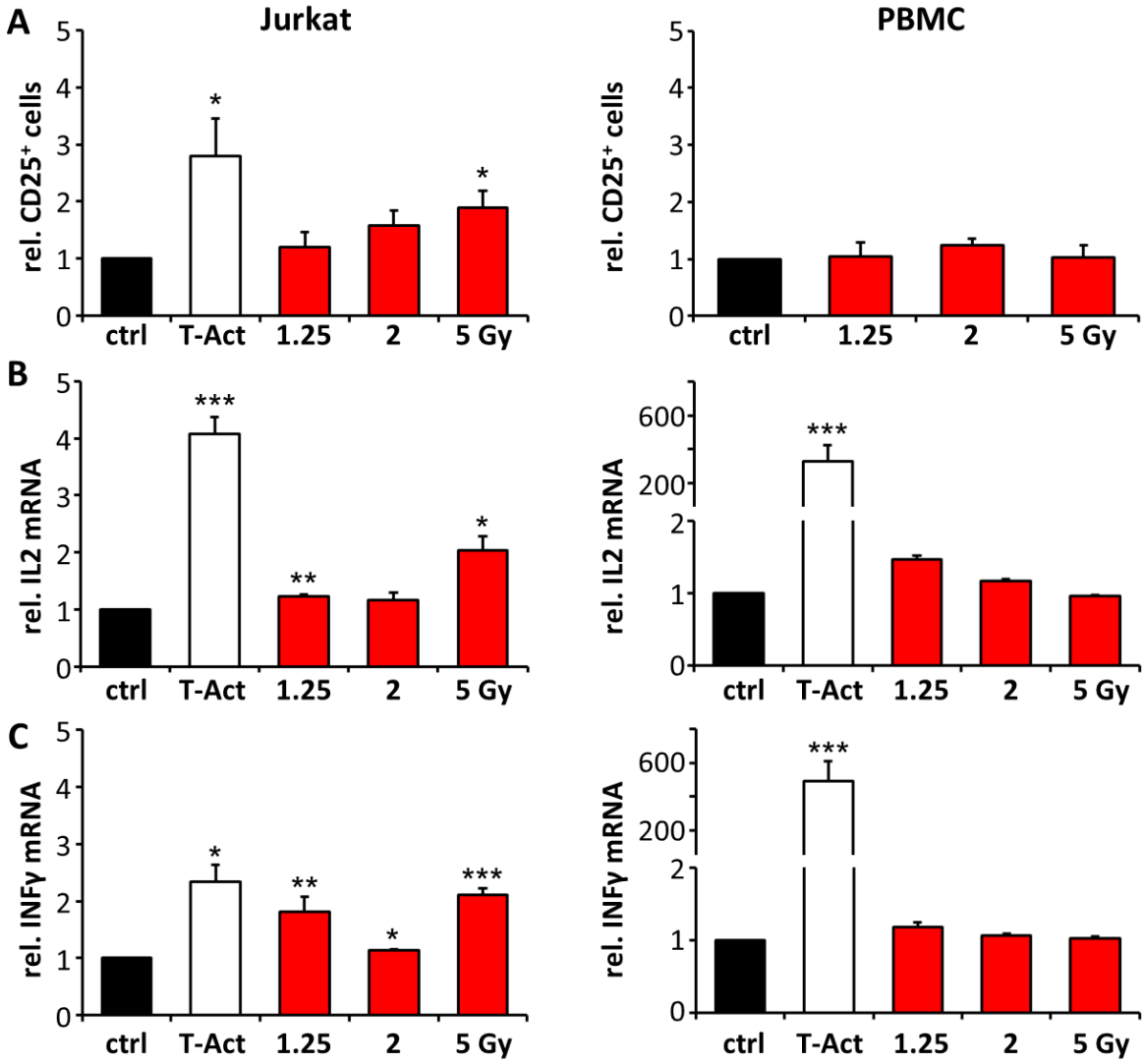

Figure 41: Irradiation stimulates immune activation in Jurkat cells and marginal changes in peripheral blood mononuclear cells (PBMC). (**A**) FACS analysis of relative CD25 surface expression in Jurkat cells and CD3-positive PBL 48 h following irradiation with doses of 1.25, 2, and 5 Gy respectively. Stimulation with 25 µl/ml of the CD3/CD28/CD2 T-cell activator (T-Act) in non-irradiated cells served as positive controls (N = 3). In PBMCs, T-act could not be applied due to inference with the CD3 stimulus. Quantification of interleukin2 (IL2) (**B**) and interferon-γ (IFNγ) (**C**) mRNA expression by quantitative real-time PCR in Jurkat cells and PBMCs 24 h after irradiation with doses of 1.25, 2, or 5 Gy respectively. Non-irradiated cells or cells stimulated with T-Act served as negative or positive control, respectively (N = 2). Data are represented as mean + SD. Student's t-test compared activator-treated or irradiated cells with non-irradiated controls; *P < 0.05, **P < 0.01, ***P < 0.001.

The results of these assays indicate a dose-dependent increase of CD25 expression after X-ray exposure in Jurkat cells (**Figure 41A, left**); the signal increase is significant compared to that in control cells. Further assays on the X-ray induced changes in the level of IFNγ and IL2 mRNA also revealed an increased expression in Jurkat cells after irradiation. The effect was most pronounced following 5 Gy exposure (**Figure 41B, C, left**). The latter effect on the RNA level of IFNγ is comparable to that obtained by the activator cocktail T-Act.

While X-ray irradiation evokes in Jurkat cells a positive signal in all three immune responses, PBMCs remain largely unaffected by the same treatment. While the positive control elicits in these cells a much higher (300-600-fold) increase in the relative amount of mRNA for IL2 and IFNγ (**Figure 41B, right**), X-ray exposure only evoked a marginal, if any, increase in the signal for IFNγ RNA (**Figure 41C, right**).

3.5.3 Conclusion and Perspectives

The morphological change in cell volume as well as the altered gene expression in response to appropriate stimuli is in T-cells mainly mediated by the NFAT signaling cascade (Diehn et al. 2002; Rosenbluth et al. 2006; MacIver et al. 2013). Therefore, the addition of the CD3/CD28/CD2 antigen cocktail, T-Act, leads to a dramatic increase in the relative number of $CD25^+$ Jurkat cells, as well as to a highly significant increase in the IL2 and IFNγ mRNA expression in Jurkat cells but even more pronounced in PBMCs. Worth noting is that the levels of the three T-cell activation markers in Jurkat cells increases in response to irradiation, but generally not as much as after addition of T-Act. In this context some scientists claim that without the assistance of appropriate co-transcription factors NFAT proteins probably do not bind properly to their DNA promotor regions *in vivo* (Macián et al. 2001; Jhun et al. 2006). This leads to the further assumption that an incomplete T-cell activation process evokes either i. the transcription of only a few target genes, ii. a small amount of the target genes or iii. even no significant increase in the RNA level and consequently also no increase of the protein level of the T-cell activation marker at all. On the basis of the present data, I conclude that irradiation triggers the NFAT signaling cascade and results in an elevated expression of some target genes like IL2 and IFNγ. With this stimulus the expression rate is not as high as when stimulating with T-Act. The reason might be the lack of additional co-stimuli and/or an inhibition of different intracellular signaling pathways, which are needed for an adequate immune response. In contrast to Jurkat cells, irradiation causes in PBMCs only marginal differences in expression of the immune markers compared to untreated control cells. The reason for this very different behavior of the two cell lines requires further investigation.

4. General Conclusion and Perspectives

A number of publications have been highlighting the complex and multifactorial relationship between radiation and the activation or suppression of the immune system (Gray et al. 1985; Nakamura et al. 1990; Feinendegen et al. 2007). It seems as if the effect of radiation on cells is strictly depending on the applied dose (Dagoglu et al. 2019) and on the type and differentiation state of the immune cell type of interest (Gray et al. 1985; Trotti et al. 2000). The goal of this work was to uncover an intracellular signal cascade, which connects primary events of IR and the subsequent long-term effects, which eventually lead to a change in the immunological activation state of exposed T-lymphocytes. Moreover, I attempt not only to find step by step responsible key regulators in the signaling pathway but also to elucidate their dynamical interplay.

4.1 Clinically relevant X-ray doses cause canonical T-lymphocyte activation

It is well established that stimulus induced Ca^{2+} signaling cascades are a key event in the activation of T-cells. Triggered by antigen binding to the TCR (Shaw et al. 1988; Mustelin et al. 1990), a downstream response mechanism is initiated, which promotes the release of Ca^{2+} from internal stores and eventually the activation of CICR (Trafford et al. 2000). In the latter process Ca^{2+} enters the cytoplasm primarily via CRAC channels and generate Ca^{2+}_{cyt} oscillations with distinct frequencies between 1-50 mHz (Salazar et al. 2008; Di Capite et al. 2009; Parekh 2011; Sharma et al. 2011) and stimuli-dependent amplitudes (Dolmetsch and Lewis 1994; Tomida et al. 2003; Parekh 2011). These dynamic changes in the concentration of the second messenger molecule are finally decoded by cytosolic Ca^{2+}-dependent target enzymes including kinases and phosphatases like calmodulin and calcineurin which consequently activate cytoplasmic, inactive transcription factors like NFAT (Erondu and Kennedy 1985; Dolmetsch et al. 2001) and foster its nuclear translocation and promoter properties (Beals et al. 1997; Crabtree and Olson 2002). With this network of signaling steps T-cells achieve precise control over essential lymphocyte functions such as cytokine production, proliferation, differentiation and cytotoxicity (Diehn et al. 2002).

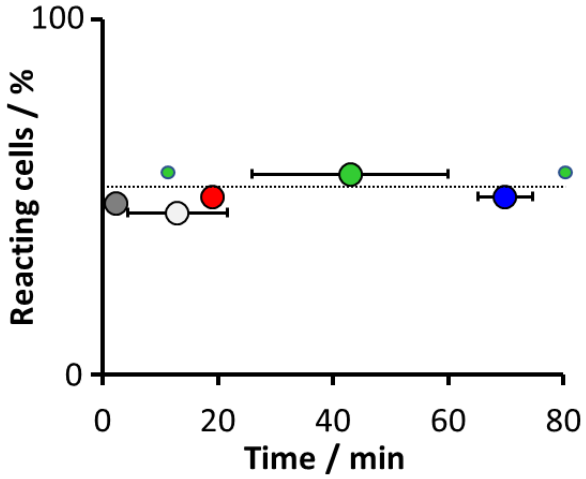

Figure 42: Dynamic range of key steps in an irradiation induced signal cascade in T-cells. Approximately 50% of Jurkat cells, irradiated with 5 Gy X-ray, show an increase in mitochondrial/cytosolic (light/dark gray) H2O2 concentration, Ca2+-release activated Ca2+ (CRAC) channel formation (red), Ca2+ oscillations with 2-4 mHz frequency (green) and nuclear translocation of the nuclear factor of activated T-cells (NFAT) (blue). Shown are the average values of the reaction times ± SD, small green data points represent fastest and slowest calcium response.

The present data now show, that the same signaling cascade involving CRAC channel activation, SOCE mediated Ca^{2+}_{cyt} excursions and translocation of NFAT from the cytosol to the nucleus and subsequent immunological modulations including IL2 and IFNγ expression and a cell size increase can be triggered in a population of T-cells by clinically relevant doses of ionizing irradiation. This is the first report which shows that X-ray irradiation can substitute a conventional antigen in triggering the same signaling cascade in these cells, which leads to immune activation. One additional aspect of the data, which further underpins this conclusion, is that also the sequence of signaling events, which is shown in **Figure 42**, is in perfect agreement with corresponding reaction times after physiological antigen stimulation as it is reported in the literature (Lewis and Cahalan 1989; Zweifach and Lewis 1995; Loh et al. 1996; Berridge et al. 1998; Sharma et al. 2011; Xia et al. 2018) reports the mean values for the times ± SD over which the signaling events take place; precisely the data in **Figure 42** indicate at which point of time 50% of the irradiated cells had initiated a defined signaling step. On the basis of these data, the signaling cascade can be decomposed into consecutive and causally related steps.

It is noticeable that the greatest variability of the cellular signaling responses is related to time of onset of the calcium oscillations; this value has the largest SD (**Figure 42**). To illustrate the overlap of this effect with the preceding formation of CRAC channels and the downstream nuclear translocation of NFAT this plot shows not only the average delay time but also the two extrema. The huge variability of the onset of the Ca^{2+} oscillations ranging in the CRAC channel and NFAT dynamic processes highlights its importance in mediating cellular effects. In this scenario the initial X-ray triggered event is a generation of ROS in the mitochondria. This causes in a direct or indirect manner a slow progressing increase in ROS in the cytosol. The latter is followed by the activation of CRAC channels, which then elicit Ca^{2+} oscillations in the cells (Grupe et al. 2010b; Bhardwaj et al. 2016). The direct consequence of this Ca^{2+} signaling is the nuclear transfer of NFAT and the subsequent activation of genes, which stimulate immune relevant molecules.

Taken together, the general paradigm provided by the present study is that IR is able to substitute the role of an antigen as stimulating agent for T-cell activation. Surprisingly this unambiguous cascade of X-ray triggered events has never been described before in T-cells. Overall, this study may help to better assess the risk of radiation therapy for tumor patients. It furthermore bears the potential of using the IR triggered hormetic effect, which is occurring in more than 50% of T-cells, as immune therapy in support of radiation therapy.

4.2 Limitations in the identification of key regulators of a radiation induced signaling cascade

Although the results of the current study already show many causal and temporal relationships between different key players of the IR induced signaling cascade, the available data are not sufficient to explain the gap between IR exposure and the onset of Ca^{2+}_{cyt} oscillations. Worth noting, however, is that also typical T-cell stimuli like phytohemagglutinin (Lewis and Cahalan 1989; Zweifach and Lewis 1993) or the addition of CD3 antibodies (Loh et al. 1996) are not causing an immediate Ca^{2+} response. In the latter case it is well established that an activation of the PLC and the generation of IP_3 is preceding the SOCE and the subsequent oscillation of Ca^{2+}_{cyt}. If the parallels between X-ray and antigens are a coincidence or based on a common mechanism like the generation of IP_3 and/or DAG upstream of SOCE needs to be investigated. The results of experiments with blockers of the PLC and the IP_3R on the X-ray induced increase in cell diameter of Jurkat cells already provide an indirect indication for an involvement of IP_3 signaling. These data are consistent with a model in which the increase in diameter is an endpoint of the immune stimulation and triggered by a Ca^{2+} signaling cascade including SOCE.

4.3 Differences in responses of the model T-cell line Jurkat and PBMCs

This study mainly employs the established Jurkat cells for analyzing immunological effects of IR. These cells have served for decades as a valid model system for immune stimulation of T-cells. But due to their immortalization they have lost their ability to differentiate and therefore consist of a very homogeneous gene pool (Abraham and Weiss 2004). Furthermore, a major difference to naïve PBMCs, which consist of many subpopulations such as T-, B-, and NK-cells, is that they do not possess a functional p53 (Vuitton et al. 1989; Lee et al. 1999). This acts as a tumor suppressor and a deficit leads to a constant proliferation of the cells (Perry and Levine 1993; Miyashita et al. 1994), whereas naive lymphocytes are not proliferating in the G0 status (Rosenbluth et al. 2006). This difference in the proliferation rate could be a reason for discriminative radiation sensitivity of the model cell line and naive PBMCs.

The present data show that many of the observations on Jurkat cells were also made in complementary experiments with PBL from healthy blood donors. This includes the X-ray stimulated clustering of STIM and Orai as well as the crucial nuclear transfer of NFAT. These data indicate that X-ray irradiation triggers in PBLs the same signaling cascade as in Jurkat cells. Still the analysis of the final markers of immune stimulation reveal some significant differences between the cell lines. This is the case for the X-ray induced CD25 surface expression and cytokine IFNγ and IL2 generation. The reasons for these differences are not known. There is compelling evidence that subpopulations of T-cells may display differential radiation sensitivities. While T-helper lymphocytes are characterized by a radiation sensitive phenotype, regulatory T-cells, appear to be more radioresistant. Notably, by comparing the effects of IR on gene expression in $CD4^+$ T-lymphocytes and in Jurkat cells, a predominant upregulation of p53 target genes in naïve $CD4^+$ positive cells is reported (Mori et al. 2004b). By contrast, Jurkat leukemic cells with a non-functional p53 gene are characterized by alterations in a more limited set of

genes. Accordingly, it can be assumed that activation of CD25 expression and cytokine response in Jurkat versus PBMCs may arise from a differential p53 dependent gene activation.

In summary, the present findings indicate that IR in a clinically relevant dose causes an immune activation in T-lymphocytes. At this point it is important to note that STIM and Orai proteins are not only present in T-cells but also in B-cells as well as in the phagocytic cells such as neutrophils, macrophages, and dendritic cells (Demaurex and Nunes 2016) where they regulate a multitude of cellular reactions (Vaeth and Feske 2018). With the general functional importance of these channel forming proteins in different types of cells it can be anticipated that IR activation of CRAC channels and the following Ca^{2+} signaling cascade may even have a more global importance in the reaction of the immune system to IR.

Altogether the present data and the reasonable speculations on the impact of X-ray irradiation on immune cells in the blood may have implications for both, toxic and secondary cancer inducing effects of radiotherapy. At the same time this information may also help to develop protocols which combine the cell killing effects of radiotherapy with a stimulation of the immune response in cancer patients.

5. List of references

Abraham RT, Weiss A. Jurkat T cells and development of the T-cell receptor signalling paradigm. Nature reviews. Immunology 2004;4:301–8.

Abuodeh Y, Venkat P, Kim S. Systematic review of case reports on the abscopal effect. Current Problems in Cancer 2016;40:25–37.

Adam-Vizi V, Starkov AA. Calcium and mitochondrial reactive oxygen species generation: how to read the facts. Journal of Alzheimer's disease : JAD 2010;20 Suppl 2:S413-26.

Alam MS, Gaida MM, Debnath S, Tagad HD, Miller Jenkins LM, Appella E, Rahman MJ, Ashwell JD. Unique properties of TCR-activated p38 are necessary for NFAT-dependent T-cell activation. PLoS biology 2018;16:e2004111.

Al-Mehdi A-B, Pastukh VM, Swiger BM, Reed DJ, Patel MR, Bardwell GC, Pastukh VV, Alexeyev MF, Gillespie MN. Perinuclear mitochondrial clustering creates an oxidant-rich nuclear domain required for hypoxia-induced transcription. Sci. Signal. 2012;5:ra47.

Alwarawrah Y, Kiernan K, MacIver NJ. Changes in Nutritional Status Impact Immune Cell Metabolism and Function. Front. Immunol. 2018;9:1055.

Ameziane-El-Hassani R, Morand S, Boucher J-L, Frapart Y-M, Apostolou D, Agnandji D, Gnidehou S, Ohayon R, Noël-Hudson M-S, Francon J, Lalaoui K, Virion A, Dupuy C. Dual oxidase-2 has an intrinsic Ca2+-dependent H2O2-generating activity. The Journal of biological chemistry 2005;280:30046–54.

Amundson J, Clapham D. Calcium waves. Current Opinion in Neurobiology 1993;3:375–82.

Apostol I, Heinstein PF, Low PS. Rapid Stimulation of an Oxidative Burst during Elicitation of Cultured Plant Cells : Role in Defense and Signal Transduction. Plant Physiology 1989;90:109–16.

Armstrong JG, Minsky BD. Radiation therapy for medically inoperable stage I and II non-small cell lung cancer. Cancer Treatment Reviews 1989;16:247–55.

Bading H, Ginty DD, Greenberg ME. Regulation of gene expression in hippocampal neurons by distinct calcium signaling pathways. Science 1993;260:181–6.

Barber EK, Dasgupta JD, Schlossman SF, Trevillyan JM, Rudd CE. The CD4 and CD8 antigens are coupled to a protein-tyrosine kinase (p56lck) that phosphorylates the CD3 complex. Proceedings of the National Academy of Sciences of the United States of America 1989;86:3277–81.

Barr VA, Bernot KM, Shaffer MH, Burkhardt JK, Samelson LE. Formation of STIM and Orai complexes: puncta and distal caps. Immunological reviews 2009;231:148–59.

Baskar R, Lee KA, Yeo R, Yeoh K-W. Cancer and radiation therapy: current advances and future directions. International Journal of Medical Sciences 2012;9:193–9.

Beals CR, Clipstone NA, Ho SN, Crabtree GR. Nuclear localization of NF-ATc by a calcineurin-dependent, cyclosporin-sensitive intramolecular interaction. Genes & Development 1997;11:824–34.

Bedard K, Krause K-H. The NOX family of ROS-generating NADPH oxidases: physiology and pathophysiology. Physiological reviews 2007;87:245–313.

Belousov VV, Fradkov AF, Lukyanov KA, Staroverov DB, Shakhbazov KS, Terskikh AV, Lukyanov S. Genetically encoded fluorescent indicator for intracellular hydrogen peroxide. Nature methods 2006;3:281–6.

Berchtold MW, Villalobo A. The many faces of calmodulin in cell proliferation, programmed cell death, autophagy, and cancer. Biochimica et biophysica acta 2014;1843:398–435.

Berridge MJ. Inositol trisphosphate and calcium signalling. Nature 1993;361:315–25.

Berridge MJ, Bootman MD, Lipp P. Calcium--a life and death signal. Nature 1998;395:645–8.

Berridge MJ, Bootman MD, Roderick HL. Calcium signalling: dynamics, homeostasis and remodelling. Nature reviews. Molecular cell biology 2003;4:517–29.

Berridge MJ, Dupont G. Spatial and temporal signalling by calcium. Current Opinion in Cell Biology 1994;6:267–74.

Berridge MJ, Lipp P, Bootman MD. The versatility and universality of calcium signalling. Nat Rev Mol Cell Biol 2000;1:11–21.

Berrier C, Besnard M, Ajouz B, Coulombe A, Ghazi A. Multiple mechanosensitive ion channels from Escherichia coli, activated at different thresholds of applied pressure. J. Membrane Biol. 1996;151:175–87.

Bhardwaj R, Hediger MA, Demaurex N. Redox modulation of STIM-ORAI signaling. Cell calcium 2016;60:142–52.

Biary N, Xie C, Kauffman J, Akar FG. Biophysical properties and functional consequences of reactive oxygen species (ROS)-induced ROS release in intact myocardium. The Journal of physiology 2011;589:5167–79.

Bienert GP, Chaumont F. Aquaporin-facilitated transmembrane diffusion of hydrogen peroxide. Biochimica et biophysica acta 2014;1840:1596–604.

Bienert GP, Møller ALB, Kristiansen KA, Schulz A, Møller IM, Schjoerring JK, Jahn TP. Specific aquaporins facilitate the diffusion of hydrogen peroxide across membranes. The Journal of biological chemistry 2007;282:1183–92.

Bilan DS, Pase L, Joosen L, Gorokhovatsky AY, Ermakova YG, Gadella TWJ, Grabher C, Schultz C, Lukyanov S, Belousov VV. HyPer-3: a genetically encoded H(2)O(2) probe with improved performance for ratiometric and fluorescence lifetime imaging. ACS chemical biology 2013;8:535–42.

Bird JJ, Brown DR, Mullen AC, Moskowitz NH, Mahowald MA, Sider JR, Gajewski TF, Wang C-R, Reiner SL. Helper T Cell Differentiation Is Controlled by the Cell Cycle. Immunity 1998;9:229–37.

Bito H, Deisseroth K, Tsien RW. CREB Phosphorylation and Dephosphorylation: A Ca2+- and Stimulus Duration–Dependent Switch for Hippocampal Gene Expression. Cell 1996;87:1203–14.

Bogeski I, Niemeyer BA. Redox regulation of ion channels. Antioxidants & redox signaling 2014;21:859–62.

Bootman MD, Rietdorf K, Collins T, Walker S, Sanderson M. Ca2+-sensitive fluorescent dyes and intracellular Ca2+ imaging. Cold Spring Harbor protocols 2013a;2013:83–99.

Bootman MD, Rietdorf K, Collins T, Walker S, Sanderson M. Loading fluorescent Ca2+ indicators into living cells. Cold Spring Harbor protocols 2013b;2013:122–5.

Boulware MJ, Marchant JS. Timing in cellular Ca2+ signaling. Current Biology 2008;18:R769-R776.

Braakman I, Helenius J, Helenius A. Manipulating disulfide bond formation and protein folding in the endoplasmic reticulum. The EMBO journal 1992;11:1717–22.

Brand K, Williams JF, Weidemann MJ. Glucose and glutamine metabolism in rat thymocytes. Biochemical Journal 1984;221:471–5.

Britschgi C, Riesterer O, Burger IA, Guckenberger M, Curioni-Fontecedro A. Report of an abscopal effect induced by stereotactic body radiotherapy and nivolumab in a patient with metastatic non-small cell lung cancer. Radiation Oncology 2018;13:102.

Browne SE, Bowling AC, MacGarvey U, Baik MJ, Berger SC, Muqit MM, Bird ED, Beal MF. Oxidative damage and metabolic dysfunction in Huntington's disease: selective vulnerability of the basal ganglia. Annals of neurology 1997;41:646–53.

Brusko TM, Wasserfall CH, Hulme MA, Cabrera R, Schatz D, Atkinson MA. Influence of membrane CD25 stability on T lymphocyte activity: implications for immunoregulation. PloS one 2009;4:e7980.

Buhrman G, Parker B, Sohn J, Rudolph J, Mattos C. Structural mechanism of oxidative regulation of the phosphatase Cdc25B via an intramolecular disulfide bond. Biochemistry 2005;44:5307–16.

Burdon RH, Rice-Evans C. Free radicals and the regulation of mammalian cell proliferation. Free radical research communications 1989;6:345–58.

Buxbaum JD, Choi EK, Luo Y, Lilliehook C, Crowley AC, Merriam DE, Wasco W. Calsenilin: a calcium-binding protein that interacts with the presenilins and regulates the levels of a presenilin fragment. Nature medicine 1998;4:1177–81.

Cahalan MD. STIMulating store-operated Ca(2+) entry. Nature cell biology 2009;11:669–77.

Cahalan MD, Chandy KG. The functional network of ion channels in T lymphocytes. Immunological reviews 2009;231:59–87.

Cai X, Nwokonko RM, Loktionova NA, Abdulqadir R, Baraniak JH, Wang Y, Trebak M, Zhou Y, Gill DL. Pore properties of Orai1 calcium channel dimers and their activation by the STIM1 ER calcium sensor. The Journal of biological chemistry 2018;293:12962–74.

Carafoli E. The release of calcium from heart mitochondria by sodium. Journal of molecular and cellular cardiology 1974;6:361–71.

Carafoli E. The regulation of intracellular calcium: Springer US. Advances in experimental medicine and biology 1982;151:461–72.

Carafoli E. Calcium signaling: a tale for all seasons. Proceedings of the National Academy of Sciences of the United States of America 2002;99:1115–22.

Carr EL, Kelman A, Wu GS, Gopaul R, Senkevitch E, Aghvanyan A, Turay AM, Frauwirth KA. Glutamine uptake and metabolism are coordinately regulated by ERK/MAPK during T lymphocyte activation. Journal of immunology (Baltimore, Md. : 1950) 2010;185:1037–44.

Carrasco S, Meyer T. STIM proteins and the endoplasmic reticulum-plasma membrane junctions. Annual review of biochemistry 2011;80:973–1000.

Castro JR, Saunders WM, Tobias CA, Chen GT, Curtis S, Lyman JT, Michael Collier J, Pitluck S, Woodruff KA, Blakely EA, Tenforde T, Char D, Phillips TL, Alpen EL. Treatment of cancer with heavy charged particles. International Journal of Radiation Oncology*Biology*Physics 1982;8:2191–8.

Cerretti DP, McKereghan K, Larsen A, Cantrell MA, Anderson D, Gillis S, Cosman D, Baker PE. Cloning, sequence, and expression of bovine interleukin 2. Proceedings of the National Academy of Sciences of the United States of America 1986;83:3223–7.

Chan JL, Lai M, Wang LH. Effect of dimerization on signal transduction and biological function of oncogenic Ros, insulin, and insulin-like growth factor I receptors. The Journal of biological chemistry 1997;272:146–53.

Chaudière J, Ferrari-Iliou R. Intracellular Antioxidants: from Chemical to Biochemical Mechanisms. Food and Chemical Toxicology 1999;37:949–62.

Choi H-J, Kim S-J, Mukhopadhyay P, Cho S, Woo J-R, Storz G, Ryu S-E. Structural Basis of the Redox Switch in the OxyR Transcription Factor. Cell 2001;105:103–13.

Clapham DE. Calcium signaling. Cell 2007;131:1047–58.

Cooling MT, Hunter P, Crampin EJ. Sensitivity of NFAT cycling to cytosolic calcium concentration: implications for hypertrophic signals in cardiac myocytes. Biophysical Journal 2009;96:2095–104.

Corre I, Niaudet C, Paris F. Plasma membrane signaling induced by ionizing radiation. Mutation research 2010;704:61–7.

Cortés-Ríos J, Torres MJ, Campos-Bustamante MP, Romero-Parra J, Letelier ME, Pessoa-Mahana D, Chung H, Faúndez M. NADPH oxidase activity: Spectrophotometric determination of superoxide using pyrogallol red. Analytical biochemistry 2017;536:96–100.

Covington ED, Wu MM, Lewis RS. Essential role for the CRAC activation domain in store-dependent oligomerization of STIM1. Molecular biology of the cell 2010;21:1897–907.

Crabtree GR, Olson EN. NFAT Signaling. Cell 2002;109:S67-S79.

Cuttler JM, Feinendegen LE, Socol Y. Evidence That Lifelong Low Dose Rates of Ionizing Radiation Increase Lifespan in Long- and Short-Lived Dogs. Dose-response : a publication of International Hormesis Society 2017;15:1559325817692903.

D Kline, J T Kline. Thapsigargin activates a calcium influx pathway in the unfertilized mouse egg and suppresses repetitive calcium transients in the fertilized egg. J. Biol. Chem. 1992;267:17624–30.

Dagoglu N, Karaman S, Caglar HB, Oral EN. Abscopal Effect of Radiotherapy in the Immunotherapy Era: Systematic Review of Reported Cases. Cureus 2019;11:e4103.

Daiber A, Di Lisa F, Oelze M, Kröller-Schön S, Steven S, Schulz E, Münzel T. Crosstalk of mitochondria with NADPH oxidase via reactive oxygen and nitrogen species signalling and its role for vascular function. British journal of pharmacology 2017;174:1670–89.

Dantzer R, Kelley KW. Stress and immunity: An integrated view of relationships between the brain and the immune system. Life Sciences 1989;44:1995–2008.

Darzynkiewicz Z, Staiano-Coico L, Melamed MR. Increased mitochondrial uptake of rhodamine 123 during lymphocyte stimulation. Proceedings of the National Academy of Sciences of the United States of America 1981;78:2383–7.

Davidson SM, Duchen MR. Calcium microdomains and oxidative stress. Cell calcium 2006;40:561–74.

Decrock E, Bock M de, Wang N, Gadicherla AK, Bol M, Delvaeye T, Vandenabeele P, Vinken M, Bultynck G, Krysko DV, Leybaert L. IP3, a small molecule with a powerful message. Biochimica et biophysica acta 2013;1833:1772–86.

Demaurex N, Nunes P. The role of STIM and ORAI proteins in phagocytic immune cells. American journal of physiology. Cell physiology 2016;310:C496-508.

Demaurex N, Poburko D. Cell biology. A revolving door for calcium. Science (New York, N.Y.) 2009;326:57–8.

Derler I, Schindl R, Fritsch R, Heftberger P, Riedl MC, Begg M, House D, Romanin C. The action of selective CRAC channel blockers is affected by the Orai pore geometry. Cell calcium 2013;53:139–51.

Di Capite J, Ng SW, Parekh AB. Decoding of cytoplasmic Ca(2+) oscillations through the spatial signature drives gene expression. Current biology : CB 2009;19:853–8.

Diebold L, Chandel NS. Mitochondrial ROS regulation of proliferating cells. Free radical biology & medicine 2016;100:86–93.

Diehn M, Alizadeh AA, Rando OJ, Liu CL, Stankunas K, Botstein D, Crabtree GR, Brown PO. Genomic expression programs and the integration of the CD28 costimulatory signal in T cell activation. Proceedings of the National Academy of Sciences of the United States of America 2002;99:11796–801.

Diercks B-P, Fliegert R, Guse AH. Mag-Fluo4 in T cells: Imaging of intra-organelle free Ca2+ concentrations. Biochimica et biophysica acta. Molecular cell research 2017;1864:977–86.

Dolmetsch RE, Lewis RS. Signaling between intracellular Ca2+ stores and depletion-activated Ca2+ channels generates Ca2+i oscillations in T lymphocytes. The Journal of general physiology 1994;103:365–88.

Dolmetsch RE, Pajvani U, Fife K, Spotts JM, Greenberg ME. Signaling to the nucleus by an L-type calcium channel-calmodulin complex through the MAP kinase pathway. Science 2001;294:333–9.

Dolmetsch RE, Xu K, Lewis RS. Calcium oscillations increase the efficiency and specificity of gene expression. Nature 1998;392:933–6.

Dong C, Kobayashi A, Konishi T, Shao C. Role of Endoplasmic Reticulum and Mitochondrion in Proton Microbeam Radiation-Induced Bystander Effect. Radiat Res 2020;193:63–72.

Dranoff G. Cytokines in cancer pathogenesis and cancer therapy. Nature reviews. Cancer 2004;4:11–22.

Driessens N, Versteyhe S, Ghaddhab C, Burniat A, Deken X de, van Sande J, Dumont J-E, Miot F, Corvilain B. Hydrogen peroxide induces DNA single- and double-strand breaks in thyroid cells and is therefore a potential mutagen for this organ. Endocrine-related cancer 2009;16:845–56.

Dröse S, Brandt U. Molecular Mechanisms of Superoxide Production by the Mitochondrial Respiratory Chain. In: Kadenbach B, editor. Mitochondrial Oxidative Phosphorylation. Nuclear-Encoded Genes, Enzyme Regulation, and Pathophysiology. New York, NY: Springer New York; 2012. p. 145–69.

Dumont A, Hehner SP, Hofmann TG, Ueffing M, Dröge W, Schmitz ML. Hydrogen peroxide-induced apoptosis is CD95-independent, requires the release of mitochondria-derived reactive oxygen species and the activation of NF-kappaB. Oncogene 1999;18:747–57.

Emmel EA, Verweij CL, Durand DB, Higgins KM, Lacy E, Crabtree GR. Cyclosporin A specifically inhibits function of nuclear proteins involved in T cell activation. Science 1989;246:1617–20.

Enyedi B, Niethammer P. H2O2: a chemoattractant? Methods in enzymology 2013;528:237–55.

Ermakova YG, Bilan DS, Matlashov ME, Mishina NM, Markvicheva KN, Subach OM, Subach FV, Bogeski I, Hoth M, Enikolopov G, Belousov VV. Red fluorescent genetically encoded indicator for intracellular hydrogen peroxide. Nature communications 2014a;5:5222.

Ermakova YG, Bilan DS, Matlashov ME, Mishina NM, Markvicheva KN, Subach OM, Subach FV, Bogeski I, Hoth M, Enikolopov G, Belousov VV. Red fluorescent genetically encoded indicator for intracellular hydrogen peroxide. Nat Commun 2014b;5:5222.

Erondu NE, Kennedy MB. Regional distribution of type II Ca2+/calmodulin-dependent protein kinase in rat brain. J. Neurosci. 1985;5:3270–7.

Exton JH. Regulation of phosphoinositide phospholipases by hormones, neurotransmitters, and other agonists linked to G proteins. Annual review of pharmacology and toxicology 1996;36:481–509.

Ezeriņa D, Takano Y, Hanaoka K, Urano Y, Dick TP. N-Acetyl Cysteine Functions as a Fast-Acting Antioxidant by Triggering Intracellular H2S and Sulfane Sulfur Production. Cell Chemical Biology 2018;25:447-459.e4.

Feinendegen LE. Reactive oxygen species in cell responses to toxic agents. Human & experimental toxicology 2002;21:85–90.

Feinendegen LE. Evidence for beneficial low level radiation effects and radiation hormesis. The British Journal of Radiology 2005;78:3–7.

Feinendegen LE, Pollycove M, Neumann RD. Whole-body responses to low-level radiation exposure: new concepts in mammalian radiobiology. Experimental Hematology 2007;35:37–46.

Ferranti CS, Cheng J, Thompson C, Zhang J, Rotolo JA, Buddaseth S, Fuks Z, Kolesnick RN. Fusion of lysosomes to plasma membrane initiates radiation-induced apoptosis. The Journal of cell biology 2020;219.

Feske S, Okamura H, Hogan PG, Rao A. Ca2+/calcineurin signalling in cells of the immune system. Biochemical and biophysical research communications 2003;311:1117–32.

Feske S, Skolnik EY, Prakriya M. Ion channels and transporters in lymphocyte function and immunity. Nature reviews. Immunology 2012;12:532–47.

Finkel T. Oxidant signals and oxidative stress. Current Opinion in Cell Biology 2003;15:247–54.

Fisher B, Wolmark N, Rockette H, Redmond C, Deutsch M, Wickerham DL, Fisher ER, Caplan R, Jones J, Lerner H. Postoperative adjuvant chemotherapy or radiation therapy for rectal cancer: results from NSABP protocol R-01. Journal of the National Cancer Institute 1988;80:21–9.

Flanagan WM, Corthésy B, Bram RJ, Crabtree GR. Nuclear association of a T-cell transcription factor blocked by FK-506 and cyclosporin A. Nature 1991;352:803–7.

Fomina AF, Fanger CM, Kozak JA, Cahalan MD. Single channel properties and regulated expression of Ca(2+) release-activated Ca(2+) (CRAC) channels in human T cells. J Cell Biol 2000;150:1435–44.

Foyer CH, Halliwell B. The presence of glutathione and glutathione reductase in chloroplasts: A proposed role in ascorbic acid metabolism. Planta 1976;133:21–5.

Fracchia KM, Pai CY, Walsh CM. Modulation of T Cell Metabolism and Function through Calcium Signaling. Frontiers in immunology 2013;4:324.

Frederick RL, Shaw JM. Moving mitochondria: establishing distribution of an essential organelle. Traffic (Copenhagen, Denmark) 2007;8:1668–75.

Fresu L, Dehpour A, Genazzani AA, Carafoli E, Guerini D. Plasma membrane calcium ATPase isoforms in astrocytes. Glia 1999;28:150–5.

Fridovich I. Superoxide anion radical (O2-.), superoxide dismutases, and related matters. The Journal of biological chemistry 1997;272:18515–7.

Fuck, S. Kurz- und Langzeiteffekte ionisierender Strahlung auf die T-Zelllinie Jurkat. Technische Universität Darmstadt 2017

Fulda S, Gorman AM, Hori O, Samali A. Cellular stress responses: cell survival and cell death. International journal of cell biology 2010;2010:214074.

Galione A, Lee HC, Busa WB. Ca(2+)-induced Ca2+ release in sea urchin egg homogenates: modulation by cyclic ADP-ribose. Science 1991;253:1143–6.

Garrity PA, Chen D, Rothenberg EV, Wold BJ. Interleukin-2 transcription is regulated in vivo at the level of coordinated binding of both constitutive and regulated factors. Molecular and cellular biology 1994;14:2159–69.

Gee KR, Brown KA, Chen WN, Bishop-Stewart J, Gray D, Johnson I. Chemical and physiological characterization of fluo-4 Ca(2+)-indicator dyes. Cell calcium 2000;27:97–106.

Ghanshani S, Wulff H, Miller MJ, Rohm H, Neben A, Gutman GA, Cahalan MD, Chandy KG. Up-regulation of the IKCa1 potassium channel during T-cell activation. Molecular mechanism and functional consequences. The Journal of biological chemistry 2000;275:37137–49.

Gibhardt CS, Vultur A, Bogeski I. Measuring Calcium and ROS by Genetically Encoded Protein Sensors and Fluorescent Dyes. Methods in molecular biology (Clifton, N.J.) 2019;1925:183–96.

Gill T, Levine AD. Mitochondria-derived hydrogen peroxide selectively enhances T cell receptor-initiated signal transduction. The Journal of biological chemistry 2013;288:26246–55.

Giusti AF, Xu W, Hinkle B, Terasaki M, Jaffe LA. Evidence that fertilization activates starfish eggs by sequential activation of a Src-like kinase and phospholipase cgamma. The Journal of biological chemistry 2000;275:16788–94.

Golden EB, Demaria S, Schiff PB, Chachoua A, Formenti SC. An abscopal response to radiation and ipilimumab in a patient with metastatic non-small cell lung cancer. Cancer Immunology Research 2013;1:365–72.

Gomes AP, Price NL, Ling AJY, Moslehi JJ, Montgomery MK, Rajman L, White JP, Teodoro JS, Wrann CD, Hubbard BP, Mercken EM, Palmeira CM, Cabo R de, Rolo AP, Turner N, Bell EL, Sinclair DA. Declining NAD(+) induces a pseudohypoxic state disrupting nuclear-mitochondrial communication during aging. Cell 2013;155:1624–38.

Görlach A, Bertram K, Hudecova S, Krizanova O. Calcium and ROS: A mutual interplay. Redox biology 2015;6:260–71.

Gouspillou G, Scheede-Bergdahl C, Spendiff S, Vuda M, Meehan B, Mlynarski H, Archer-Lahlou E, Sgarioto N, Purves-Smith FM, Konokhova Y, Rak J, Chevalier S, Taivassalo T, Hepple RT, Jagoe RT. Anthracycline-containing chemotherapy causes long-term impairment of mitochondrial respiration and increased reactive oxygen species release in skeletal muscle. Sci Rep 2015;5:8717.

Grabarek Z. Structural basis for diversity of the EF-hand calcium-binding proteins. Journal of molecular biology 2006;359:509–25.

Gray WC, Chretien PB, Suter CM, Revie DR, Tomazic VT, Blanchard CL, Aygun C, Amornmarn R, Ordonez JV. Effects of radiation therapy on T-lymphocyte subpopulations in patients with head and neck cancer. Otolaryngology--head and neck surgery : official journal of American Academy of Otolaryngology-Head and Neck Surgery 1985;93:650–60.

Gross E, Sevier CS, Heldman N, Vitu E, Bentzur M, Kaiser CA, Thorpe C, Fass D. Generating disulfides enzymatically: reaction products and electron acceptors of the endoplasmic reticulum thiol oxidase Ero1p. Proceedings of the National Academy of Sciences of the United States of America 2006;103:299–304.

Grumont R, Lock P, Mollinari M, Shannon FM, Moore A, Gerondakis S. The mitogen-induced increase in T cell size involves PKC and NFAT activation of Rel/NF-kappaB-dependent c-myc expression. Immunity 2004;21:19–30.

Grupe M, Myers G, Penner R, Fleig A. Activation of store-operated I(CRAC) by hydrogen peroxide. Cell calcium 2010a;48:1–9.

Grupe M, Myers G, Penner R, Fleig A. Activation of store-operated I(CRAC) by hydrogen peroxide. Cell calcium 2010b;48:1–9.

Guerini D, Coletto L, Carafoli E. Exporting calcium from cells. Cell calcium 2005;38:281–9.

Guse AH, Wolf IMA. Ca(2+) microdomains, NAADP and type 1 ryanodine receptor in cell activation. Biochimica et biophysica acta 2016;1863:1379–84.

Gwack Y, Feske S, Srikanth S, Hogan PG, Rao A. Signalling to transcription: store-operated Ca2+ entry and NFAT activation in lymphocytes. Cell calcium 2007;42:145–56.

Hafer K, Konishi T, Schiestl RH. Radiation-induced long-lived extracellular radicals do not contribute to measurement of intracellular reactive oxygen species using the dichlorofluorescein method. Radiation research 2008;169:469–73.

Hajnóczky G, Csordás G, Das S, Garcia-Perez C, Saotome M, Sinha Roy S, Yi M. Mitochondrial calcium signalling and cell death: approaches for assessing the role of mitochondrial Ca2+ uptake in apoptosis. Cell calcium 2006;40:553–60.

Hajnóczky G, Robb-Gaspers LD, Seitz MB, Thomas AP. Decoding of cytosolic calcium oscillations in the mitochondria. Cell 1995;82:415–24.

Hallahan DE, Virudachalam S, Kuchibhotla J, Kufe DW, Weichselbaum RR. Membrane-derived second messenger regulates x-ray-mediated tumor necrosis factor alpha gene induction. Proceedings of the National Academy of Sciences of the United States of America 1994;91:4897–901.

Halliwell B. SUPEROXIDE DISMUTASE, CATALASE AND GLUTATHIONE PEROXIDASE: SOLUTIONS TO THE PROBLEMS OF LIVING WITH OXYGEN. New Phytol 1974;73:1075–86.

Hecquet CM, Ahmmed GU, Vogel SM, Malik AB. Role of TRPM2 channel in mediating H2O2-induced Ca2+ entry and endothelial hyperpermeability. Circulation research 2008;102:347–55.

Hempel N, Trebak M. Crosstalk between calcium and reactive oxygen species signaling in cancer. Cell calcium 2017;63:70–96.

Hiniker SM, Chen DS, Reddy S, Chang DT, Jones JC, Mollick JA, Swetter SM, Knox SJ. A systemic complete response of metastatic melanoma to local radiation and immunotherapy. Translational Oncology 2012;5:404–7.

Hogan PG. Calcium-NFAT transcriptional signalling in T cell activation and T cell exhaustion. Cell calcium 2017;63:66–9.

Hogan PG, Lewis RS, Rao A. Molecular basis of calcium signaling in lymphocytes: STIM and ORAI. Annual review of immunology 2010;28:491–533.

Hoth M, Penner R. Depletion of intracellular calcium stores activates a calcium current in mast cells. Nature 1992;355:353–6.

Huang K, Caplan J, Sweigard JA, Czymmek KJ, Donofrio NM. Optimization of the HyPer sensor for robust real-time detection of hydrogen peroxide in the rice blast fungus. Molecular plant pathology 2017;18:298–307.

Hughes-Fulford M. Signal transduction and mechanical stress. Sci. STKE 2004;2004:RE12.

Imboden JB, Stobo JD. Transmembrane signalling by the T cell antigen receptor. Perturbation of the T3-antigen receptor complex generates inositol phosphates and releases calcium ions from intracellular stores. J Exp Med 1985;161:446–56.

Iñarrea P, Moini H, Han D, Rettori D, Aguiló I, Alava MA, Iturralde M, Cadenas E. Mitochondrial respiratory chain and thioredoxin reductase regulate intermembrane Cu,Zn-superoxide dismutase activity: implications for mitochondrial energy metabolism and apoptosis. The Biochemical journal 2007;405:173–9.

Jackson SH, Devadas S, Kwon J, Pinto LA, Williams MS. T cells express a phagocyte-type NADPH oxidase that is activated after T cell receptor stimulation. Nature immunology 2004;5:818–27.

Jhun BS, Lee JY, Oh YT, Lee JH, Choe W, Baik HH, Kim SS, Yoon K-S, Ha J, Kang I. Inhibition of AMP-activated protein kinase suppresses IL-2 expression through down-regulation of NF-AT and AP-1 activation in Jurkat T cells. Biochemical and biophysical research communications 2006;351:986–92.

Jiang F, Zhang Y, Dusting GJ. NADPH oxidase-mediated redox signaling: roles in cellular stress response, stress tolerance, and tissue repair. Pharmacological reviews 2011;63:218–42.

Kahn CR. Membrane receptors for hormones and neurotransmitters. J Cell Biol 1976;70:261–86.

Kam WW-Y, Banati RB. Effects of ionizing radiation on mitochondria. Free radical biology & medicine 2013;65:607–19.

Kamiński MM, Röth D, Krammer PH, Gülow K. Mitochondria as oxidative signaling organelles in T-cell activation: physiological role and pathological implications. Archivum immunologiae et therapiae experimentalis 2013;61:367–84.

Kar P, Mirams GR, Christian HC, Parekh AB. Control of NFAT Isoform Activation and NFAT-Dependent Gene Expression through Two Coincident and Spatially Segregated Intracellular Ca2+ Signals. Molecular cell 2016;64:746–59.

Katz S, Boland R, Santillán G. Modulation of ERK 1/2 and p38 MAPK signaling pathways by ATP in osteoblasts: involvement of mechanical stress-activated calcium influx, PKC and Src activation. The International Journal of Biochemistry & Cell Biology 2006;38:2082–91.

Kawasaki T, Lange I, Feske S. A minimal regulatory domain in the C terminus of STIM1 binds to and activates ORAI1 CRAC channels. Biochemical and biophysical research communications 2009;385:49–54.

Kehlenbach RH, Dickmanns A, Gerace L. Nucleocytoplasmic shuttling factors including Ran and CRM1 mediate nuclear export of NFAT In vitro. J Cell Biol 1998;141:863–74.

Khodorov B, Pinelis V, Storozhevykh T, Yuravichus A, Khaspekhov L. Blockade of mitochondrial Ca 2+ uptake by mitochondrial inhibitors amplifies the glutamate-induced calcium response in cultured cerebellar granule cells. FEBS Letters 1999;458:162–6.

Kiani A, García-Cózar FJ, Habermann I, Laforsch S, Aebischer T, Ehninger G, Rao A. Regulation of interferon-gamma gene expression by nuclear factor of activated T cells. Blood 2001;98:1480–8.

Kil IS, Lee SK, Ryu KW, Woo HA, Hu M-C, Bae SH, Rhee SG. Feedback control of adrenal steroidogenesis via H2O2-dependent, reversible inactivation of peroxiredoxin III in mitochondria. Molecular cell 2012;46:584–94.

Kim H, Kim Y-N, Kim H, Kim C-W. Oxidative stress attenuates Fas-mediated apoptosis in Jurkat T cell line through Bfl-1 induction. Oncogene 2005a;24:1252–61.

Kim H, Kim Y-N, Kim H, Kim C-W. Oxidative stress attenuates Fas-mediated apoptosis in Jurkat T cell line through Bfl-1 induction. Oncogene 2005b;24:1252–61.

Krishnamoorthy K, Veerapandian M, Zhang L-H, Yun K, Kim SJ. Antibacterial Efficiency of Graphene Nanosheets against Pathogenic Bacteria via Lipid Peroxidation. J. Phys. Chem. C 2012;116:17280–7.

Kubis H-P, Scheibe RJ, Meissner JD, Hornung G, Gros G. Fast-to-slow transformation and nuclear import/export kinetics of the transcription factor NFATc1 during electrostimulation of rabbit muscle cells in culture. The Journal of physiology 2002;541:835–47.

L Legendre, Y G Yueh, R Crain, N Haddock, P F Heinstein, P S Low. Phospholipase C activation during elicitation of the oxidative burst in cultured plant cells. J. Biol. Chem. 1993;268:24559–63.

La Monte SM de, Tong M. Brain metabolic dysfunction at the core of Alzheimer's disease. Biochemical pharmacology 2014;88:548–59.

Laleu B, Gaggini F, Orchard M, Fioraso-Cartier L, Cagnon L, Houngninou-Molango S, Gradia A, Duboux G, Merlot C, Heitz F, Szyndralewiez C, Page P. First in class, potent, and orally bioavailable NADPH oxidase isoform 4 (Nox4) inhibitors for the treatment of idiopathic pulmonary fibrosis. Journal of Medicinal Chemistry 2010;53:7715–30.

Lam K-P, Kühn R, Rajewsky K. In Vivo Ablation of Surface Immunoglobulin on Mature B Cells by Inducible Gene Targeting Results in Rapid Cell Death. Cell 1997;90:1073–83.

Lambeth JD. NOX enzymes and the biology of reactive oxygen. Nature reviews. Immunology 2004;4:181–9.

Large M, Hehlgans S, Reichert S, Gaipl US, Fournier C, Rödel C, Weiss C, Rödel F. Study of the anti-inflammatory effects of low-dose radiation: The contribution of biphasic regulation of the antioxidative system in endothelial cells. Strahlentherapie und Onkologie : Organ der Deutschen Rontgengesellschaft … [et al] 2015;191:742–9.

Laver DR, Kong CHT, Imtiaz MS, Cannell MB. Termination of calcium-induced calcium release by induction decay: an emergent property of stochastic channel gating and molecular scale architecture. Journal of molecular and cellular cardiology 2013;54:98–100.

Le Caër S. Water Radiolysis: Influence of Oxide Surfaces on H2 Production under Ionizing Radiation. Water 2011;3:235–53.

Lee I-T, Yang C-M. Role of NADPH oxidase/ROS in pro-inflammatory mediators-induced airway and pulmonary diseases. Biochemical pharmacology 2012;84:581–90.

Lee KP, Yuan JP, Zeng W, So I, Worley PF, Muallem S. Molecular determinants of fast Ca2+-dependent inactivation and gating of the Orai channels. PNAS 2009;106:14687–92.

Lee W, Wang C, Chien M. Virus antigen expression and alterations in peripheral blood mononuclear cell subpopulations after classical swine fever virus infection. Veterinary Microbiology 1999;67:17–29.

Lemasters JJ, Theruvath TP, Zhong Z, Nieminen A-L. Mitochondrial calcium and the permeability transition in cell death. Biochimica et biophysica acta 2009;1787:1395–401.

Lewis RS, Cahalan MD. Mitogen-induced oscillations of cytosolic Ca2+ and transmembrane Ca2+ current in human leukemic T cells. Cell regulation 1989;1:99–112.

Leybaert L. IP3, still on the move but now in the slow lane. Science signaling 2016;9:fs17.

Li H-H, Wang Y-W, Chen R, Zhou B, Ashwell JD, Fornace AJ. Ionizing Radiation Impairs T Cell Activation by Affecting Metabolic Reprogramming. International journal of biological sciences 2015;11:726–36.

Lin Z, Fillmore GC, Um T-H, Elenitoba-Johnson KSJ, Lim MS. Comparative microarray analysis of gene expression during activation of human peripheral blood T cells and leukemic Jurkat T cells. Laboratory investigation; a journal of technical methods and pathology 2003;83:765–76.

Lioudyno MI, Kozak JA, Penna A, Safrina O, Zhang SL, Sen D, Roos J, Stauderman KA, Cahalan MD. Orai1 and STIM1 move to the immunological synapse and are up-regulated during T cell activation. PNAS 2008;105:2011–6.

Lock JT, Smith IF, Parker I. Spatial-temporal patterning of Ca2+ signals by the subcellular distribution of IP3 and IP3 receptors. Seminars in cell & developmental biology 2019;94:3–10.

Lodygin D, Odoardi F, Schläger C, Körner H, Kitz A, Nosov M, van den Brandt J, Reichardt HM, Haberl M, Flügel A. A combination of fluorescent NFAT and H2B sensors uncovers dynamics of T cell activation in real time during CNS autoimmunity. Nature medicine 2013;19:784–90.

Loh C, Carew JA, Kim J, Hogan PG, Rao A. T-cell receptor stimulation elicits an early phase of activation and a later phase of deactivation of the transcription factor NFAT1. Molecular and cellular biology 1996;16:3945–54.

Luckey TD. Radiation hormesis: the good, the bad, and the ugly. Dose-response : a publication of International Hormesis Society 2006;4:169–90.

Lyte M, Nelson SG, Thompson ML. Innate and adaptive immune responses in a social conflict paradigm. Clinical Immunology and Immunopathology 1990;57:137–47.

Ma G, Zheng S, Ke Y, Zhou L, He L, Huang Y, Wang Y, Zhou Y. Molecular Determinants for STIM1 Activation During Store-Operated Ca2+ Entry. Current molecular medicine 2017;17:60–9.

Macian F. NFAT proteins: key regulators of T-cell development and function. Nature reviews. Immunology 2005;5:472–84.

Macián F, López-Rodríguez C, Rao A. Partners in transcription: NFAT and AP-1. Oncogene 2001;20:2476–89.

MacIver NJ, Michalek RD, Rathmell JC. Metabolic regulation of T lymphocytes. Annual review of immunology 2013;31:259–83.

MacLennan IC, Vinuesa CG. Dendritic Cells, BAFF, and APRIL. Immunity 2002;17:235–8.

Malaney P, Nicosia SV, Davé V. One mouse, one patient paradigm: New avatars of personalized cancer therapy. Cancer Letters 2014;344:1–12.

Malek TR. The biology of interleukin-2. Annual review of immunology 2008;26:453–79.

Manda K, Glasow A, Paape D, Hildebrandt G. Effects of ionizing radiation on the immune system with special emphasis on the interaction of dendritic and T cells. Front. Oncol. 2012;2:102.

Mangialavori IC, Ferreira-Gomes MS, Saffioti NA, González-Lebrero RM, Rossi RC, Rossi JPFC. Conformational changes produced by ATP binding to the plasma membrane calcium pump. The Journal of biological chemistry 2013;288:31030–41.

Marban E, Wier WG. Ryanodine as a tool to determine the contributions of calcium entry and calcium release to the calcium transient and contraction of cardiac Purkinje fibers. Circulation research 1985;56:133–8.

Markvicheva KN, Bilan DS, Mishina NM, Gorokhovatsky AY, Vinokurov LM, Lukyanov S, Belousov VV. A genetically encoded sensor for H2O2 with expanded dynamic range. Bioorganic & medicinal chemistry 2011;19:1079–84.

Maruyama T, Kanaji T, Nakade S, Kanno T, Mikoshiba K. 2APB, 2-aminoethoxydiphenyl borate, a membrane-penetrable modulator of Ins(1,4,5)P3-induced Ca2+ release. J Biochem 1997;122:498–505.

Mazars C, Thuleau P, Lamotte O, Bourque S. Cross-talk between ROS and calcium in regulation of nuclear activities. Molecular plant 2010;3:706–18.

McDermott U, Settleman J. Personalized cancer therapy with selective kinase inhibitors: an emerging paradigm in medical oncology. Journal of clinical oncology : official journal of the American Society of Clinical Oncology 2009;27:5650–9.

Medzhitov R, Janeway CA. Innate immune recognition and control of adaptive immune responses. Seminars in Immunology 1998;10:351–3.

Meesungnoen J, Jay-Gerin J-P. High-LET ion radiolysis of water: oxygen production in tracks. Radiation research 2009;171:379–86.

Meric-Bernstam F, Mills GB. Overcoming implementation challenges of personalized cancer therapy. Nat Rev Clin Oncol 2012;9:542–8.

Mikkelsen RB, Wardman P. Biological chemistry of reactive oxygen and nitrogen and radiation-induced signal transduction mechanisms. Oncogene 2003;22:5734–54.

Minamikawa T, Sriratana A, Williams DA, Bowser DN, Hill JS, Nagley P. Chloromethyl-X-rosamine (MitoTracker Red) photosensitises mitochondria and induces apoptosis in intact human cells. Journal of cell science 1999;112 (Pt 14):2419–30.

Mishina NM, Markvicheva KN, Bilan DS, Matlashov ME, Shirmanova MV, Liebl D, Schultz C, Lukyanov S, Belousov VV. Visualization of intracellular hydrogen peroxide with HyPer, a genetically encoded fluorescent probe. Methods in enzymology 2013;526:45–59.

Miyashita T, Krajewski S, Krajewska M, Wang HG, Lin HK, Liebermann DA, Hoffman B, Reed JC. Tumor suppressor p53 is a regulator of bcl-2 and bax gene expression in vitro and in vivo. Oncogene 1994;9:1799–805.

Miyazaki S, Shirakawa H, Nakada K, Honda Y. Essential role of the inositol 1,4,5-trisphosphate receptor/Ca2+ release channel in Ca2+ waves and Ca2+ oscillations at fertilization of mammalian eggs. Developmental Biology 1993;158:62–78.

Mogami H, Lloyd Mills C, Gallacher DV. Phospholipase C inhibitor, U73122, releases intracellular Ca2+, potentiates Ins(1,4,5)P3-mediated Ca2+ release and directly activates ion channels in mouse pancreatic acinar cells. Biochem J 1997;324 (Pt 2):645–51.

Mori M, Benotmane MA, Tirone I, Hooghe-Peters EL, Desaintes C. Transcriptional response to ionizing radiation in lymphocyte subsets. Cellular and molecular life sciences : CMLS 2005;62:1489–501.

Mori M, Benotmane MA, Vanhove D, van Hummelen P, Hooghe-Peters EL, Desaintes C. Effect of ionizing radiation on gene expression in CD4+ T lymphocytes and in Jurkat cells: unraveling novel pathways in radiation response. Cellular and molecular life sciences : CMLS 2004a;61:1955–64.

Mori M, Benotmane MA, Vanhove D, van Hummelen P, Hooghe-Peters EL, Desaintes C. Effect of ionizing radiation on gene expression in CD4+ T lymphocytes and in Jurkat cells: unraveling novel pathways in radiation response. Cellular and molecular life sciences : CMLS 2004b;61:1955–64.

Murphy MP. How mitochondria produce reactive oxygen species. The Biochemical journal 2009;417:1–13.

Mustelin T, Coggeshall K, Isakov N, Altman A. T cell antigen receptor-mediated activation of phospholipase C requires tyrosine phosphorylation. Science 1990;247:1584–7.

Nahorski SR, Young KW, John Challiss RA, Nash MS. Visualizing phosphoinositide signalling in single neurons gets a green light. Trends in Neurosciences 2003;26:444–52.

Nakamura N, Kusunoki Y, Akiyama M. Radiosensitivity of CD4 or CD8 Positive Human T-Lymphocytes by an in Vitro Colony Formation Assay. Radiation research 1990;123:224.

Nambiar D, Rajamani P, Singh RP. Effects of phytochemicals on ionization radiation-mediated carcinogenesis and cancer therapy. Mutation research 2011;728:139–57.

Narayanan PK, Goodwin EH, Lehnert BE. Alpha particles initiate biological production of superoxide anions and hydrogen peroxide in human cells. Cancer research 1997;57:3963–71.

Neuenschwander U, Vernooij B, Friedrich L, Uknes S, Kessmann H, Ryals J. Is hydrogen peroxide a second messenger of salicylic acid in systemic acquired resistance? Plant J 1995;8:227–33.

Ng CF, Schafer FQ, Buettner GR, Rodgers VGJ. The rate of cellular hydrogen peroxide removal shows dependency on GSH: mathematical insight into in vivo H2O2 and GPx concentrations. Free radical research 2007;41:1201–11.

Nguyen NT, Ma G, Lin E, D'Souza B, Jing J, He L, Huang Y, Zhou Y. CRAC channel-based optogenetics. Cell calcium 2018;75:79–88.

Nicotera P, Bellomo G, Orrenius S. Calcium-mediated mechanisms in chemically induced cell death. Annual review of pharmacology and toxicology 1992;32:449–70.

Nwokonko RM, Zhou Y, Cai X, Loktionova N, Trebak M, Gill DL. STIM Proteins Cluster Orai1 Channels and Modulate Receptor-Mediated Calcium Signals. Biophysical Journal 2018;114:285a.

Odermatt A, Taschner PE, Khanna VK, Busch HF, Karpati G, Jablecki CK, Breuning MH, MacLennan DH. Mutations in the gene-encoding SERCA1, the fast-twitch skeletal muscle sarcoplasmic reticulum Ca2+ ATPase, are associated with Brody disease. Nature Genetics 1996;14:191–4.

Ogura A, Oowada S, Kon Y, Hirayama A, Yasui H, Meike S, Kobayashi S, Kuwabara M, Inanami O. Redox regulation in radiation-induced cytochrome c release from mitochondria of human lung carcinoma A549 cells. Cancer Letters 2009;277:64–71.

Okuno T, Kondelis N. Evaluation of dithiothreitol (DTT) for inactivation of IgM antibodies. Journal of Clinical Pathology 1978;31:1152–5.

Orrenius S, McCabe MJ, Nicotera P. Ca2+-dependent mechanisms of cytotoxicity and programmed cell death. Toxicology Letters 1992;64-65:357–64.

Osinalde N, Moss H, Arrizabalaga O, Omaetxebarria MJ, Blagoev B, Zubiaga AM, Fullaondo A, Arizmendi JM, Kratchmarova I. Interleukin-2 signaling pathway analysis by quantitative phosphoproteomics. Journal of proteomics 2011;75:177–91.

Ozinsky A, Underhill DM, Fontenot JD, Hajjar AM, Smith KD, Wilson CB, Schroeder L, Aderem A. The repertoire for pattern recognition of pathogens by the innate immune system is defined by cooperation between toll-like receptors. Proceedings of the National Academy of Sciences of the United States of America 2000;97:13766–71.

Parekh AB. Decoding cytosolic Ca2+ oscillations. Trends in biochemical sciences 2011;36:78–87.

Park CY, Hoover PJ, Mullins FM, Bachhawat P, Covington ED, Raunser S, Walz T, Garcia KC, Dolmetsch RE, Lewis RS. STIM1 clusters and activates CRAC channels via direct binding of a cytosolic domain to Orai1. Cell 2009;136:876–90.

Passwell JH, Levanon M, Davidsohn J, Kohen F, Ramot B. The effect of human monocytes and macrophages on lymphocyte proliferation. Immunology 1982;47:175–81.

Patel DM, Arnold PY, White GA, Nardella JP, Mannie MD. Class II MHC/peptide complexes are released from APC and are acquired by T cell responders during specific antigen recognition. Journal of immunology (Baltimore, Md. : 1950) 1999;163:5201–10.

Patwardhan RS, Sharma D, Checker R, Thoh M, Sandur SK. Spatio-temporal changes in glutathione and thioredoxin redox couples during ionizing radiation-induced oxidative stress regulate tumor radio-resistance. Free radical research 2015;49:1218–32.

Pedersen PL, Carafoli E. Ion motive ATPases. I. Ubiquity, properties, and significance to cell function. Trends in biochemical sciences 1987;12:146–50.

Peglow M, Niemeyer BA, Hoth M, Rieger H. Interplay of channels, pumps and organelle location in calcium microdomain formation. New J. Phys. 2013;15:55022.

Perry ME, Levine AJ. Tumor-suppressor p53 and the cell cycle. Current Opinion in Genetics & Development 1993;3:50–4.

Persechini A, Moncrief ND, Kretsinger RH. The EF-hand family of calcium-modulated proteins. Trends in Neurosciences 1989;12:462–7.

Phillips MJ, Voeltz GK. Structure and function of ER membrane contact sites with other organelles. Nature reviews. Molecular cell biology 2016;17:69–82.

Politi A, Gaspers LD, Thomas AP, Höfer T. Models of IP3 and Ca2+ oscillations: frequency encoding and identification of underlying feedbacks. Biophysical Journal 2006;90:3120–33.

Pouget J-P, Lozza C, Deshayes E, Boudousq V, Navarro-Teulon I. Introduction to radiobiology of targeted radionuclide therapy. Frontiers in medicine 2015;2:12.

Pozzan T, Rizzuto R, Volpe P, Meldolesi J. Molecular and cellular physiology of intracellular calcium stores. Physiological reviews 1994;74:595–636.

Prakriya M, Lewis RS. CRAC channels: activation, permeation, and the search for a molecular identity. Cell calcium 2003;33:311–21.

Putney JW. A model for receptor-regulated calcium entry. Cell calcium 1986;7:1–12.

R. Mole. Whole body irradiation; radiobiology or medicine? The British Journal of Radiology 1953.

Raucher D, Stauffer T, Chen W, Shen K, Guo S, York JD, Sheetz MP, Meyer T. Phosphatidylinositol 4,5-Bisphosphate Functions as a Second Messenger that Regulates Cytoskeleton–Plasma Membrane Adhesion. Cell 2000;100:221–8.

Reinherz EL, Kung PC, Goldstein G, Levey RH, Schlossman SF. Discrete stages of human intrathymic differentiation: analysis of normal thymocytes and leukemic lymphoblasts of T-cell lineage. Proceedings of the National Academy of Sciences of the United States of America 1980;77:1588–92.

Renard-Rooney DC, Joseph SK, Seitz MB, Thomas AP. Effect of oxidized glutathione and temperature on inositol 1,4,5-trisphosphate binding in permeabilized hepatocytes. Biochem J 1995;310 (Pt 1):185–92.

Reth M. Hydrogen peroxide as second messenger in lymphocyte activation. Nat Immunol 2002;3:1129–34.

Rizzuto R, Brini M, Murgia M, Pozzan T. Microdomains with high Ca2+ close to IP3-sensitive channels that are sensed by neighboring mitochondria. Science 1993;262:744–7.

Rizzuto R, Pinton P, Carrington W, Fay FS, Fogarty KE, Lifshitz LM, Tuft RA, Pozzan T. Close contacts with the endoplasmic reticulum as determinants of mitochondrial Ca2+ responses. Science 1998;280:1763–6.

Rizzuto R, Simpson AW, Brini M, Pozzan T. Rapid changes of mitochondrial Ca2+ revealed by specifically targeted recombinant aequorin. Nature 1992;358:325–7.

Rodemann HP, Blaese MA. Responses of normal cells to ionizing radiation. Seminars in radiation oncology 2007;17:81–8.

Rolink A, Melchers F. Molecular and cellular origins of B lymphocyte diversity. Cell 1991;66:1081–94.

Rosenbluth MJ, Lam WA, Fletcher DA. Force microscopy of nonadherent cells: a comparison of leukemia cell deformability. Biophysical Journal 2006;90:2994–3003.

Roth B, Gibhardt CS, Becker P, Gebhardt M, Knoop J, Fournier C, Moroni A, Thiel G. Low-dose photon irradiation alters cell differentiation via activation of hIK channels. Pflugers Archiv : European journal of physiology 2015;467:1835–49.

Roth O, LaVerne JA. Effect of pH on H2O2 production in the radiolysis of water. The journal of physical chemistry. A 2011;115:700–8.

Russell JT. Imaging calcium signals in vivo: a powerful tool in physiology and pharmacology. British journal of pharmacology 2011;163:1605–25.

S. Demaria, N. Kawashima, Anne Marie Yang, M. Devitt, J. Babb, J. Allison, S. Formenti. Immune-mediated inhibition of metastases after treatment with local radiation and CTLA-4 blockade in a mouse model of breast cancer. Clinical cancer research : an official journal of the American Association for Cancer Research 2005.

Saito Y, Nishio K, Ogawa Y, Kimata J, Kinumi T, Yoshida Y, Noguchi N, Niki E. Turning point in apoptosis/necrosis induced by hydrogen peroxide. Free radical research 2006;40:619–30.

Salazar C, Politi AZ, Höfer T. Decoding of calcium oscillations by phosphorylation cycles: analytic results. Biophysical Journal 2008;94:1203–15.

Sampieri A, Santoyo K, Asanov A, Vaca L. Association of the IP3R to STIM1 provides a reduced intraluminal calcium microenvironment, resulting in enhanced store-operated calcium entry. Scientific reports 2018;8:13252.

Schaue D, Ratikan JA, Iwamoto KS, McBride WH. Maximizing tumor immunity with fractionated radiation. International journal of radiation oncology, biology, physics 2012;83:1306–10.

Schreck R, Baeuerle PA. A role for oxygen radicals as second messengers. Trends in cell biology 1991;1:39–42.

Schwartz RH. T cell anergy. Annual review of immunology 2003;21:305–34.

Shaposhnikova VV, Korystova AF, Emel'yanov MO, Kublik LN, Kudryavtsev AA, Levitman MK, Kim YA, Korystov YN. Effect of ionizing radiation on multidrug resistance of human larynx cancer HEp-2 cells. Biochem. Moscow Suppl. Ser. A 2007;1:294–300.

Sharma S, Findlay GM, Bandukwala HS, Oberdoerffer S, Baust B, Li Z, Schmidt V, Hogan PG, Sacks DB, Rao A. Dephosphorylation of the nuclear factor of activated T cells (NFAT) transcription factor is regulated by an RNA-protein scaffold complex. PNAS 2011;108:11381–6.

Shaw JP, Utz PJ, Durand DB, Toole JJ, Emmel EA, Crabtree GR. Identification of a putative regulator of early T cell activation genes. Science 1988;241:202–5.

Shaw PJ, Qu B, Hoth M, Feske S. Molecular regulation of CRAC channels and their role in lymphocyte function. Cellular and molecular life sciences : CMLS 2013;70:2637–56.

Shim AH-R, Tirado-Lee L, Prakriya M. Structural and functional mechanisms of CRAC channel regulation. Journal of molecular biology 2015;427:77–93.

Sies H. Hydrogen peroxide as a central redox signaling molecule in physiological oxidative stress: Oxidative eustress. Redox biology 2017;11:613–9.

Sies H, Berndt C, Jones DP. Oxidative Stress. Annual review of biochemistry 2017;86:715–48.

Simeoni L, Bogeski I. Redox regulation of T-cell receptor signaling. Biological chemistry 2015a;396:555–68.

Simeoni L, Bogeski I. Redox regulation of T-cell receptor signaling. Biological chemistry 2015b;396:555–68.

Sloan-Lancaster J, Evavold BD, Allen PM. Induction of T-cell anergy by altered T-cell-receptor ligand on live antigen-presenting cells. Nature 1993;363:156–9.

Smedler E, Uhlén P. Frequency decoding of calcium oscillations. Biochimica et biophysica acta 2014;1840:964–9.

Smeets RL, Fleuren WWM, He X, Vink PM, Wijnands F, Gorecka M, Klop H, Bauerschmidt S, Garritsen A, Koenen HJPM, Joosten I, Boots AMH, Alkema W. Molecular pathway profiling of T lymphocyte signal transduction pathways; Th1 and Th2 genomic fingerprints are defined by TCR and CD28-mediated signaling. BMC immunology 2012;13:12.

Smith-Garvin JE, Koretzky GA, Jordan MS. T cell activation. Annual review of immunology 2009;27:591–619.

Soboloff J, Madesh M, Gill DL. Sensing cellular stress through STIM proteins. Nature chemical biology 2011;7:488–92.

Soboloff J, Rothberg BS, Madesh M, Gill DL. STIM proteins: dynamic calcium signal transducers. Nature reviews. Molecular cell biology 2012;13:549–65.

Soto-Nieves N, Puga I, Abe BT, Bandyopadhyay S, Baine I, Rao A, Macian F. Transcriptional complexes formed by NFAT dimers regulate the induction of T cell tolerance. The Journal of experimental medicine 2009;206:867–76.

Stathopulos PB, Le Zheng, Li G-Y, Plevin MJ, Ikura M. Structural and mechanistic insights into STIM1-mediated initiation of store-operated calcium entry. Cell 2008;135:110–22.

Stein KT, Moon SJ, Nguyen AN, Sikes HD. Kinetic modeling of H2O2 dynamics in the mitochondria of HeLa cells. PLoS computational biology 2020;16:e1008202.

Suzuki K, Yamashita S. Radiation-Induced Bystander Response: Mechanism and Clinical Implications. Advances in wound care 2014;3:16–24.

Szatrowski TP, Nathan CF. Production of large amounts of hydrogen peroxide by human tumor cells. Cancer research 1991;51:794–8.

Tafani M, Sansone L, Limana F, Arcangeli T, Santis E de, Polese M, Fini M, Russo MA. The Interplay of Reactive Oxygen Species, Hypoxia, Inflammation, and Sirtuins in Cancer Initiation and Progression. Oxidative medicine and cellular longevity 2016;2016:3907147.

Tavassolifar MJ, Vodjgani M, Salehi Z, Izad M. The Influence of Reactive Oxygen Species in the Immune System and Pathogenesis of Multiple Sclerosis. Autoimmune diseases 2020;2020:5793817.

Thastrup O, Cullen PJ, Drøbak BK, Hanley MR, Dawson AP. Thapsigargin, a tumor promoter, discharges intracellular Ca2+ stores by specific inhibition of the endoplasmic reticulum Ca2(+)-ATPase. Proceedings of the National Academy of Sciences of the United States of America 1990;87:2466–70.

Thillaiappan NB, Chakraborty P, Hasan G, Taylor CW. IP3 receptors and Ca2+ entry. Biochimica et biophysica acta. Molecular cell research 2019;1866:1092–100.

Thome M, Duplay P, Guttinger M, Acuto O. Syk and ZAP-70 mediate recruitment of p56lck/CD4 to the activated T cell receptor/CD3/zeta complex. J Exp Med 1995;181:1997–2006.

Tomida T, Hirose K, Takizawa A, Shibasaki F, Iino M. NFAT functions as a working memory of Ca2+ signals in decoding Ca2+ oscillation. The EMBO journal 2003;22:3825–32.

Tomita K, Takashi Y, Ouchi Y, Kuwahara Y, Igarashi K, Nagasawa T, Nabika H, Kurimasa A, Fukumoto M, Nishitani Y, Sato T. Lipid peroxidation increases hydrogen peroxide permeability leading to cell death in cancer cell lines that lack mtDNA. Cancer science 2019;110:2856–66.

Tough DF, Sprent J. Turnover of naive- and memory-phenotype T cells. J Exp Med 1994;179:1127–35.

Trachootham D, Lu W, Ogasawara MA, Nilsa R-DV, Huang P. Redox regulation of cell survival. Antioxidants & redox signaling 2008;10:1343–74.

Trafford AW, Díaz ME, Sibbring GC, Eisner DA. Modulation of CICR has no maintained effect on systolic Ca2+: simultaneous measurements of sarcoplasmic reticulum and sarcolemmal Ca2+ fluxes in rat ventricular myocytes. The Journal of physiology 2000;522 Pt 2:259–70.

Treberg JR, Munro D, Banh S, Zacharias P, Sotiri E. Differentiating between apparent and actual rates of H2O2 metabolism by isolated rat muscle mitochondria to test a simple model of mitochondria as regulators of H2O2 concentration. Redox biology 2015;5:216–24.

Triplett TA, Curti BD, Bonafede PR, Miller WL, Walker EB, Weinberg AD. Defining a functionally distinct subset of human memory CD4+ T cells that are CD25POS and FOXP3NEG. European journal of immunology 2012;42:1893–905.

Trotti A, Byhardt R, Stetz J, Gwede C, Corn B, Fu K, Gunderson L, McCormick B, Morris∫ M, Rich T, Shipley W, Curran W. Common toxicity criteria: version 2.0. an improved reference for grading the acute effects of cancer treatment: impact on radiotherapy. International Journal of Radiation Oncology*Biology*Physics 2000;47:13–47.

Tsien RY, Pozzan T, Rink TJ. Calcium homeostasis in intact lymphocytes: cytoplasmic free calcium monitored with a new, intracellularly trapped fluorescent indicator. J Cell Biol 1982;94:325–34.

Tu BP, Ho-Schleyer SC, Travers KJ, Weissman JS. Biochemical basis of oxidative protein folding in the endoplasmic reticulum. Science 2000;290:1571–4.

Tucker MA, Jones PH, Boice JD, Robison LL, Stone BJ, Stovall M, Jenkin RD, Lubin JH, Baum ES, Siegel SE. Therapeutic radiation at a young age is linked to secondary thyroid cancer. The Late Effects Study Group. Cancer research 1991;51:2885–8.

Turner MD, Nedjai B, Hurst T, Pennington DJ. Cytokines and chemokines: At the crossroads of cell signalling and inflammatory disease. Biochimica et biophysica acta 2014;1843:2563–82.

Vaca L, Sampieri A. Calmodulin modulates the delay period between release of calcium from internal stores and activation of calcium influx via endogenous TRP1 channels. The Journal of biological chemistry 2002;277:42178–87.

Vaeth M, Feske S. Ion channelopathies of the immune system. Current Opinion in Immunology 2018;52:39–50.

van Anken E, Braakman I. Versatility of the endoplasmic reticulum protein folding factory. Critical Reviews in Biochemistry and Molecular Biology 2005;40:191–228.

van BLITTERSWIJK WJ, van der LUIT AH, VELDMAN RJ, VERHEIJ M, BORST J. Ceramide: second messenger or modulator of membrane structure and dynamics? Biochem J 2003;369:199–211.

van Parijs L, Abbas AK. Homeostasis and self-tolerance in the immune system: turning lymphocytes off. Science 1998;280:243–8.

Voos P, Fuck S, Weipert F, Babel L, Tandl D, Meckel T, Hehlgans S, Fournier C, Moroni A, Rödel F, Thiel G. Ionizing Radiation Induces Morphological Changes and Immunological Modulation of Jurkat Cells. Frontiers in immunology 2018;9:922.

Vuitton DA, Bresson-Hadni S, Laroche L, Kaiserlian D, Guerret-Stocker S, Bresson JL, Gillet M. Cellular immune response in Echinococcus multilocularis infection in humans. II. Natural killer cell activity and cell subpopulations in the blood and in the periparasitic granuloma of patients with alveolar echinococcosis. Clinical and Experimental Immunology 1989;78:67–74.

Waldmann R, Lazdunski M. H+-gated cation channels: neuronal acid sensors in the NaC/DEG family of ion channels. Current Opinion in Neurobiology 1998;8:418–24.

Wang X, Wang Y, Zhou Y, Hendron E, Mancarella S, Andrake MD, Rothberg BS, Soboloff J, Gill DL. Distinct Orai-coupling domains in STIM1 and STIM2 define the Orai-activating site. Nature communications 2014;5:3183.

Wang Y, Deng X, Zhou Y, Hendron E, Mancarella S, Ritchie MF, Tang XD, Baba Y, Kurosaki T, Mori Y, Soboloff J, Gill DL. STIM protein coupling in the activation of Orai channels. PNAS 2009;106:7391–6.

Weinberg SE, Sena LA, Chandel NS. Mitochondria in the regulation of innate and adaptive immunity. Immunity 2015;42:406–17.

Wilder RL. Neuroendocrine-immune system interactions and autoimmunity. Annual review of immunology 1995;13:307–38.

Woods NM, Cuthbertson K, Cobbold PH. Agonist-induced oscillations in cytoplasmic free calcium concentration in single rat hepatocytes. Cell calcium 1987;8:79–100.

Xia F, Qian C-R, Xun Z, Hamon Y, Sartre A-M, Formisano A, Mailfert S, Phelipot M-C, Billaudeau C, Jaeger S, Nunès JA, Guo X-J, He H-T. TCR and CD28 Concomitant Stimulation Elicits a Distinctive Calcium Response in Naive T Cells. Front. Immunol. 2018;9:2864.

Y Sagara, G Inesi. Inhibition of the sarcoplasmic reticulum Ca2+ transport ATPase by thapsigargin at subnanomolar concentrations. J. Biol. Chem. 1991;266:13503–6.

Yang Y, Jin X, Jiang C. S-glutathionylation of ion channels: insights into the regulation of channel functions, thiol modification crosstalk, and mechanosensing. Antioxidants & redox signaling 2014;20:937–51.

Yissachar N, Sharar Fischler T, Cohen AA, Reich-Zeliger S, Russ D, Shifrut E, Porat Z, Friedman N. Dynamic response diversity of NFAT isoforms in individual living cells. Molecular cell 2013a;49:322–30.

Yissachar N, Sharar Fischler T, Cohen AA, Reich-Zeliger S, Russ D, Shifrut E, Porat Z, Friedman N. Dynamic response diversity of NFAT isoforms in individual living cells. Molecular cell 2013b;49:322–30.

Zhang JZ, Wu Y, Williams BY, Rodney G, Mandel F, Strasburg GM, Hamilton SL. Oxidation of the skeletal muscle Ca2+ release channel alters calmodulin binding. The American journal of physiology 1999;276:C46-53.

Zhang S, Ehlers MD, Bernhardt JP, Su C-T, Huganir RL. Calmodulin Mediates Calcium-Dependent Inactivation of N-Methyl-D-Aspartate Receptors. Neuron 1998;21:443–53.

Zhang X, Gibhardt CS, Will T, Stanisz H, Körbel C, Mitkovski M, Stejerean I, Cappello S, Pacheu-Grau D, Dudek J, Tahbaz N, Mina L, Simmen T, Laschke MW, Menger MD, Schön MP, Helms V, Niemeyer BA, Rehling P, Vultur A, Bogeski I. Redox signals at the ER-mitochondria interface control melanoma progression. The EMBO journal 2019;38:e100871.

Zheng S, Zhou L, Ma G, Zhang T, Liu J, Li J, Nguyen NT, Zhang X, Li W, Nwokonko R, Zhou Y, Zhao F, Liu J, Huang Y, Gill DL, Wang Y. Calcium store refilling and STIM activation in STIM- and Orai-deficient cell lines. Pflugers Archiv : European journal of physiology 2018;470:1555–67.

Zhitkovich A. N-Acetylcysteine: Antioxidant, Aldehyde Scavenger, and More. Chemical Research in Toxicology 2019;32:1318–9.

Zhou Y, Nwokonko RM, Cai X, Loktionova NA, Abdulqadir R, Xin P, Niemeyer BA, Wang Y, Trebak M, Gill DL. Cross-linking of Orai1 channels by STIM proteins. Proceedings of the National Academy of Sciences of the United States of America 2018;115:E3398-E3407.

Zhou YD, Fang XF, Cui ZJ. UVA-induced calcium oscillations in rat mast cells. Cell calcium 2009;45:18–28.

Zhu J, Yamane H, Paul WE. Differentiation of effector CD4 T cell populations (*). Annual review of immunology 2010;28:445–89.

Zhu L, Song S, Pi Y, Yu Y, She W, Ye H, Su Y, Hu Q. Cumulated $Ca2^{+}$ spike duration underlies $Ca2^{+}$ oscillation frequency-regulated NFκB transcriptional activity. Journal of cell science 2011;124:2591–601.

Zorov DB, Filburn CR, Klotz LO, Zweier JL, Sollott SJ. Reactive oxygen species (ROS)-induced ROS release: a new phenomenon accompanying induction of the mitochondrial permeability transition in cardiac myocytes. J Exp Med 2000;192:1001–14.

Zorov DB, Juhaszova M, Sollott SJ. Mitochondrial ROS-induced ROS release: an update and review. Biochimica et biophysica acta 2006;1757:509–17.

Zorov DB, Juhaszova M, Sollott SJ. Mitochondrial reactive oxygen species (ROS) and ROS-induced ROS release. Physiological reviews 2014;94:909–50.

Zweifach A, Lewis RS. Mitogen-regulated Ca2+ current of T lymphocytes is activated by depletion of intracellular Ca2+ stores. Proceedings of the National Academy of Sciences of the United States of America 1993;90:6295–9.

Zweifach A, Lewis RS. Rapid inactivation of depletion-activated calcium current (ICRAC) due to local calcium feedback. J Gen Physiol 1995;105:209–26.

Zweifach A, Lewis RS. Calcium-dependent potentiation of store-operated calcium channels in T lymphocytes. J Gen Physiol 1996;107:597–610.

6. Appendix

List of abbreviations

ALX	Alexa fluophor
APC	antigen presenting cell
ATP	adenosintriphosphat
BAPTA-AM	1,2-bis(o-aminophenoxy)ethane-N,N,N',N'-tetraacetic acid
BSA	bovine serumalbumin
($[Ca^{2+}]_{cyt}$)	free cytosolic calcium ions
Ca^{2+}	calcium-ion
CD3	cluster of differentiation 3
CD4	cluster of differentiation 4
CICR	Ca^{2+} induced Ca^{2+} release
CIRR	Ca^{2+} induced ROS release
CLSM	confocal laser scanning microscopy)
CRAC	calcium-release activated calcium
CsA	cycloyporin A
Ctrl	control
DAG	diacylglycerine
DNA	deoxyribonucleic acid
DTT	dithiothreitol
ER	endoplasmatic reticulum
FACS	fluorescence-activated cell sorting
Fluo4-AM	2-{[2-(2-{5-[bis(carboxymethyl)amino]-2-methylphenoxy}ethoxy)-4-(2,7-difluoro-6-hydroxy-3-oxo-3H-xanthen-9yl)phenyl](carboxymethyl)amino}acetic acid
FRET	Förster resonance energy transfer
Gd^{3+}	gadolinium
GPCR	g-protein coupled receptor
H_2O_2	hydrogen peroxide
IL2	Interleukin-2
IP_3	inositol-1,4,5-trisphosphate
IP_3R	inositol-1,4,5-trisphosphate receptor

IR	ionizing radiation
ITAM	immunoreceptor tyrosine-based activation motif
MAPK	mitogen-activated protein kinase
MCU	mitochondrial calcium uniporter
MHC	major histocompatibility complex
NAC	N-Acetylcystein
NES	nuclear export signal
NFAT	nuclear factor of activated T-cells
NFKB	nuclear factor 'kappa-light-chain-enhancer' of activated B-cells
NLS	nuclear localisation sequence
NOX	nicotinamide adenine dinucleotide phosphate oxidase
PBMC	peripheral blood mononuclear cells
PIP_2	phosphatidylinositol 4,5-bisphosphate
PLC	phospholipase C
PMCA	plasmamembrane Ca^{2+} ATPase
PMA	para-methoxyamphetamine
RICR	ROS induced Ca^{2+} release
RIRR	ROS induced ROS release
RNA	ribonuclein acid
ROS	reactive oxygen species
qRT-PCR	quantitative real-time polymerase chain reaction
SERCA	sarcoplasmic/endoplasmic reticulum calcium ATPase
SOCE	store operated Ca^{2+} entry
SOD	superoxisdismutase
STIM	stromal interaction molecule
T-Act	CD3/CD28/CD2 T-cell activation mix
TCR	T-cell receptor
Tg	thapsigargin
TRP-channels	transient receptor potential channels

Declaration / Ehrenwörtliche Erklärung

Ich erkläre hiermit ehrenwörtlich, dass ich die vorliegende Arbeit entsprechend den Regeln guter wissenschaftlicher Praxis selbstständig und ohne unzulässige Hilfe Dritter angefertigt habe.

Sämtliche aus fremden Quellen direkt oder indirekt übernommenen Gedanken sowie sämtliche von Anderen direkt oder indirekt übernommenen Daten, Techniken und Materialien sind als solche kenntlich gemacht. Die Arbeit wurde bisher bei keiner anderen Hochschule zu Prüfungszwecken eingereicht.

Darmstadt, den 03.12.2020

_____

Dominique Tandl